

AD632198



Technical Report 122 MECHANICS OF PENETRATION OF PILES INTO PERMAFROST

by

Jacques Charest, Philippe Duler
and
John S. Rinehart

SEPTEMBER, 1965

U.S. ARMY MATERIEL COMMAND
COLD REGIONS RESEARCH & ENGINEERING LABORATORY
HANOVER, NEW HAMPSHIRE

Colorado School of Mines Research Foundation, Inc.
Contract DA-11-190-ENG-92

CLEARINGHOUSE FOR FEDERAL SCIENTIFIC AND TECHNICAL INFORMATION		
Hardcopy	Microfiche	
\$4.00	\$0.75	108 pp
ARCHIVE COPY		



code 6

Errata - Technical Report 122

Page 47, para. 2, line 1

"100°" should read "110°"

Page 58, para. 4, line 2

"normal" should read "nominal"

BLANK PAGE



Technical Report 122
MECHANICS OF PENETRATION
OF
PILES INTO PERMAFROST

by

Jacques Charest, Philippe Duler
and
John S. Rinehart

SEPTEMBER, 1965

U.S. ARMY MATERIEL COMMAND
COLD REGIONS RESEARCH & ENGINEERING LABORATORY
HANOVER, NEW HAMPSHIRE

Colorado School of Mines Research Foundation, Inc.

Contract DA-11-190-ENG-92



DDC AVAILABILITY NOTICE
DISTRIBUTION OF THIS
DOCUMENT IS UNLIMITED

PREFACE

This investigation was carried out for U. S. Army Snow, Ice and Permafrost Research Establishment* by the Colorado School of Mines Research Foundation, Inc. under Contract DA-11-190-ENG-92, "Mechanics of penetration of piles into permafrost." The purpose of this investigation was twofold: to study the mechanics of piles penetrating permafrost under the influence of their impact kinetic energies alone and to investigate the feasibility of driving full-size piles into natural permafrost, using a rocket as the driving agent.

The investigation was initiated by W. K. Boyd, then chief of USA SIPRE's Applied Research Branch. The report was prepared for the Applied Research Branch (Dr. A. Assur, then chief), Experimental Engineering Division (K. A. Linell, chief).

Dr. J. S. Rinehart was principal investigator of this project. The laboratory work was done at the Mining Research Laboratory, Colorado School of Mines, Golden, Colorado, by J. Charest and P. F. Duler. The field work was conducted near Fairbanks, Alaska, by J. F. Whalen, under the direction of Fred L. Smith.

Buckling of piles when shot into the ground is one of the problems in practical application. Appendix H, by Sp/4 C. Goetze, USA CRREL, gives a theoretical treatment of this problem.

USA CRREL is an Army Material Command laboratory.

Manuscript received 15 July 1962

*Redesignated U. S. Army Cold Regions Research and Engineering Laboratory, Feb 1962.

CONTENTS

	Page
Preface	ii
Summary	vi
Introduction	1
Experimental	1
Artificial permafrost	1
Piles	2
Guns	3
Impact velocity measurement technique	7
Firing procedure	7
Phase I	7
Impact velocity dependence	8
Mass dependence	8
Shape factor dependence	12
Theoretical considerations	12
Constant force model	17
Variable force model	18
Combined force model	18
First investigation, phase II	19
Penetration-time measurement technique	19
Determination of penetration-time curves	19
Study of penetration-time curves	21
Physical model	23
Discussion of the physical model	29
Second investigation, phase II	34
Piles of the same projected area	34
Effective projected area	34
Thick piles	35
Thin piles	46
Solid circular piles with conical and ogival tips	46
Discussion	47
Field tests	55
Experimental	55
Results	58
Proposal for an integrated pile-rocket	60
Conclusions and recommendations	61
Literature cited	61
Appendix A: Data on artificial permafrost	63
Appendix B: Characteristics of piles used in laboratory and field work	64
Appendix C: Firing data of phase I	66
Appendix D: Firing data of the first investigation of phase II	73
Appendix E: Firing data of the second investigation of phase II	79
Appendix F: Determination of the shape factor Q	89
Appendix G: Firing record of Alaskan tests	92
Appendix H: Buckling of piles under deceleration	94

ILLUSTRATIONS

Figure		Page
1.	Aluminum container assembly	2
2.	Pile assembly used in laboratory	3
3.	Pile-rocket assembly used for field tests	4
4.	50-caliber gun assembly	4
5.	50-caliber gun as a conventional gun	5

CONTENTS (Cont'd)

ILLUSTRATIONS (Cont'd)

Figure	Page
6. 50-caliber gun as an air gun-----	5
7. 1 $\frac{1}{4}$ -in. gun as a conventional gun-----	6
8. Breaking-wire system-----	6
9. Electrical diagram of the breaking-wire system-----	7
10. Penetration of a 7/16 in. diam pile vs impact velocity--	9
11. Penetration of a 1.0 in. diam pile vs impact velocity---	10
12. Penetration of 6/16 in. diam piles vs impact velocity --	10
13. Penetration of 6/16 in. diam piles vs mass-----	11
14. Reduced penetration of 6/16 in. diam piles vs impact velocity-----	11
15. Reduced penetration of 1.0 in. diam piles vs impact velocity-----	13
16. Penetration vs impact velocity, piles with various shape factors-----	13
17. Penetration vs shape factor at 200 ft/sec-----	16
18. Reduced penetration vs impact velocity, piles with various shape factors-----	16
19. Reduced penetration vs impact velocity, piles with various masses and shape factors-----	17
20. Principle of the penetration-time measurement technique	20
21. Electrical diagram of the penetration-time measurement technique-----	21
22. Trace of an oscilloscope record of the penetration-time measurement technique-----	22
23. Determination of a penetration-time curve-----	22
24. Instantaneous deceleration vs instantaneous penetration	25
25. Impact deceleration vs impact velocity-----	25
26. Total deceleration-----	26
27. Frictional deceleration region-----	28
28. Frictional deceleration vs instantaneous penetration----	28
29. Friction factor vs instantaneous velocity-----	30
30. Experimental and calculated values of penetration-----	30
31. Penetration vs impact velocity, piles of different materials	31
32. Normal pile and wall-reduced pile --	31
33. Penetration vs impact velocity, piles with different wall characteristics-----	32
34. Reduced penetration vs impact velocity, piles with various masses-----	33
35-39. Penetration vs impact velocity for various pile shapes -	36
40-42. Penetration vs impact velocity, various projected areas	41
43. Reduced penetration vs impact velocity for thick piles with the same projected areas-----	44
44. Reduced penetration vs impact velocity for thick piles with various projected areas-----	48
45. Penetration vs impact velocity, 1.0 in. diam cross- shaped pile-----	49
46. Penetration vs impact velocity, 7/16 in. diam cross- shaped pile-----	49
47. Penetration vs projected area, thick piles with same shape-----	50
48. Penetration vs projected area, various piles-----	50
49. Penetration vs impact velocity, piles with various tips -	51
50. Penetration ratio vs $\cos \beta$ (linear scales)-----	53
51. Penetration ratio vs $\cos \beta$ (log-log scales)-----	53
52. Penetration vs impact velocity for piles having conical and ogival tips-----	54

CONTENTS (Cont'd)

ILLUSTRATIONS (Cont'd)

Figure	Page
53. Arrangement of the launching stand-----	57
54. Reinforcement shoes-----	58
55. Reduced penetration vs impact velocity, field test results-----	59
56. Integrated pile-rocket assembly-----	60

TABLES

Table	
I. Values of A, B, C -----	23
II. Values of P_i , v , a , t -----	24
III. Calculated penetrations-----	32
IV. Characteristics of thick piles -----	45
V. Penetration of circular piles at 100 ft/sec -----	47
VI. Penetration ratios of conical-tipped piles-----	47
VII. Comparison between two relationships for thick piles --	48
VIII. Description of drill hole 1 -----	56
IX. Description of drill hole 2 -----	56
X. Analyses of permafrost samples from drill holes 1 and 2	57

SUMMARY

A comprehensive study was made of rapid pile driving into permafrost. The experimental work was limited to the study of piles penetrating permafrost under the influence of their kinetic energies alone. Laboratory tests were conducted by driving various model piles with guns into artificial permafrost. A single series of field tests was made near Fairbanks, Alaska, in which hollow, circular, full-size piles were launched into permafrost, using an Army practice solid-fuel rocket as the driving agent. Impact velocities were measured with a breaking-wire system in both laboratory and field tests.

The penetration of piles into permafrost was studied as a function of impact velocity, mass, and pile-shape factor. The range of impact velocity explored for both laboratory and field tests was 40 to 525 ft/sec. The mass of the piles ranged from 0.05 to 5.0 lb in the laboratory tests and from 115 to 350 lb for field tests. Solid circular piles used in the laboratory ranged from 0.246 to 7/16 in. diam; hollow piles ranged from 3/16 to 0.83 in. ID and from 5/16 to 1 in. OD. Other types of piles also used for laboratory work — cross-shaped, rectangular, and square piles — did not exceed 1.0 in. in maximum transverse dimension. The diameters of the hollow circular piles investigated during the field tests ranged from 1.93 to 8.18 ID and from 2.37 to 8.62 OD. In both laboratory and field tests the ratio of pile penetration to maximum transverse pile dimension was limited to less than 20.

The artificial permafrost used for most of the laboratory tests was prepared from graded Ottawa sand, type Wausau 3/0, saturated with water and frozen at -6C. This mixture has an average density of 1.77 g/cm³ and an average water content of 23%. Other more limited testing was done with a few other types of permafrost made with bauxite, fine Ottawa sand, pure ice, Golden sand, and ground silica. The similarity of results obtained with different types of artificial permafrost indicates that the relationships developed in the laboratory could be applicable to field-test results.

Phase I of the laboratory work showed that the penetration of thin-walled, hollow, circular piles into permafrost made with Wausau sand 3/0 closely followed the empirical equation,

$$P = KM^{0.8} V^{1.5} / (D_1^2 - D_2^2)^{0.4}$$

where P is the penetration of the pile, K is a constant which, for a given shape of pile, depends upon the properties of the permafrost, M is the mass of the pile, V the velocity, and D_1 and D_2 are the external and internal diameters of the pile.

During a second phase of the laboratory work, additional parameters were measured in an effort to establish a physical basis for

SUMMARY (Cont'd)

eq 1. This phase consisted of two separate investigations: the first, to determine the displacement of a thin, hollow, circular pile during its penetration, and the second to determine the influence of pile shape on pile penetration.

An optical technique was developed which made it possible to measure pile penetration at any instant and obtain penetration-time curves, from which pile velocity and deceleration at any instant of penetration could be calculated.

A study of penetration-time curves showed that the total force resisting pile penetration could be resolved into three types: crushing and drag forces acting at the tip of the pile and friction forces acting along the walls of the pile.

The crushing force can be considered the minimum force required to destroy the structure of the permafrost and allow the pile to penetrate. The drag force is the force necessary to displace particles of permafrost, and could also include a possible increase of the crushing force with velocity.

The friction forces acting along the walls of the pile would be similar to friction forces common to fluid flow. On the basis of a few assumptions and from the analysis of a series of tests, a differential equation was found to provide a good model of penetration. This differential equation, based on constant crushing forces, drag forces varying with velocity, and friction forces varying with penetration and velocity can be written,

$$-d(Mv^2/2) = M(C_1 + C_2 v^2 + C_3 P_i e^{-kv}) dP_i$$

or

$$-vdv = (C_1 + C_2 v^2 + C_3 P_i e^{-kv}) dP_i$$

where M is the mass of the pile, v its instantaneous velocity, C_1 a constant crushing force, $C_2 \cdot v^2$ a drag force, $C_3 \cdot P_i \cdot e^{-kv}$ a friction force, P_i the instantaneous penetration, and C_1 , C_2 , C_3 and k are empirical constants.

When this equation is numerically integrated using the experimentally obtained values of C_1 , C_2 , C_3 , and k it closely approximates the experimental results within the range of the tests; it closely approximates the 1.5 velocity power dependence and the 0.8 mass power dependence of the penetration given by the empirical equation; it predicts the penetration, within the range explored during the experiments, when the mass of the pile is changed; and it predicts a mass power dependence of penetration close to unity at low penetration, which was observed experimentally.

During the second investigation of phase II, model cross-shaped, solid-circular, rectangular, and square piles were tested. The study of flat-tipped piles showed that, for a constant projected area, the shape of a pile affected its penetration. This observation led to the definition of a parameter, effective pile thickness τ , defined as twice the average sum (with respect to the projected area of the pile) of the respective displacements of the individual particles of permafrost. This parameter provided a means of comparing flat-tipped piles of various shapes, using the following equations:

SUMMARY (Cont'd)

$$P = K_1 / (p\tau)^{0.6} \quad (p/\tau < 50, \text{ thick piles})$$

$$P = K_2 / (p\tau)^{0.4} \quad (p/\tau > 70, \text{ thin piles})$$

where \underline{P} = penetration, \underline{p} = perimeter of pile cross section, and K_1 and K_2 are constants, for piles having identical masses and impact velocities. For piles having identical shapes, masses, and impact velocities:

$$P = K_3 / S^{0.6} \quad (p/\tau < 50)$$

$$P = K_4 / S^{0.4} \quad (p/\tau > 70)$$

where K_3 and K_4 are defined as above and \underline{S} is the projected area of the piles. The dependence of the penetration as the inverse of the 0.4 power of the projected area of the piles is in very good agreement with the empirical equation.

For solid, circular, conically tipped piles, the penetration was found to vary as the cube of $\cos \beta$ (2β = apex angle of the conical tip). The penetration of ogival-tipped piles was found to be 20 to 40% greater than that of conical-tipped piles having the same apex angle.

The empirical equation derived during the first phase of the laboratory work provided a good relationship for reducing field-test results. The M-17-AL Army practice rocket used during the field tests had insufficient thrust to achieve a 6 to 8 ft penetration of natural permafrost with 6.0 in. diam piles. To achieve that penetration with a 10 ft long pile weighing approximately 400 lb, a rocket must, in view of the Alaskan tests, have 100,000-lb thrust and a burning duration of 80 msec.

A design of an integrated pile-rocket assembly having the above characteristics and capabilities was proposed. The estimated cost of this integrated pile-rocket assembly is \$1200 per unit in small lots. While this technique of rapid pile driving appears technically feasible, the rocket design must be perfected and fully tested and evaluated in the field.

MECHANICS OF PENETRATION OF PILES INTO PERMAFROST

by

Jacques Charest, Philippe Duler and John S. Rinehart

INTRODUCTION

As a result of recent military and research developments in Alaska and Northern Canada, problems of building construction have been encountered. The annual freezing and thawing of the ground surface is a serious handicap to the use of conventional construction techniques. However, this difficulty can be overcome by driving piles into the permanently frozen layer of the ground, the permafrost layer, and using them as foundation supports.

An unusual pile-driving technique has been proposed for rapid pile driving into permafrost. A fast-burning rocket could be fixed to the end of a pile, a steel tube for example, and launched vertically in the direction of the ground, letting the pile penetrate under the influence of its kinetic energy alone. This technique could be valuable in remote areas where conventional pile-driving equipment is not available. A literature survey indicated that a study on this subject has never been done before, although much work has been done in connection with the conventional technique of pile driving. This study was approached experimentally by conducting laboratory and field tests.

The first part of the laboratory work, Phase I, consisted of driving hollow circular model piles with guns into artificial permafrost. The measured parameters were the penetrations and the impact velocities of piles having various masses and various external and internal diameters.

The main purpose of Phase II was the measurement of parameters in order to find a physical meaning of the empirical equation developed in Phase I. It consisted of two investigations. The first investigation was devoted to measuring the instantaneous penetrations of thin (walled), hollow, circular, model piles as a function of their times of penetration. The experiments were conducted with piles having various external and internal diameters but the same mass. The artificial permafrost used was the same as the one used during Phase I. The second investigation consisted of measuring the penetrations and the impact velocities of model piles having various shapes but the same masses.

The field test program consisted of driving thin, hollow, full-size piles into natural permafrost using a rocket as the driving agent. The measured parameters were the penetrations and the impact velocities of piles having various masses and various external and internal diameters. The purpose of these tests was to collect data and to obtain technical information necessary for the development of this technique of rapid pile driving.

EXPERIMENTAL

Artificial permafrost

The artificial permafrost used in the laboratory experiments had to be homogeneous and easy to reproduce. To obtain those qualities, a standard method of preparation was adopted. This method, which is described below, proved very satisfactory and constant physical properties of the permafrost were obtained.

Sands. Graded Ottawa sand, type Wausau 3/0, was used for most of the experimental work. This very fine sand, being mostly pure silica, exhibits a great ability to flow and to absorb water when dry. These characteristics of the sand are very important to avoid trapped air and to obtain homogeneous permafrost. Two shipments, designated Sand 1 and Sand 2, were used for the laboratory experiments. Although Sands 1 and 2 had practically the same screen analysis, the penetrations into Sand 2

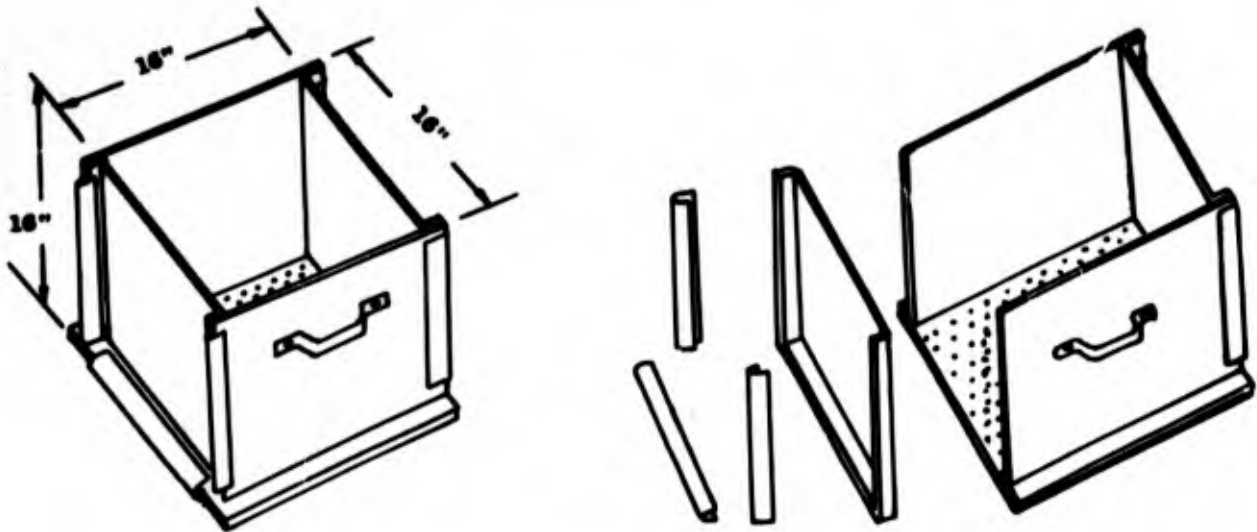


Figure 1. Aluminum container assembly.

permafrost were approximately 15% higher than the penetrations into Sand 1 permafrost. Sand 1 was used for most of Phase I and the first part of Phase II. Sand 2 was used for most of the second part of Phase II. In addition, a few penetration tests were conducted with permafrost prepared from other materials. The description of all materials is given in Appendix A.

Container. It was found during preliminary experiments that a minimum-size permafrost sample had to be used for easy manipulation of the samples and to avoid crack formation. These factors were considered when choosing the container to be used for preparing the samples. The container used (Fig. 1) was made of aluminum, and arranged so that it could be easily taken apart, permitting rapid removal of samples for water content and specific gravity determination. The perforated bottom permitted water absorption during sample preparation.

Sample preparation. A layer of porous paper was placed in the bottom of the container, to prevent the dry sand from escaping through the perforated bottom; sand was poured in and shaken until no appreciable settling was observed. The container was put into a large pan of water for about 15 hours at room temperature to allow complete saturation of the sand. The saturation was accomplished only by capillary action. The container of saturated sand was then put into a freezing unit at -6°C for at least 2 days. Thermocouples in the samples indicated that a uniform temperature was obtained after this period of time.

Water-contents and densities of the artificial permafrost are given in Table AV. The precision of water-content and density measurements were of the same order of magnitude. Due to the high rate of flow of the artificial permafrost, tests to determine its compressive strength were abandoned.

Piles

A penetration of 6 to 8 ft into natural permafrost with full-size piles was desired, and it was believed that hollow circular piles would have good mechanical qualities for field operations. The model piles for the laboratory tests were designed to permit easy changes in their physical characteristics and to establish a scale factor with full-size piles. Figure 2 shows the arrangement of the model pile. It consists essentially of three parts: a hollow steel cylinder, an adapter, and a driving head.

Hollow cylinder. The hollow cylinder was made of cold-drawn seamless steel tubing. The cylinder was 12 in. long for pile diameters smaller than $7/16$ in., and

24 in. for pile diameters of 1 in. In most cases the tip of the pile was flat. Brass piles were also used for special tests, and piles of other shapes were used in the second part of the Phase II tests. All piles used are described in Appendix B.

Adapter. The adapter, made of cold-rolled steel, was used to hold the steel tube and driving head together. The adapter, $1\frac{1}{2}$ in. long, was a push-fit type at one end and a screw-fit type at the other. A hole made on the side of the push-fit end permitted air to escape from the interior of the pile during penetration.

Driving head. The driving head, made of cold-rolled steel or aluminum alloy, served a double purpose. Being the same dimension as the internal diameter of the gun barrel, the driving head permitted firing the pile assembly into the permafrost. Secondly, it permitted changing the total mass of the pile when desired. This pile arrangement was found to be very flexible for laboratory work.

Figure 3 shows the pile and rocket assembly used during the field tests.

Guns

The easiest and safest way to launch model piles into the laboratory permafrost was by using a gun. Use of a gun permitted obtaining many experimental results with a minimum of equipment. A 50-caliber and a $1\frac{1}{4}$ -in. gun were used, both mounted vertically.

50-caliber gun. The 50-caliber gun assembly (Fig. 4) consisted of a 5 ft long 3 in. diam barrel mounted vertically. For pile velocity greater than 150 ft/sec, this gun was operated as a conventional gun, using 50-caliber shell cases and Du Pont gunpowder No. 310 (Fig. 5). The powder was contained in a 50-caliber shell case, and the driving head of the pile assembly was simply put in the place of the bullet. A screw-type breech was used, which adapted to the barrel of the gun by external threads made on the barrel itself. As shown in Figure 4, a hammer, released by an electromagnetic device, was used to fire the gun.

For lower velocity, compressed air was used to give better reproduction of velocity. Figure 6 shows the mechanical arrangement of the gun when used as an air gun. A 25 in. long, $1\frac{1}{2}$ in. diam copper tube was connected to a commercial air cylinder. The copper tube was used as a high pressure air reservoir and was capable of safely holding a pressure of 600 psi. The upper part of the high-pressure reservoir was provided with a fast-opening valve (valve 2) followed by a flexible tube and terminated by a 50-caliber shell case. The air gun was operated by pushing the driving head inside the 50-caliber shell case, inserting the shell and the pile assembly in the gun chamber, and clamping the whole with the system shown at the right of Figure 6. After the reservoir was filled to the desired pressure, the gun was fired by a quick opening of valve 2.

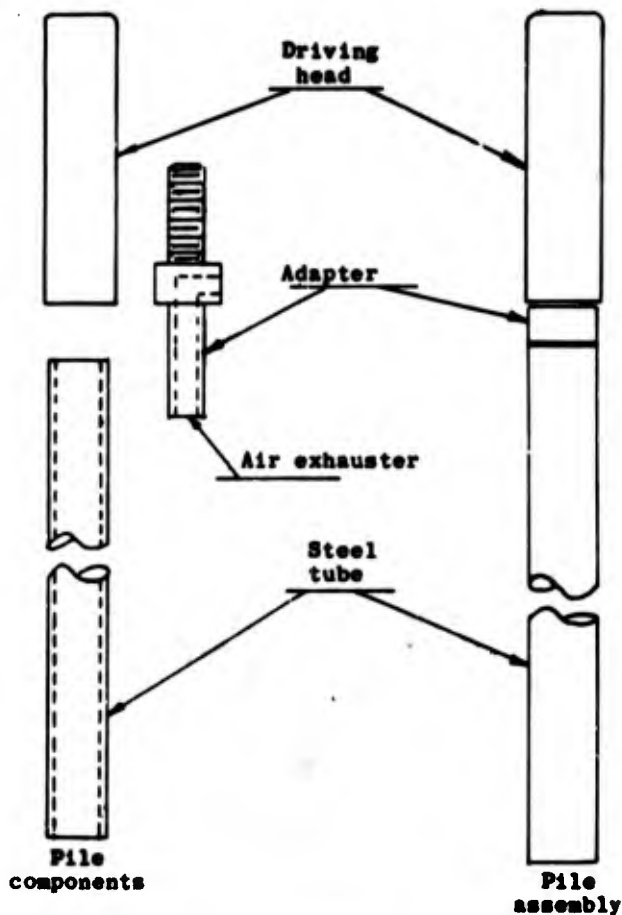


Figure 2. Pile assembly used in laboratory.

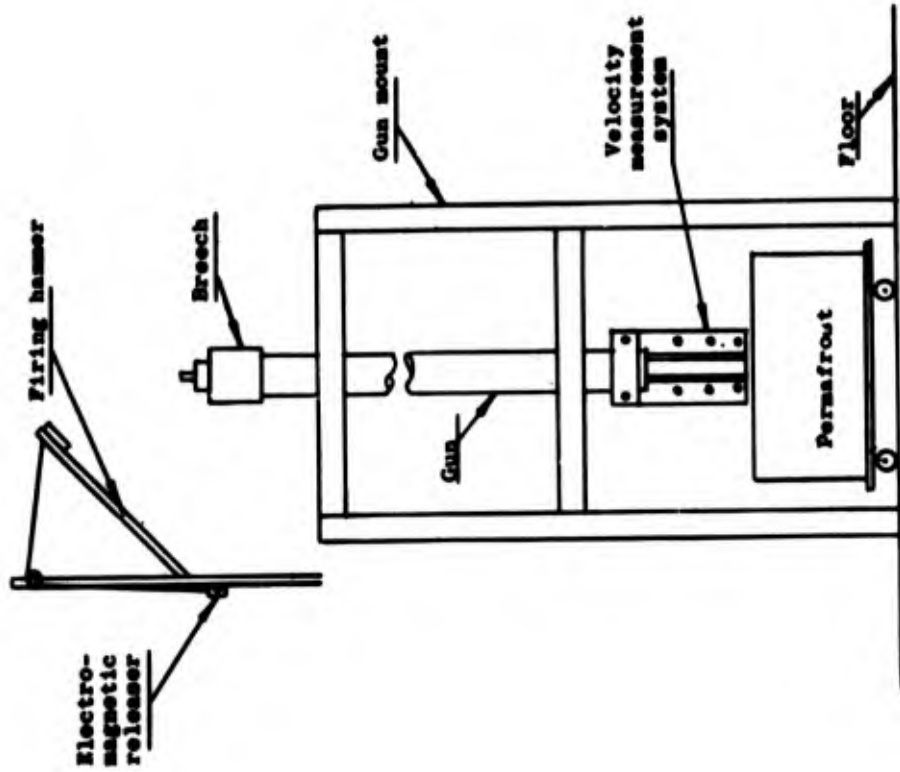


Figure 4. 50-caliber gun assembly.

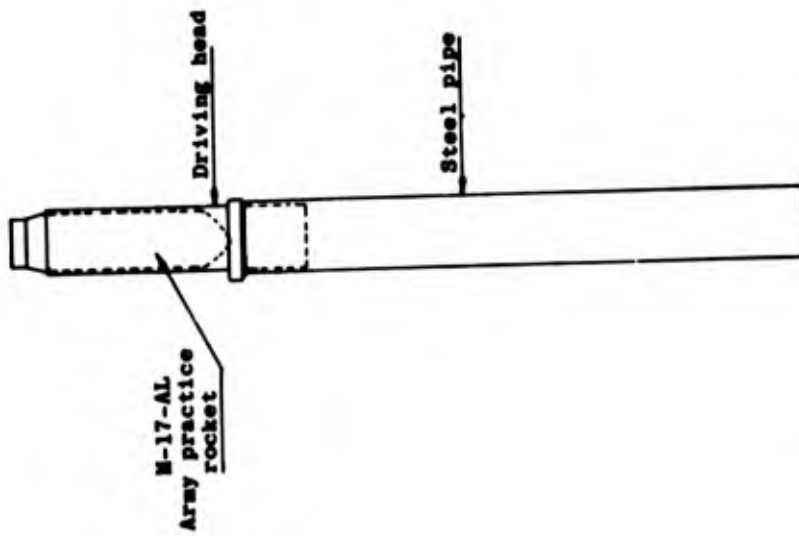


Figure 3. Pile-rocket assembly used for field tests.

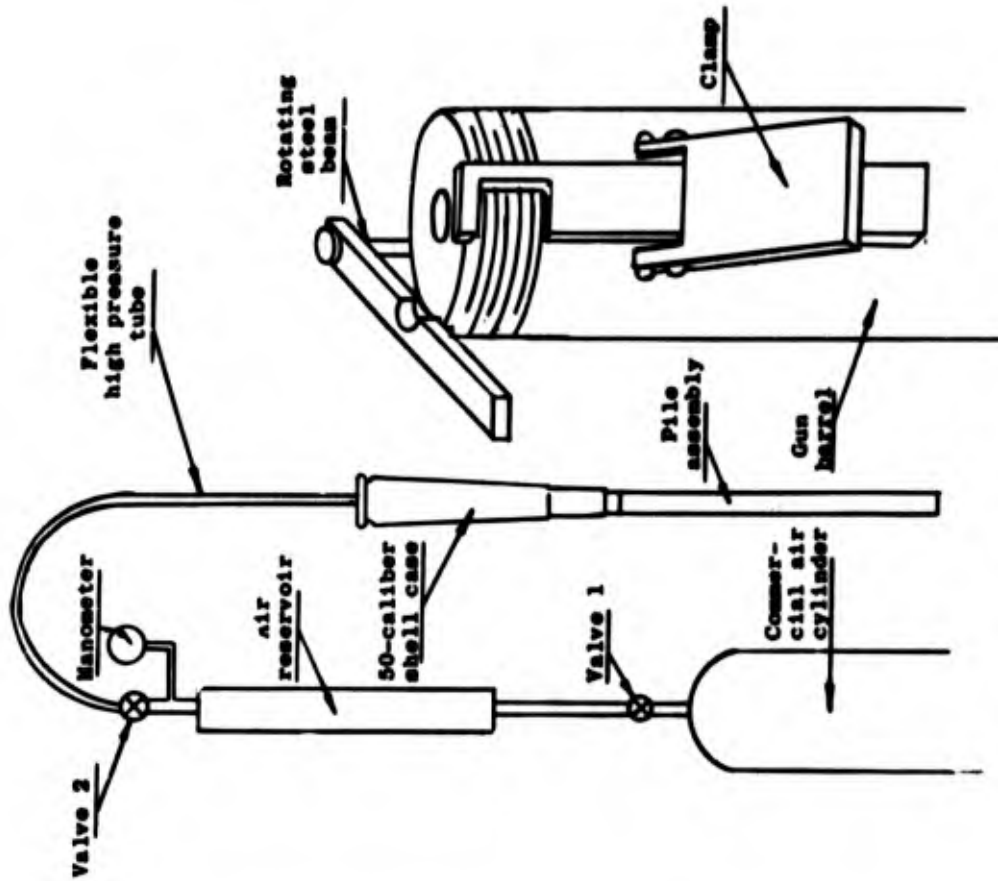


Figure 6. 50-caliber gun as an air gun.

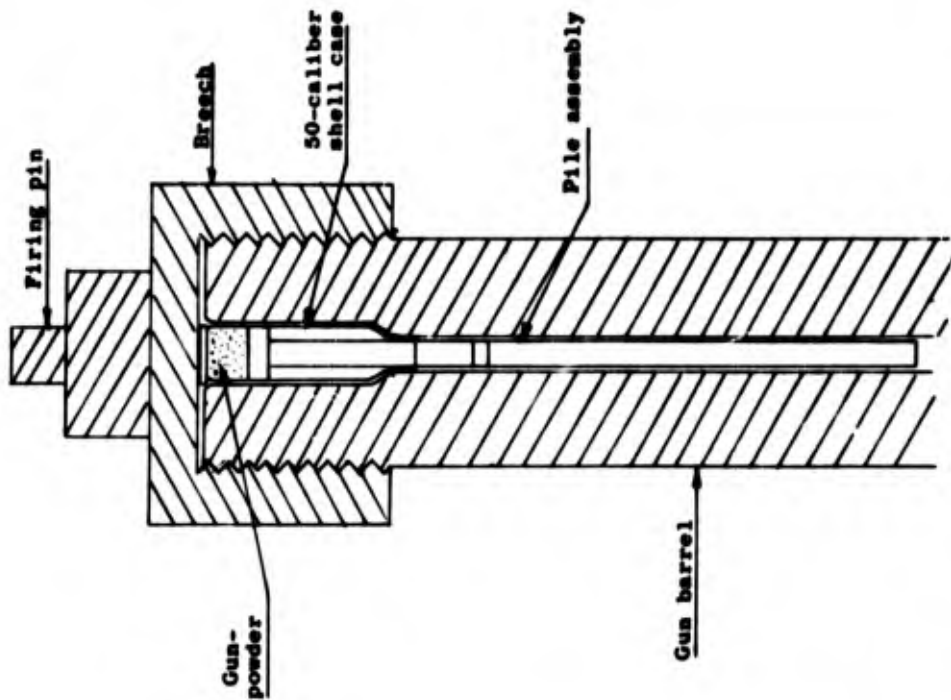


Figure 5. 50-caliber gun as a conventional gun.

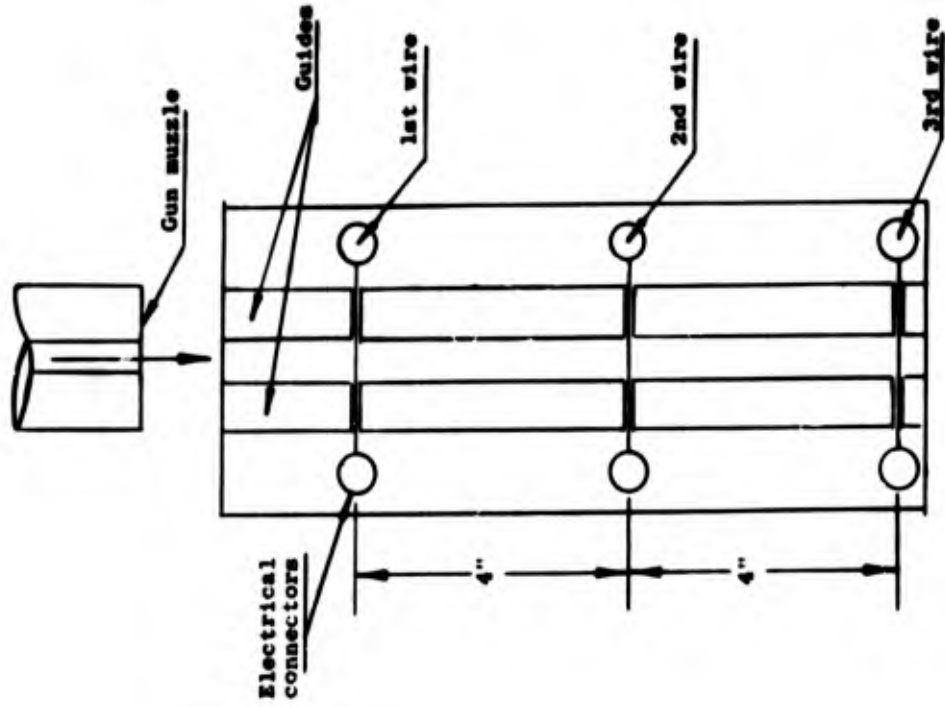


Figure 8. Breaking-wire system.

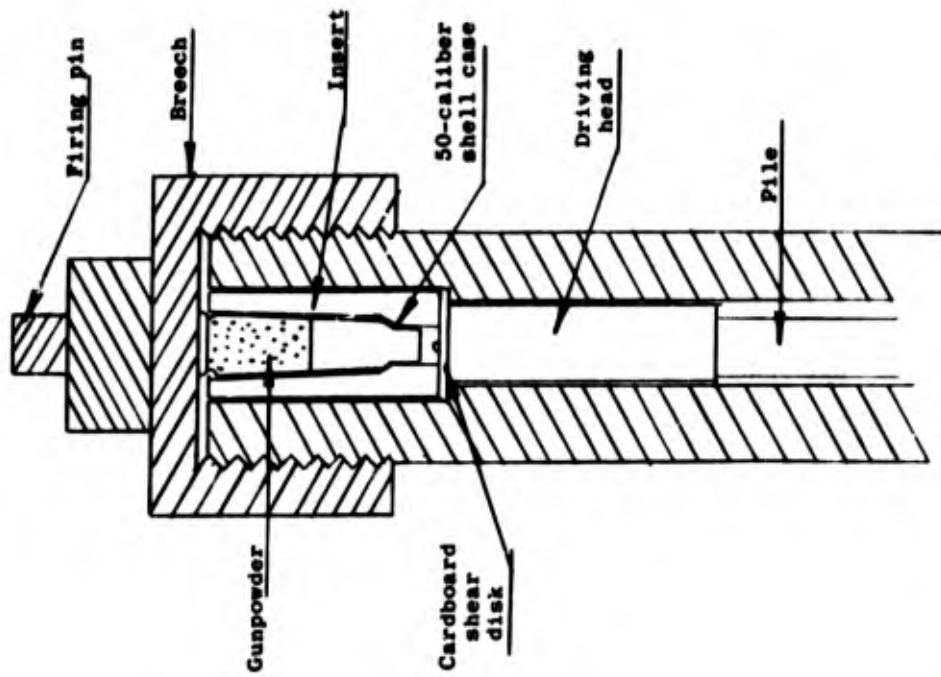


Figure 7. 1 1/4-in. gun as a conventional gun.

1¼-in. gun. The 1¼-in. gun was used to launch the 1 in. diam piles. Used as a conventional gun, it was mounted exactly as was the 50-caliber gun. It was designed to permit the use of 50-caliber shell cases which contained the powder charge. Figure 7 shows the adaption of the 50-caliber shell case to the 1¼-in. gun and the use of a shear disk to prevent the pile assembly from falling due to gravity.

Impact velocity measurement technique

The velocity of a pile before impact with the permafrost was measured with a breaking-wire system, consisting of tiny wires stretched across the trajectory line of the pile (Fig. 8). Electrical impulses obtained when these wires were ruptured by the pile were recorded by a counter (Hewlett-Packard type 423-B) and the velocity of the pile was calculated from the time interval between them.

The guides shown on the sketch were used to reduce the sag of the wires at the instant of rupture, thus reducing errors in the time measurements. The wire used during the experiments was 0.003-in. Nichrome wire. This technique, checked with the penetration-time measurement technique described later, showed an accuracy of 3% or better in the velocity measurements, which was acceptable for the present work. Figure 9 is a diagram of the electrical circuit used with the velocity measurement system.

Firing procedure

The samples of permafrost were not taken out of the freezer until the gun and the instrumentation were ready to operate; the maximum time lapse from the instant the samples were taken out of the freezer, fired into, and returned to the freezer did not exceed 45 sec; the penetrations were measured inside the freezing unit with a precision of ± 0.03 in. The firing rate was limited to a minimum interval of 15 min and was generally made according to an increasing order of penetration.

PHASE I

Experimental data from Phase I tests are given in Appendix C.

At an early stage, an empirical equation was derived from the experimental results for hollow circular piles (Charest, Duler, and Rinehart, 1961):

$$P = K_5 [M^{0.75} V^{1.5} / (D_1^2 - D_2^2)^{0.5}] \quad (1)$$

where P is total penetration of the pile in permafrost, M is the mass of the pile, V is its impact velocity, D_1 and D_2 are, respectively, the external and internal diameters of the pile, and K_5 is a constant which depends on the properties of the permafrost.

Equation 1 was derived from results obtained with both thin and thick (walled), hollow, circular piles and, in fact, included a solid circular pile. The influence of pile shape was studied extensively in Phase II with additional work in Phase I being limited to thin, hollow, circular piles. A thin, hollow, circular pile is defined as a pile for which the ratio of wall thickness, T , to external diameter D_1 , T/D_1 , is smaller than or equal to 0.2.

An empirical equation giving the penetration of a thin, hollow, circular pile as a function of the impact velocity, the mass, and the shape factor was derived. The

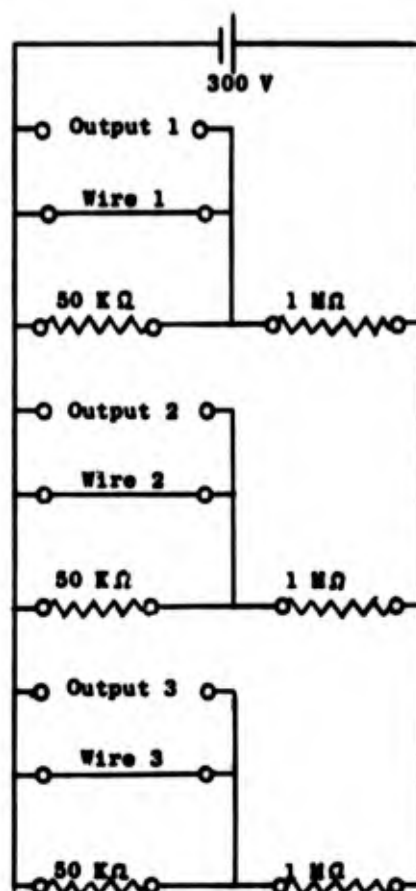


Figure 9. Electrical diagram of the breaking-wire system.

experimental results were plotted on log-log scales because they provided an expedient and rapid way for establishing the law of penetration as a function of the parameters of the pile.

Impact velocity dependence

The penetration of piles into permafrost was first studied as a function of impact velocity, i. e., the velocity at which the pile hits the surface of the permafrost. One must recall that penetration takes place only under the influence of the kinetic energies of the piles, which correspond to their respective impact velocities. Figures 10a and 10b show the penetration vs impact velocity curves for a 7/16 in. diam pile, penetrating various types of permafrost, including pure ice. The mass of the pile was kept constant. The slopes of these curves are very close to 1.5. For some materials, ice for instance, the slope is slightly higher. For others, such as fine Ottawa sand, the slope is slightly less. The differences in penetration at the same velocity are due to the differences in the physical properties of the materials involved. Figure 11 shows the penetration of a 1.0 in. diam pile into permafrost made with local soil (Golden soil). The slope of this curve is also close to 1.5. It is thus possible to write an expression giving the penetration of a given pile as a function of the impact velocity:

$$P = K_6 V^{1.5} \quad (2)$$

where P is penetration, K_6 is a constant, and V is impact velocity. Most of the experimental results obtained in this work agree very closely with eq 2 within the range of penetration studied. Because scaling between the field and laboratory work was desirable, the range of penetration studied in the laboratory was limited to values of the ratio P/D_1 between 2.0 and 20.0, the range of practical interest.

Mass dependence

The second parameter investigated was the mass of the pile. Figure 12 shows the penetration of 6/16 in. diam piles of various masses as a function of impact velocity. All these curves show a dependence on velocity close to a 1.5 power. The penetration given by each curve at a 300 ft/sec impact velocity plotted as a function of the mass of the pile (Fig. 13) shows a slope of approximately 0.78, and since the curves of Figure 12 are almost parallel, we can write

$$P = K_7 M^{0.78} \quad (3)$$

where K_7 is a constant and M is the mass of the pile.

The combination of eq 2 and 3 gives

$$P = K_8 M^{0.78} V^{1.5} \quad (4)$$

where K_8 is a constant.

Multiplying both sides of eq 4 by $(M_0/M)^{0.78}$, one obtains

$$P_M = P (M_0/M)^{0.78} = K_9 V^{1.5} \quad (5)$$

where P_M is the reduced penetration, M_0 is a reference mass, and K_9 is a constant.

Reducing the experimental results of Figure 12 by the factor $(M_0/M)^{0.78}$, making M_0 equal to 0.38 lb, gives the reduced penetration P_M as a function of the impact velocity (Fig. 14). The slope of this curve is also very close to 1.5.

The reduced-penetration curve for 1.0 in. diam piles in Golden soil is shown on Figure 15. These experimental results show a better agreement with the following equation:

$$P_M = P (M_0/M)^{0.75} = K_{10} V^{1.5} \quad (6)$$

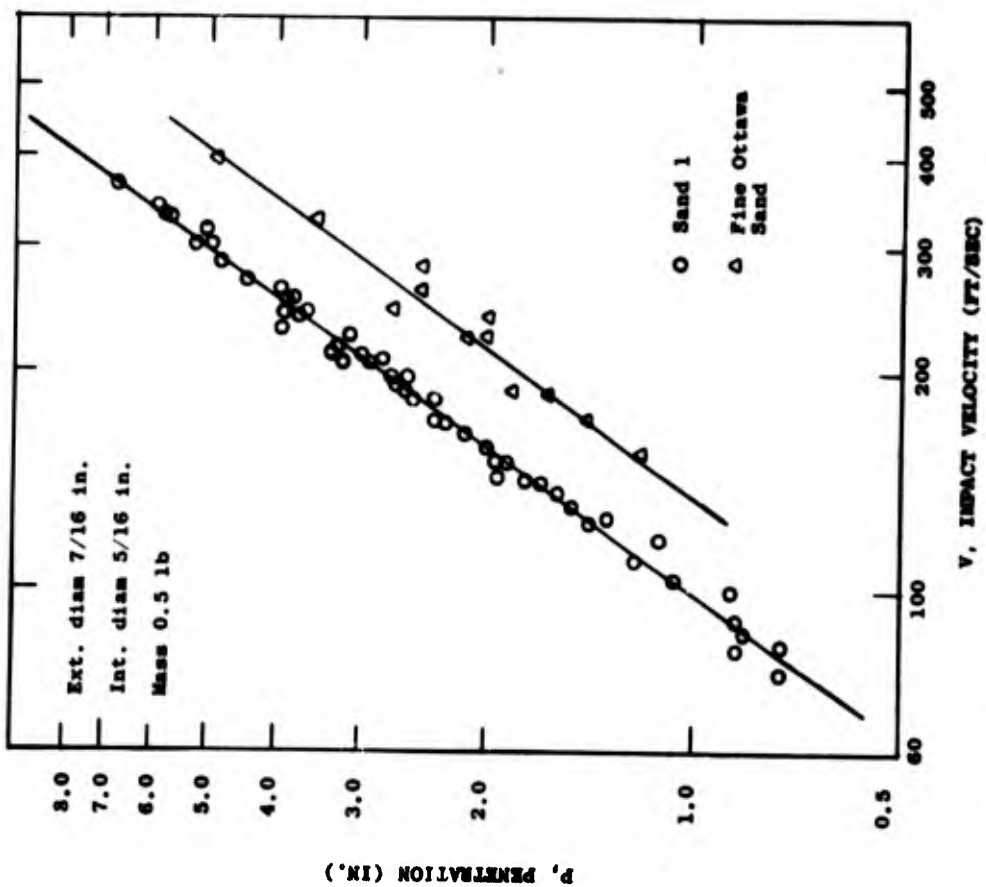


Figure 10a. Penetration of 7/16 in. diam pile vs impact velocity.

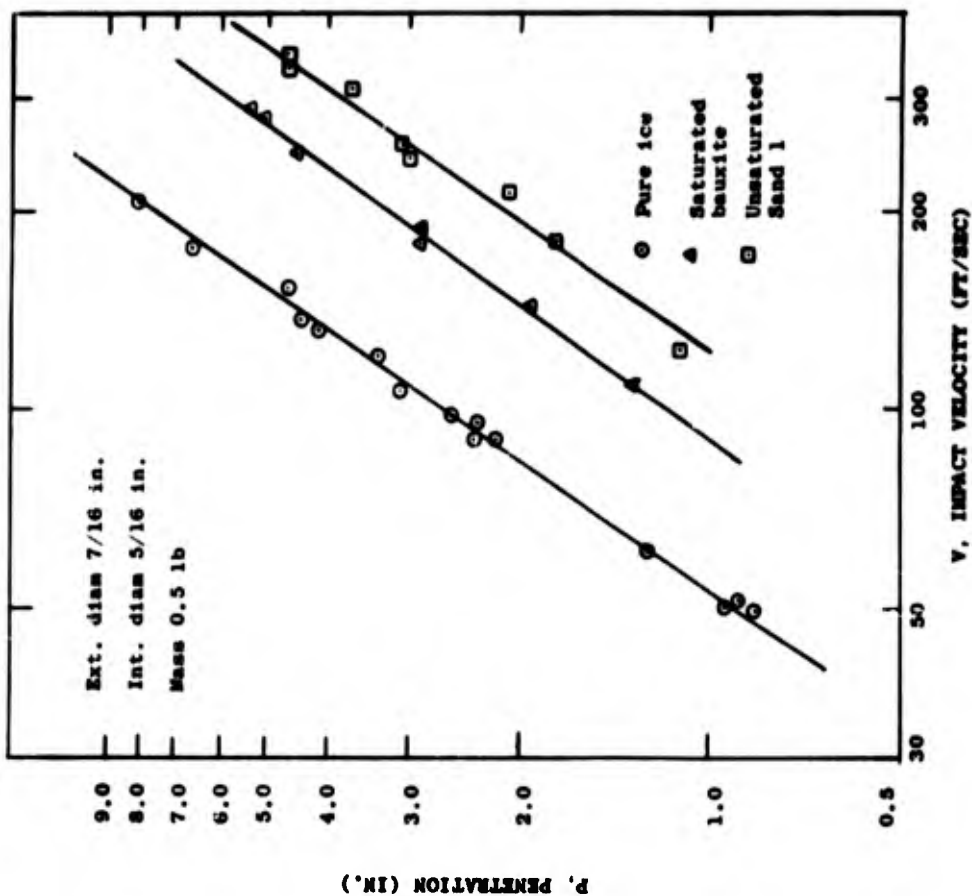


Figure 10b. Penetration of a 7/16 in. diam pile vs impact velocity.

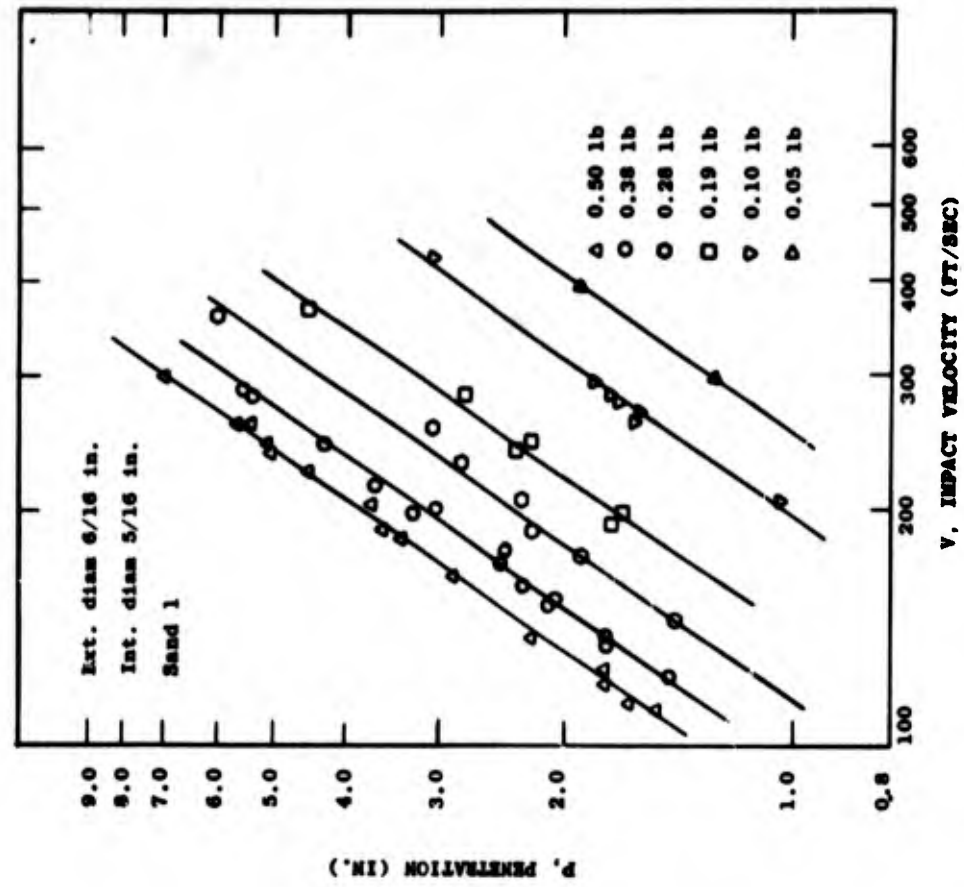


Figure 12. Penetration of 6/16 in. diam piles vs impact velocity for piles having various masses.

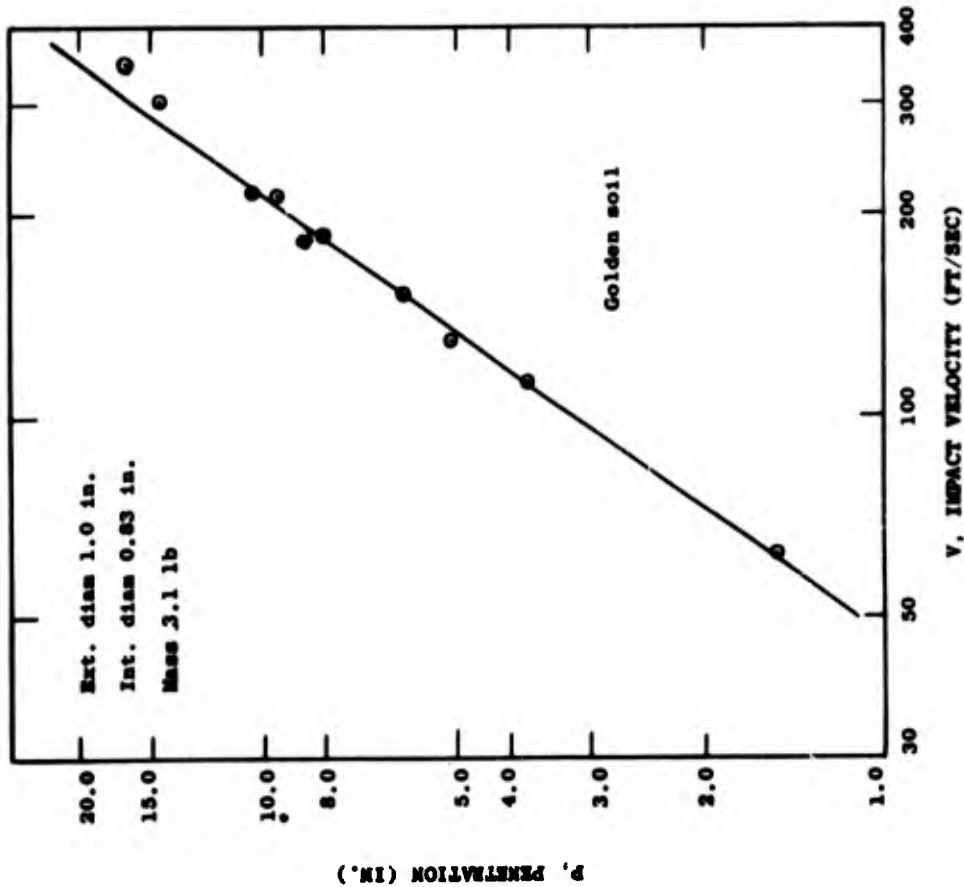


Figure 11. Penetration of a 1.0 in. diam pile vs impact velocity.

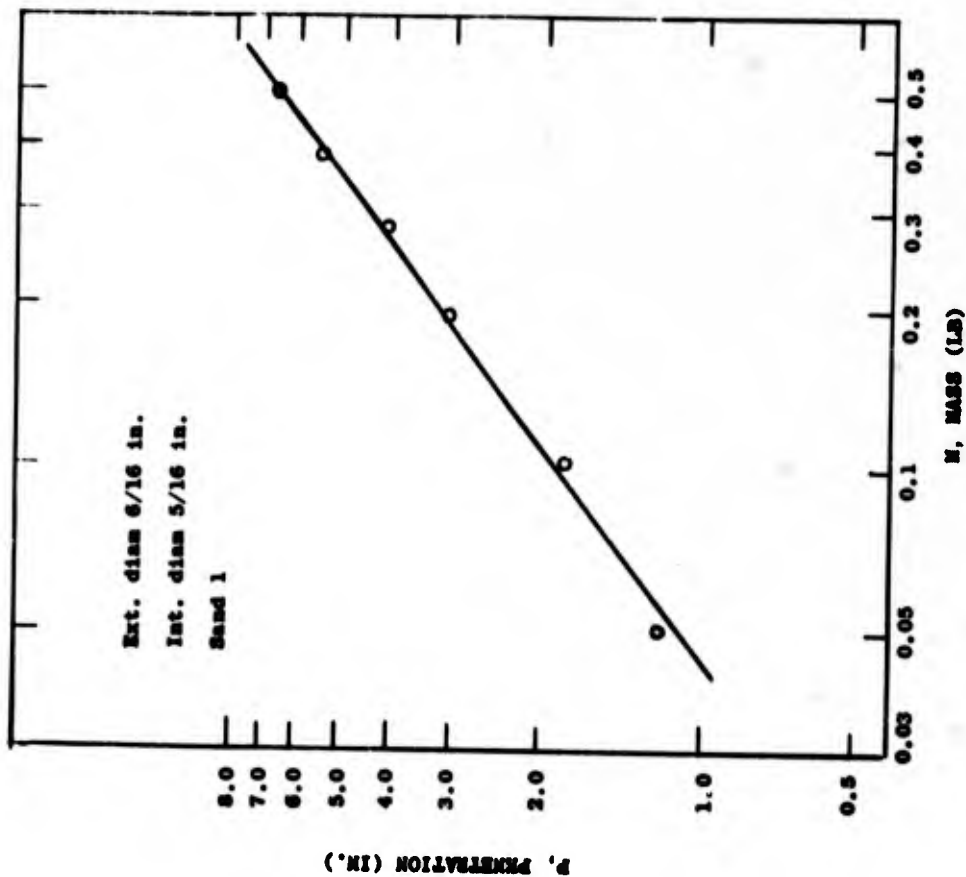


Figure 13. Penetration of 6/16 in. diam piles vs mass at 300 ft/sec.

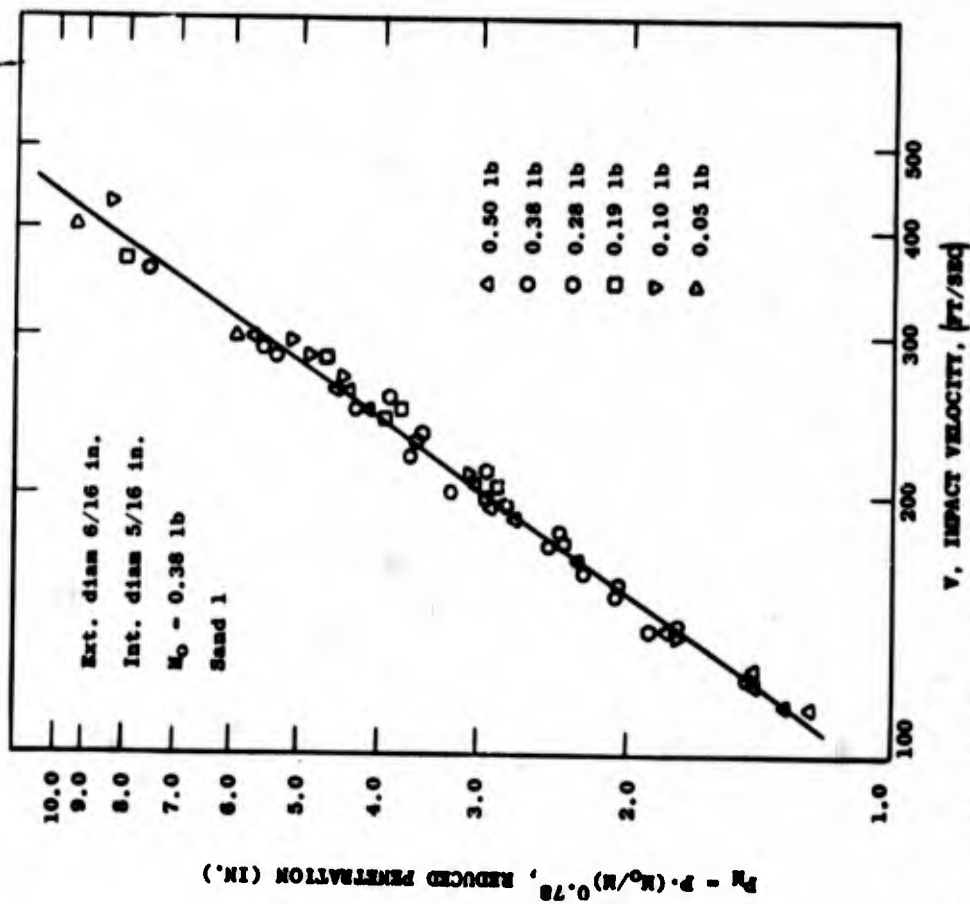


Figure 14. Reduced penetration of 6/16 in. diam piles vs impact velocity for piles having various masses.

The mass of the pile has been expressed in pound mass to conform to the four-unit engineering system $F = Ma/g_c$, where F is lb-force, M is lb-mass, a is ft/sec² and g_c is 32.12 lb-mass x ft/lb-force x sec² (See Comings, 1940, for extended discussion).

Shape factor dependence

The shape factor is defined by $(D_1^2 - D_2^2)$, where D_1 is the external diameter and D_2 the internal diameter of the pile. This shape factor, which is directly proportional to the projected area of the pile, is very significant for studying bodies moving rapidly through deformable media.

The curves showing the penetration of 0.5-lb piles having different shape factors (Fig. 16a-e) are in good agreement with the 1.5-power velocity dependence of penetration. All the curves are shown in Figure 16e, and the penetration at 200 ft/sec is plotted versus the shape factor $(D_1^2 - D_2^2)$ in Figure 17. The dotted curve of Figure 17, showing an approximate slope of -0.5, represents the average effect of the shape factor considering both thin-walled and thick-walled piles throughout. This gives the factor $(D_1^2 - D_2^2)^{0.5}$ appearing in eq 1.

The solid curve represents experimental data obtained with piles for which the ratio T/D_1 is equal to or smaller than 0.2. The change in mode of dependence on the shape factor from thin to thick piles is discussed later. The slope of the solid curve of Figure 17 being approximately -0.4, one may write:

$$P = K_{11} (D_1^2 - D_2^2)^{-0.4}. \quad (7)$$

The curves of Figure 16e being parallel, one may write

$$P = K_{12} [V^{1.5} / (D_1^2 - D_2^2)^{0.4}]. \quad (8)$$

Multiplying both sides of eq 8 by $[(D_1^2 - D_2^2) / (D_{10}^2 - D_{20}^2)]^{0.4}$ one obtains

$$P_S = P [(D_1^2 - D_2^2) / (D_{10}^2 - D_{20}^2)]^{0.4} = K_{13} V^{1.5} \quad (9)$$

where P_S is the reduced penetration, $(D_{10}^2 - D_{20}^2)$ is a reference shape factor, and K_{13} is a constant.

Figure 18 shows the reduced penetration as a function of impact velocity, using the 7/16 OD, 5/16 ID pile for the reference shape factor, $(D_{10}^2 - D_{20}^2) = 24$. The slope of this curve is close to 1.5.

Letting $M_0 = 0.5$ lb and $(D_{10}^2 - D_{20}^2) = 24$, the experimental data used in this chapter are represented with reasonable scatter by the following equation:

$$P_* = P [(M_0/M)]^{0.8} [(D_1^2 - D_2^2) / (D_{10}^2 - D_{20}^2)]^{0.4} = K_{14} V^{1.5} \quad (10)$$

where P_* is the reduced penetration and K_{14} is a constant. Figure 19 gives the curve of the experimental data reduced by eq 10. The data for thick-walled piles, lower curves of Figures 16c and 16d, are not used in Figure 19. The curve through the experimental points is almost the same as the curve for the reference pile (upper part of Fig. 10a). Thus

$$P = K_{15} [(M^{0.8} V^{1.5}) / (D_1^2 - D_2^2)^{0.4}] \quad (11)$$

represents a possible empirical equation giving the penetration of thin, hollow, circular piles into artificial permafrost, under the present experimental conditions.

THEORETICAL CONSIDERATIONS

It is the purpose of this section to establish a sound and reasonable physical basis for empirically derived equations 1 and 11. They may have a physical meaning in the same sense as the simple equation

$$E_K = \frac{1}{2} MV^2 \quad (12)$$

giving the kinetic energy, E_K , of a moving body as a function of its mass, M , and its velocity, V .

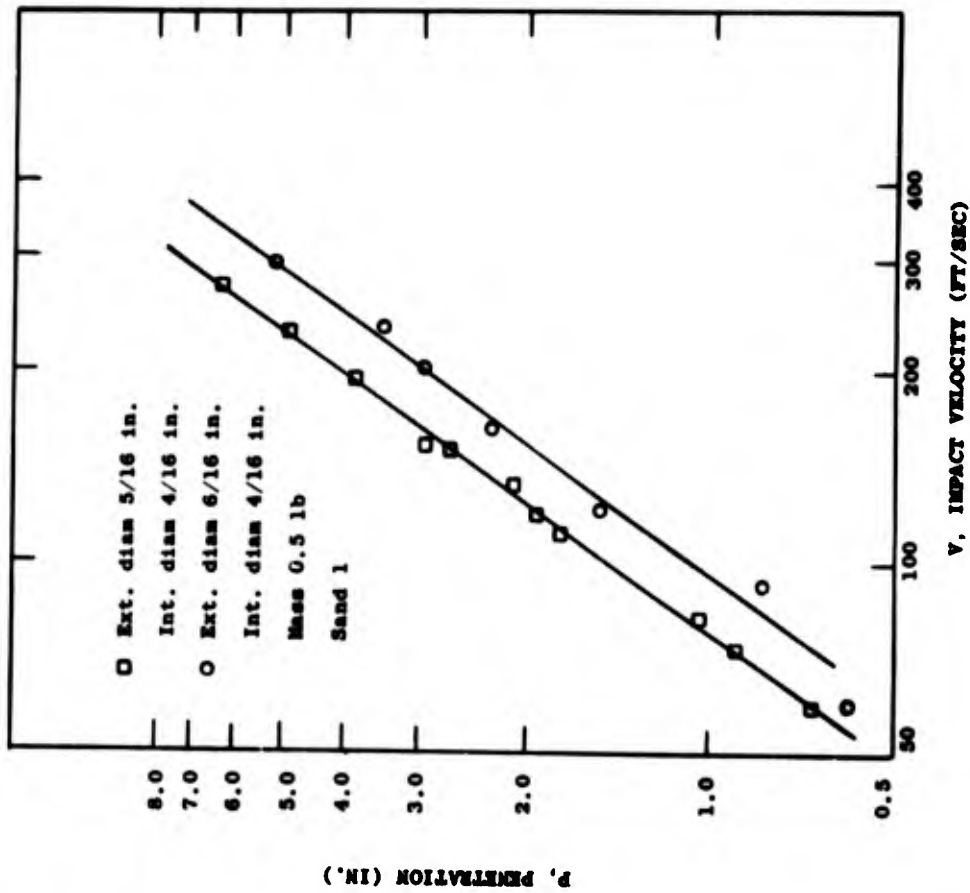


Figure 16a. Penetration vs impact velocity for piles having various shape factors.

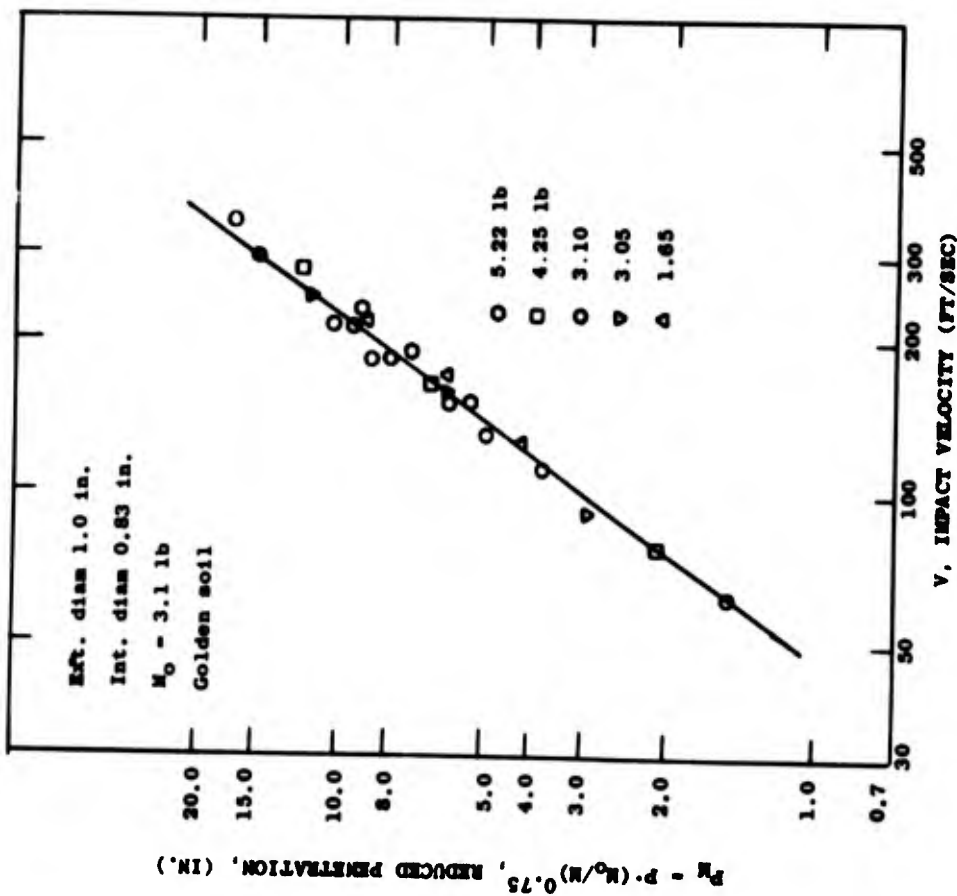


Figure 15. Reduced penetration of 1.0 in. diam piles vs impact velocity for piles having various masses.

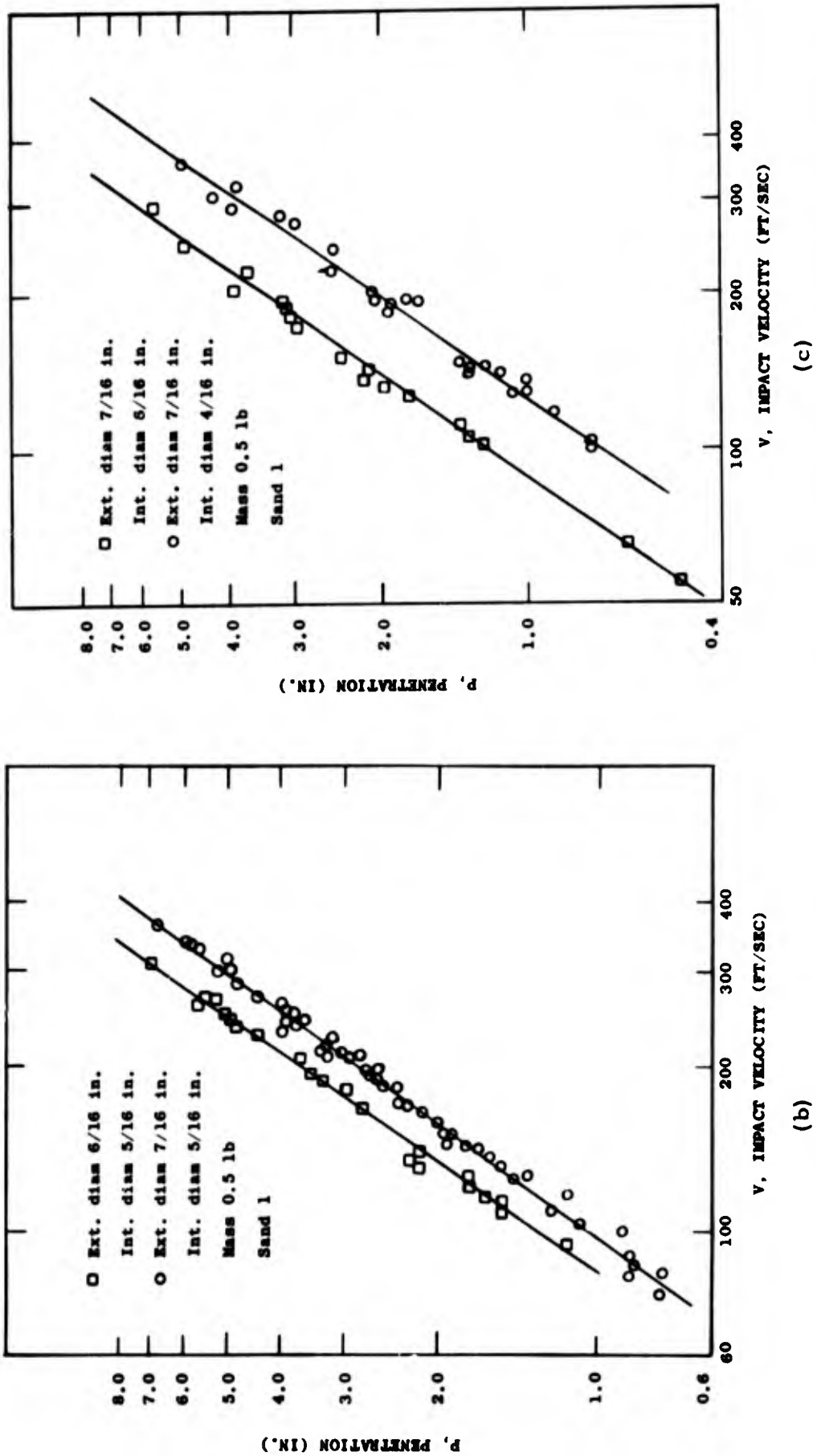


Figure 16 (Cont'd). Penetration vs impact velocity for piles having various shape factors.

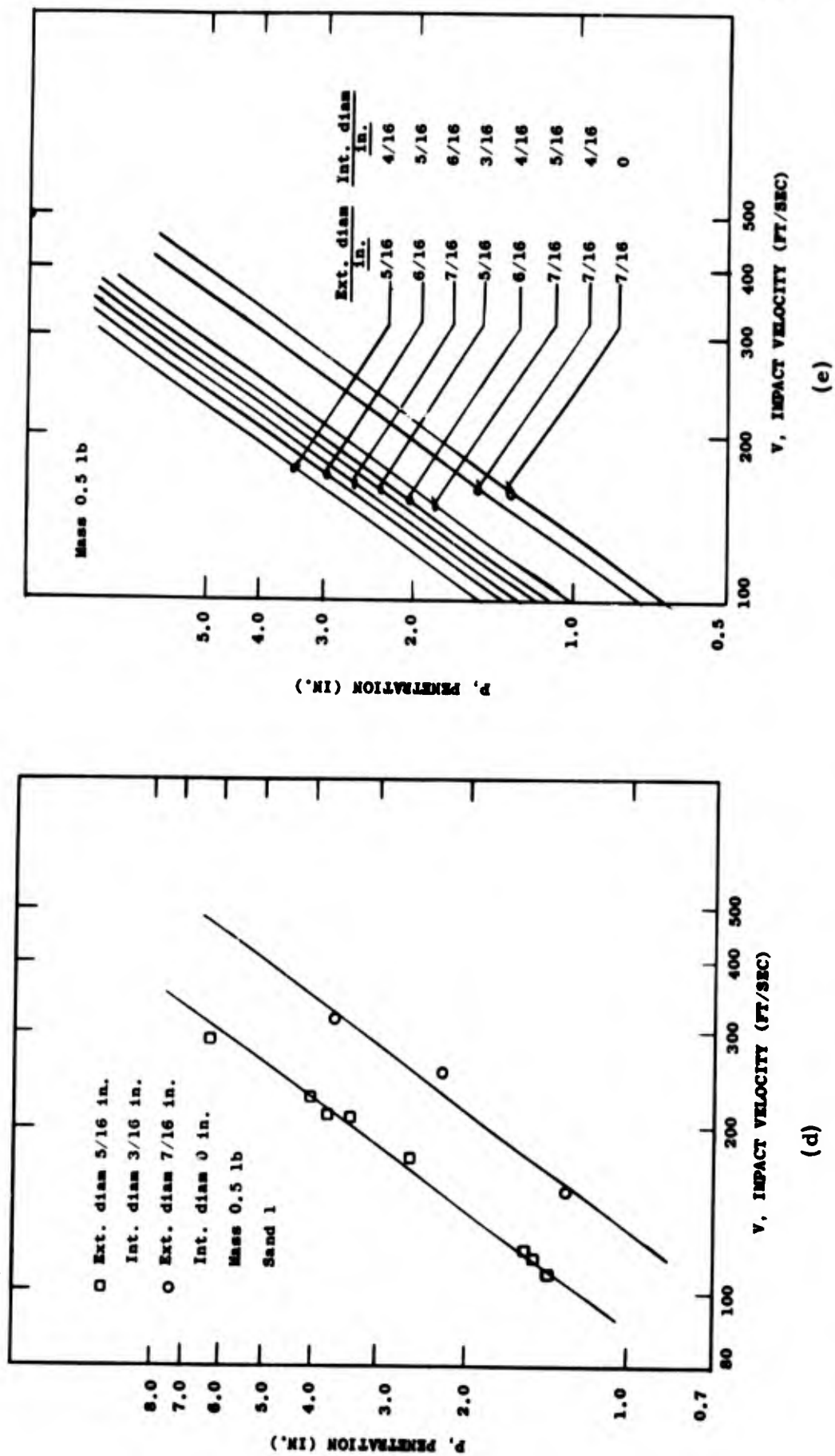


Figure 16 (Cont'd). Penetration vs impact velocity for piles having various shape factors.

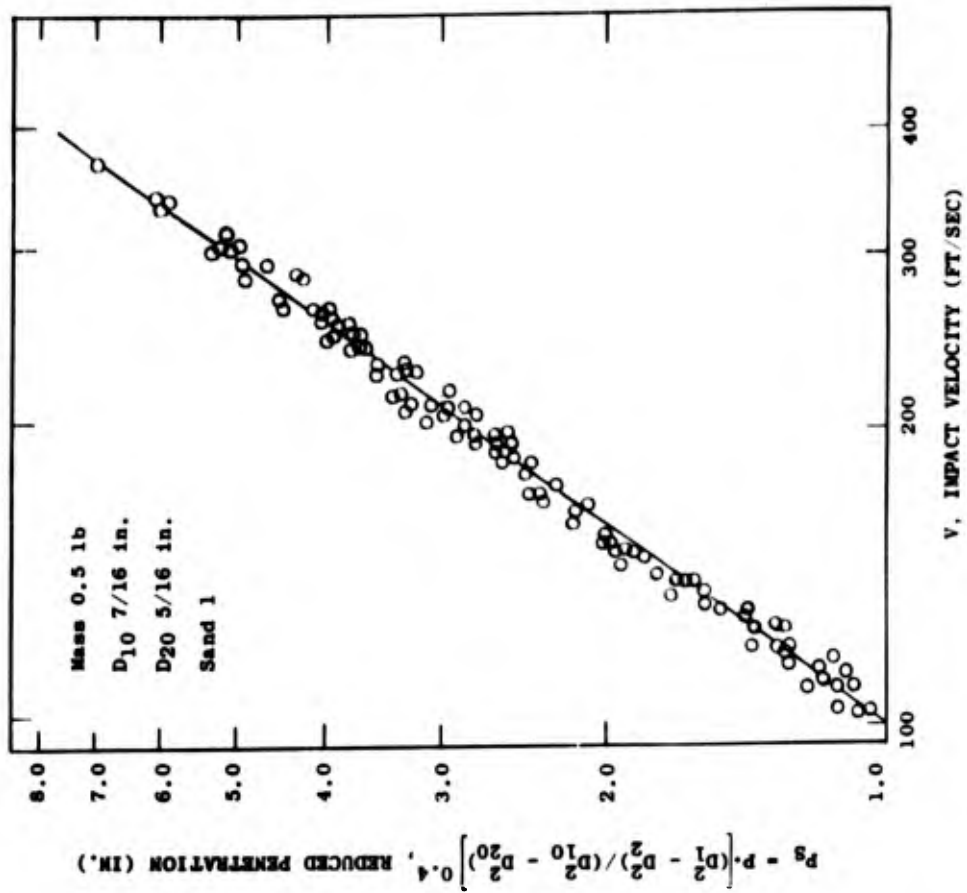


Figure 18. Reduced penetration vs impact velocity for piles having various shape factors.

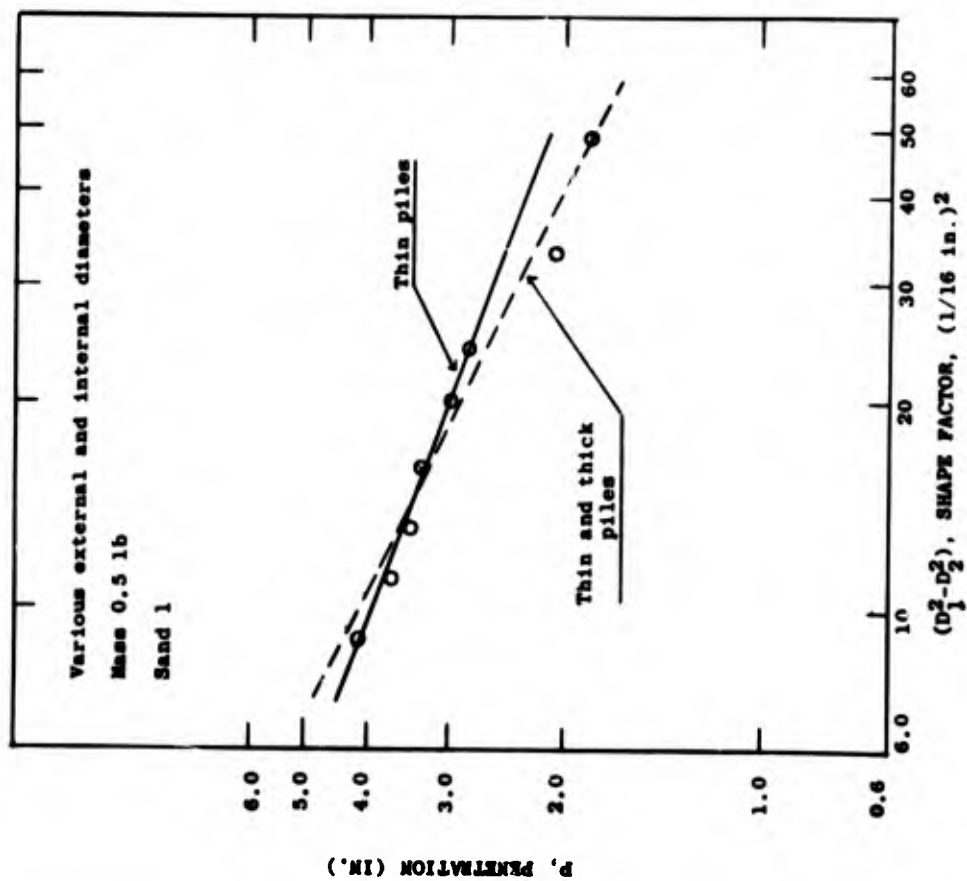


Figure 17. Penetration vs shape factor at 200 ft/sec.

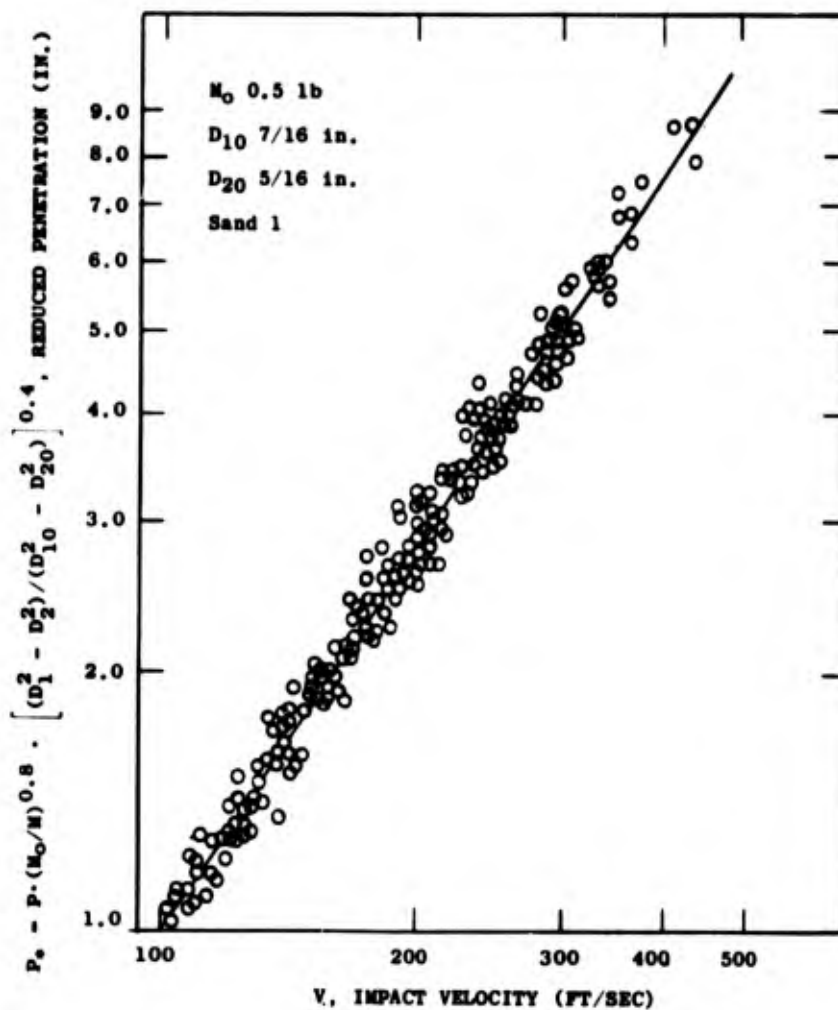


Figure 19. Reduced penetration vs impact velocity for piles having various masses and shape factors.

To make a comparison, the following hypothetical models are discussed.

Constant force model

A pile is launched in the direction of a visco-solid material, such as permafrost, and the penetration takes place solely under the influence of the pile's kinetic energy. For simplicity, it is assumed that the only strength acting against the pile during penetration is a constant crushing strength at the tip of the pile; this force is also assumed to be proportional to the projected area of the pile. Other possible forces are neglected. Under these conditions, the differential equation for movement of the pile, based on the principle of the equivalence of the loss of kinetic energy and the work done, can be written:

$$c_1 S dP_i = -d\left(\frac{1}{2}Mv^2\right) \quad (13)$$

where c_1 is a proportionality constant, S is the area of the pile projected on a plane perpendicular to its trajectory, P_i is the instantaneous penetration, M is the mass, and v the instantaneous velocity. Equation 3 becomes:

$$c_1 S dP_i = -Mvdv \quad (14)$$

which after integration becomes

$$P = \frac{1}{2}MV^2 / (c_1 S) \quad (15)$$

where P is total penetration and V is impact velocity.

Equation 15 shows that the penetration of the pile under the above conditions is directly proportional to its mass, is directly proportional to the square of its impact velocity, and is inversely proportional to its projected area.

Variable force model

As a second extreme case it is assumed that only frictional forces act against the pile during penetration. For simplicity, the total force is assumed to be proportional to the area of the pile in contact with the permafrost. Therefore, the force can be expressed as the product of the instantaneous penetration of the pile and of the perimeter of its cross section. Then the following differential equation can be written:

$$c_3 p P_i dP_i = -d(\frac{1}{2}Mv^2) \quad (16)$$

where c_3 is a proportionality constant, p is the perimeter of the cross section of the pile, M is its mass, v its instantaneous velocity, and P_i its instantaneous penetration. Equation 16 becomes, after integration,

$$P = M^{\frac{1}{2}} V / (c_3 p)^{\frac{1}{2}} \quad (17)$$

where P is total penetration and V is impact velocity.

Equation 17 shows that the penetration of the pile under those conditions is proportional to the square root of its mass, is proportional to its impact velocity, and is inversely proportional to the square root of the perimeter of its cross section.

By comparing eq 15 and 17, one sees that both these simple hypothetical models lead to well-defined mathematical formulations, each having a clear physical meaning. The different structures of eq 15 and 17 are the result of the different nature of the force involved in each case. The following question now comes to the mind: What would happen to the mathematical formulation if the pile simultaneously experienced both a crushing force and a friction force during penetration?

Combined force model

Assuming that crushing force and friction force both act against the pile during penetration, one can write

$$(c_1 S + c_3 p P_i) dP_i = -d(\frac{1}{2}Mv^2). \quad (18)$$

Equation 18 becomes after integration:

$$P = \frac{-c_1 S}{c_3 p} + \left[\left(\frac{c_1 S}{c_3 p} \right)^2 + \frac{MV^2}{c_3 p} \right]^{\frac{1}{2}}. \quad (19)$$

To show the effect of doubling the mass, an arbitrary value of unity is given to c_1 , c_3 , M , V , S , and p in eq 19. Then, eq 19 gives $P_1 = 0.414$ units of penetration. Doubling the mass while keeping the other parameters constant gives $P_2 = 0.731$ units of penetration; thus doubling the mass increases penetration by a factor $P_2 / P_1 = 0.731 / 0.414 = 1.77$.

According to eq 15, doubling the mass increases penetration by a factor of 2, and eq 17 indicates that penetration would be increased by $\sqrt{2}$ or 1.414. Equation 19 gives an intermediate value between eq 15 and 17. Moreover, it can be shown by other simple calculations that any other intermediate value between eq 15 and 17 is possible, depending upon the relative importance of the two forces c_1 and c_3 .

Anticipating the results presented in the next chapter, it is no longer surprising to find empirical equations containing nonrational exponents since the forces acting against piles during the penetration process are mainly of three types: a crushing force, a drag force, and a friction force. Since laboratory experiments consisted of measuring total penetration, which is controlled by three forces of different nature, it becomes clear that the 0.75 or 0.8-mass power dependence of eq 1 or 11 can be interpreted physically. The same arguments can be used to explain the power dependence on velocity and shape factor.

FIRST INVESTIGATION, PHASE II

Penetration-time measurement technique

The piles used during the first investigation of Phase II were modified as follows for penetration vs time measurements.

With a conventional lathe, shallow grooves, equally spaced, were cut along half the length of the piles with a flat-head cutting tool. The grooves were painted black, resulting in a succession of alternate black and metallic stripes on the piles. The piles were then turned slowly on a special lathe, and a thin band of white paint was applied with a drafting pen to the metallic stripes. The piles then had alternating black and white stripes along half their length.

This procedure was found to be very reliable. The constant distance between the white stripes could be controlled with great precision; the demarcation lines between white and black stripes were very sharp; and it was very easy to repaint the stripes when necessary. A special lathe was designed for this operation. Made of Plexiglas, it used a small synchronous motor with an output revolution of 4 rpm. After each complete revolution the drafting pen was simply shifted by hand and the next white stripe was applied. The distance between each white stripe was 0.100 ± 0.003 in.

Figure 20 is a schematic representation of the principle of the penetration-time measurement technique. An arrangement of a small bright-light source, S , and a lens system L_1 and L_2 , gives a stationary spot of light S^1 , focused above the surface of the permafrost on the trajectory line of the pile. A photo-multiplier tube is located behind a masking arrangement inside a camera, C . The camera is focused in such a way that the image of S^1 coincides with a small hole in the mask, permitting only the light reflected from an object located at S^1 to reach the cathode of the photo-multiplier tube. As the pile passes in front of the spot of light, impulses of light reflected from the white stripes on the pile emerge onto the photo-multiplier, are converted into electrical impulses by an electrical circuit, and fed into an oscilloscope.

The light source, S , was an automobile headlight bulb, Westinghouse type 2330, 6-8 volts. This bulb, of relatively small filament, gave a strong-intensity light. The bulb was operated with direct current to avoid 60-cycle fluctuations, which could have been easily recorded by the photo-multiplier tube.

Lens L_1 was an aerial photo type having a 24-in. focal length at $f/4.0$. The large focal length minimized the effect of the size of the filament bulb with respect to the focal length of the lens. For these experiments, the ratio of filament size to focal length was $3/610$. Lens L_2 was a simple converging lens, 2.4 in. in focal length. The spot of light S^1 was 0.04 in. in diameter. The distances SL_1 , L_1L_2 and L_2S_1 were, respectively, 39, 91, and 2 in.

An aerial photo camera with a 7-in. focal length lens was used. The photo-multiplier tube was a R. C. A. type 931A. Figure 21 shows the electrical circuit which was used with the penetration-time measurement technique. The oscilloscope, a Hewlett-Packard model 123-A, was triggered by the output signal of the third wire of the velocity measurement system.

Determination of penetration-time curves

A typical oscilloscope record is traced in Figure 22. The lower signal is a measurement of the amount of light reflected from the pile and each peak of the signal corresponds to the instant at which each white stripe of the pile passed the directed spot of light S^1 (see Fig. 20). The upper signal is a reference time base signal. Using a traveling microscope, the distance of each successive peak of the lower signal is compared with the distance of the upper reference signal to obtain the relative time at which each white stripe passed light spot S^1 . As the distance between each white stripe of the pile is 0.1 in., this gives the displacement of the pile with respect to the first white stripe (first-left peak of the lower signal) as a function of time. Portion AC of the plot shown in Figure 23 gives displacement of the pile as a function of relative time. Points A and C of Figure 23 correspond, respectively, to the first

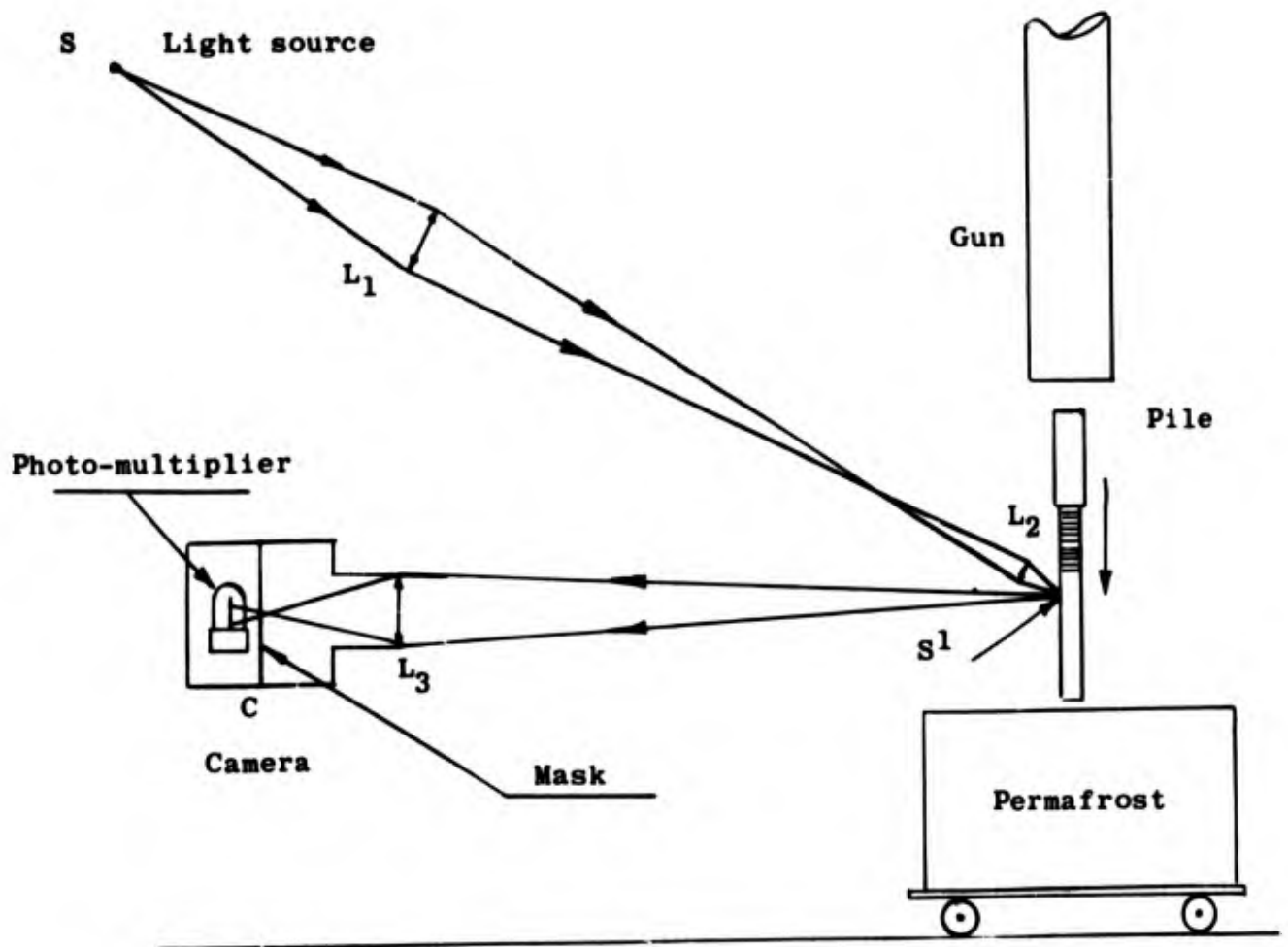


Figure 20. Principle of the penetration-time measurement technique.

and last white stripe which passed in front of light spot S' . The ordinate or displacement of point A was chosen as zero to simplify the calculations. The abscissa of point A could not always be made equal to zero because of some mechanical limitations of the traveling microscope used; this limitation caused no difficulty in determining the penetration-time curves.

Segment AC of the curve shown in Figure 23 is not the penetration-time curve; three determinations must be made to establish that curve: the final penetration; displacement and time coordinates of the beginning of penetration; and the time at which the pile comes to rest.

Final penetration. Immediately after firing the pile into permafrost, the in-place pile was visually inspected and a count made of the white stripes which had passed light spot S' . The purpose of this count was two-fold: to compare the number of white stripes which had passed the light spot with the number of peaks of the oscilloscope signal and to determine final penetration. Point C of Figure 23 represents the last-right peak of the oscilloscope signal, but the final position of light spot S' after the pile had come to rest could lie between the white stripe corresponding to point C and the next stripe. The distance that the light spot lay beyond the white stripe corresponding to point C was added to the ordinate of point C to establish the ordinate of final penetration designated by line D in Figure 23. That distance, designated "correction," could not be measured with a greater accuracy than 0.03.

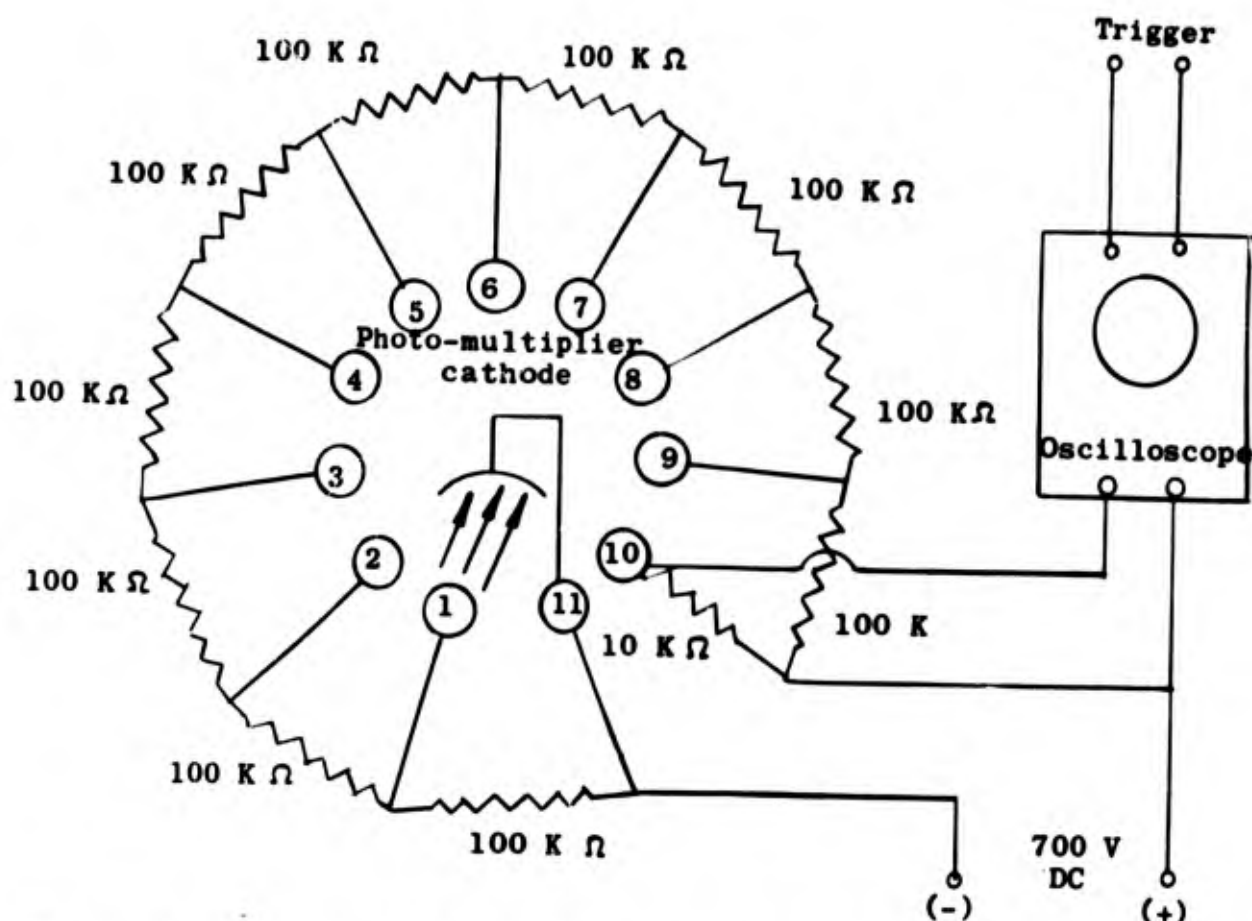


Figure 21. Electrical diagram of the penetration-time measurement technique.

Beginning of penetration. The total penetration of the pile, measured as in Phase I, subtracted from the ordinate of point D in Figure 23, gives a point B which defines the beginning of penetration. This point must be on curve AC. Giving point B coordinates 0, 0 on the penetration vs time scales of Figure 23 and making the proper shift for the rest of the experimental points, one obtains the segment BC of the penetration-time curve.

Final time of penetration. To find the abscissa of point D, t_p , which represents the total time of penetration, curve BC is extrapolated to the horizontal line passed through point D. The intersection of extrapolated curve BC and the horizontal line through point D then gives the total or final time of penetration t_p . Segment BD of the experimental curve then becomes the penetration-time curve. Segment AB corresponds to the free flight of the pile before impacting the permafrost. The slope of the straight line AB provides a good means of measuring the impact velocity of the pile.

Study of penetration-time curves

From a series of firings made in the same sample of permafrost, a set of penetration-time curves was obtained. The data of these curves are given in Appendix D, Tables DI-DIX. During this series of tests, a steel pile having a 0.5-lb mass and external and internal diameters of 7/16 in. and 6/16 in. was used. It was found that most of these curves could fit, within 1% deviation for most of their length, a third order time-dependent equation of the type,

$$P_i = At + Bt^2 + Ct^3 \quad (20)$$

where P_i is instantaneous penetration (penetration at the given instant), t is time, and A , B , and C are constants, characteristic of a given penetration-time curve.

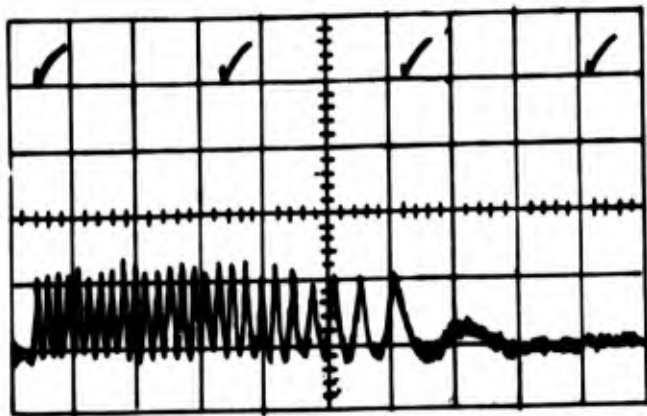


Figure 22. Trace of an oscilloscope record of the penetration-time measurement technique.

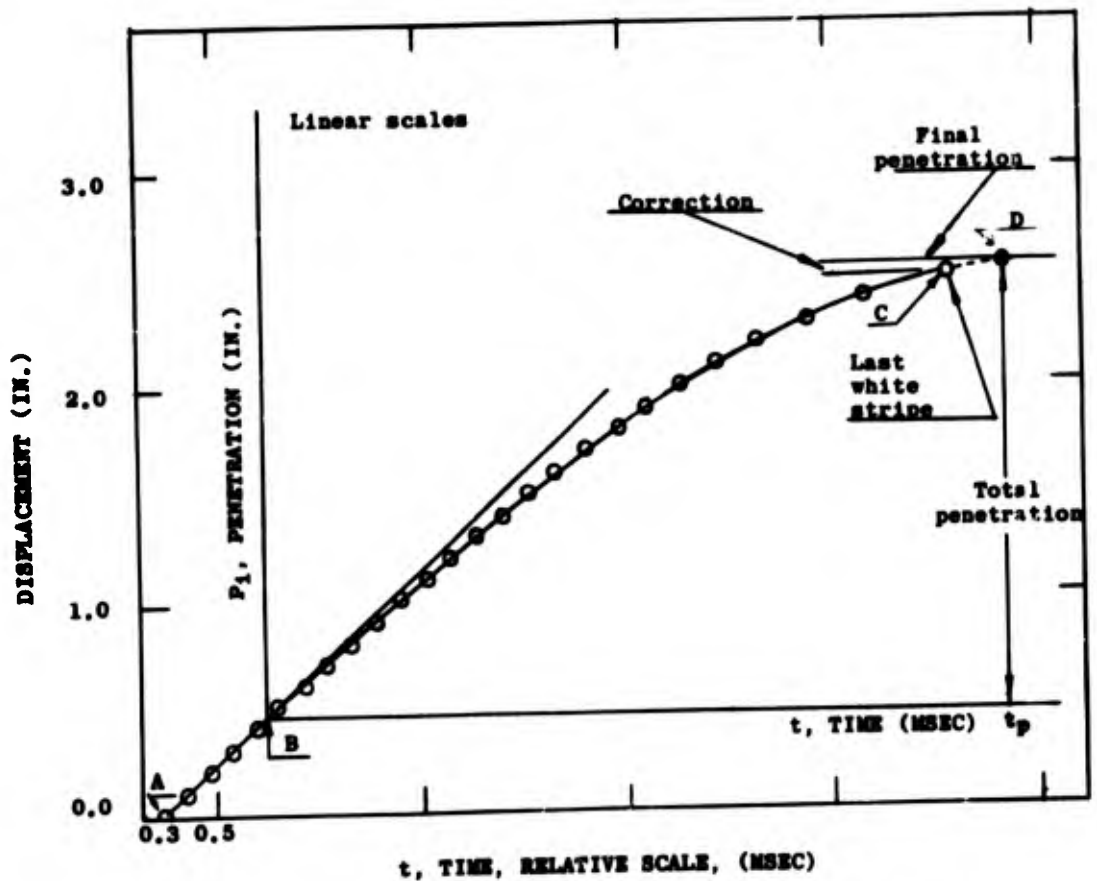


Figure 23. Determination of a penetration-time curve.

No time-dependent term appears in eq 20, since by definition the penetration is zero at time zero. Knowing the values of coefficients A, B, and C of a given penetration-time curve, it is possible to calculate the velocity and deceleration of the pile at any instant of penetration by evaluating the first and the second time derivatives of eq 20.

Determination of A, B, C. Coefficient A corresponds to impact velocity V, which is measured experimentally. This is seen by evaluating the first derivative of eq 20 at time zero,

$$(dP_i/dt)_{t=0} = A = V.$$

Two points are chosen along the experimental penetration-time curve, and a pair of simultaneous linear equations in B and C are solved:

$$P_{i1} = Vt_1 + Bt_1^2 + Ct_1^3$$

$$P_{i2} = Vt_2 + Bt_2^2 + Ct_2^3$$

where t_1 and t_2 are the measured times of penetration corresponding to measured penetration P_{i1} and P_{i2} . Calculated values of A, B, and C for the data given in Tables DI-DIX are given in Table I.

Deceleration-penetration curves. An example of the determination of a deceleration-penetration curve follows. The A, B, C values for the Table DIV data give:

$$P_i = 2.21t - 0.327t^2 - 0.022t^3. \quad (21)$$

The penetration-time data of Table DIV and the calculated values of the first and second derivatives of eq 21, give Table II and the deceleration-penetration curve corresponding to eq 21. The numerical values of Table II will be used later for the evaluation of experimental constants. These data were used because the total penetration in these tests closely represents the middle range of penetrations covered by this series of tests. Moreover, eq 21 shows a very good fit with the penetration-time data from which it was derived.

Table I. Values of the coefficients A, B, C of eq 20 after the penetration-time data given in Appendix D.

Data of table	A (in. /msec)	B (in. /msec ²)	C (in. /msec ³)
DI	2.87	-0.360	-0.016
DII	2.37	-0.330	-0.008
DIII	2.26	-0.310	-0.033
DIV	2.21	-0.327	-0.022
DV	2.00	-0.282	-0.018
DVI	1.54	-0.245	-0.025
DVII	1.51	-0.260	-0.027
DVIII	1.47	-0.260	-0.020
DIX	1.18	-0.270	-0.010
*	0.80	-0.255	-0.000
*	0.68	-0.235	-0.000

*Data not given in Appendix D.

Physical model

From the series of tests made at different velocities (Tables DI-DIX) a set of deceleration-penetration curves were obtained. As sketched in Figure 24, these curves show two characteristics: a well-defined impact deceleration a_0 at penetration zero, increasing with impact velocity V, and an increase in the deceleration a with the instantaneous penetration P_i . These two characteristics suggest the following model of penetration.

Table II. Values of P_i , v , $a = 2Bt^2$ and t after eq 21 and after Table DIV of Appendix D.

Penetration P_i (in.)	Velocity v (in./msec)	Deceleration a (in./msec ²)	Time t (msec)
0.000	2.210	0.654	0.0
0.820	1.948	0.710	0.4
1.540	1.645	0.760	0.8
2.140	1.330	0.812	1.2
2.600	0.995	0.865	1.6
2.936	0.638	0.918	2.0
3.040	0.450	0.944	2.2
3.115	0.260	0.971	2.4
3.150	0.000	1.000	2.6

Impact deceleration. Figure 25 shows the absolute values of impact deceleration a_0 plotted as a function of impact velocity V . In other words, this graph is the plot of the absolute numerical value $2B$ as a function of the corresponding numerical value $\frac{A}{V}$ given in Table I. One recalls from eq 20 that $(dP_i/dt)_{t=0} = A = V$ and $-(d^2 P_i/dt^2)_{t=0} = -2B = a_0$.

An examination of the curve shown in Figure 25 indicates a non-linear increase of impact deceleration a_0 with an increase of impact velocity V . Moreover, a curve passed through the experimental values definitely crosses the a_0 axis at a positive value a_C . These two observations of the impact deceleration-impact velocity curve suggest that the two following phenomena occur at the beginning of penetration and, by extension, during the penetration process.

Crushing force. For the pile to penetrate permafrost, a minimum force is required. This force is necessary to destroy the structure of the permafrost and permit the pile to penetrate. Since this crushing force acts at the tip of the pile, it must be present for the duration of the penetration process. As deceleration of the pile is directly proportional to the resisting force, the value of a_C in Figure 25 would correspond to this crushing force.

Drag force. The increase of impact deceleration a_0 with increase of impact velocity V suggests that, besides a crushing force, a dynamic force must also be present during the penetration process. By analogy with fluid dynamics, this second force would be similar to the drag force experienced by a solid body moving through a fluid medium. It might be regarded as the force necessary to displace the particles of crushed permafrost. This drag force might also include an increase of crushing force with increased velocity. On the basis of theoretical considerations and of the non-linear increase of the observed impact deceleration, one can pass through the experimental data of Figure 25 a curve of the following type:

$$a_0 = a_C + a_{D_0} \quad (22)$$

where a_0 is impact deceleration, a_C is crushing deceleration, and a_{D_0} is an impact drag deceleration which is a function of impact velocity.

Assuming the drag force to be proportional to the square of velocity, one obtains:

$$a_0 = a_C + C_2 V^2 \quad (23)$$

where C_2 is a drag coefficient and V is impact velocity. Drag deceleration a_D or $C_2 V^2$ would then correspond to the drag force acting at the tip of the pile. Since drag deceleration is a function of velocity, it must be present during the complete penetration process. Its value at any instant of penetration then becomes:

$$a_D = C_2 v^2 \quad (24)$$

where a_D is instantaneous drag deceleration and v the instantaneous velocity.

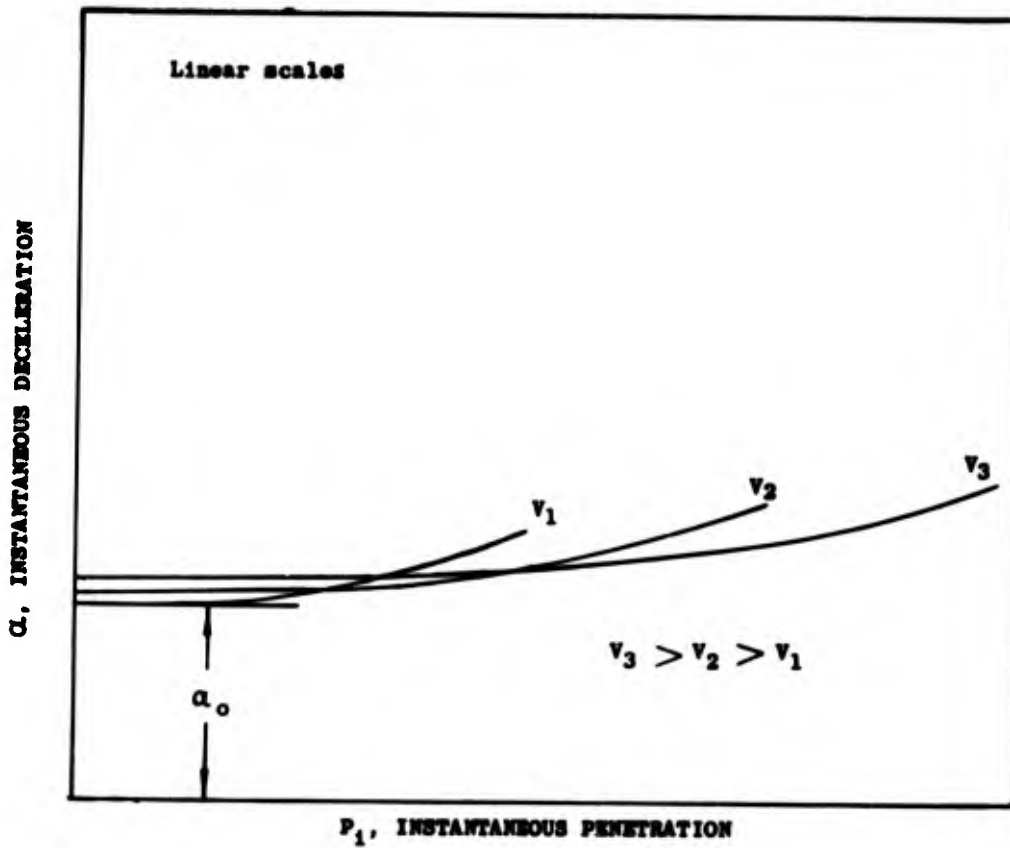


Figure 24. Instantaneous deceleration vs instantaneous penetration for various impact velocities.

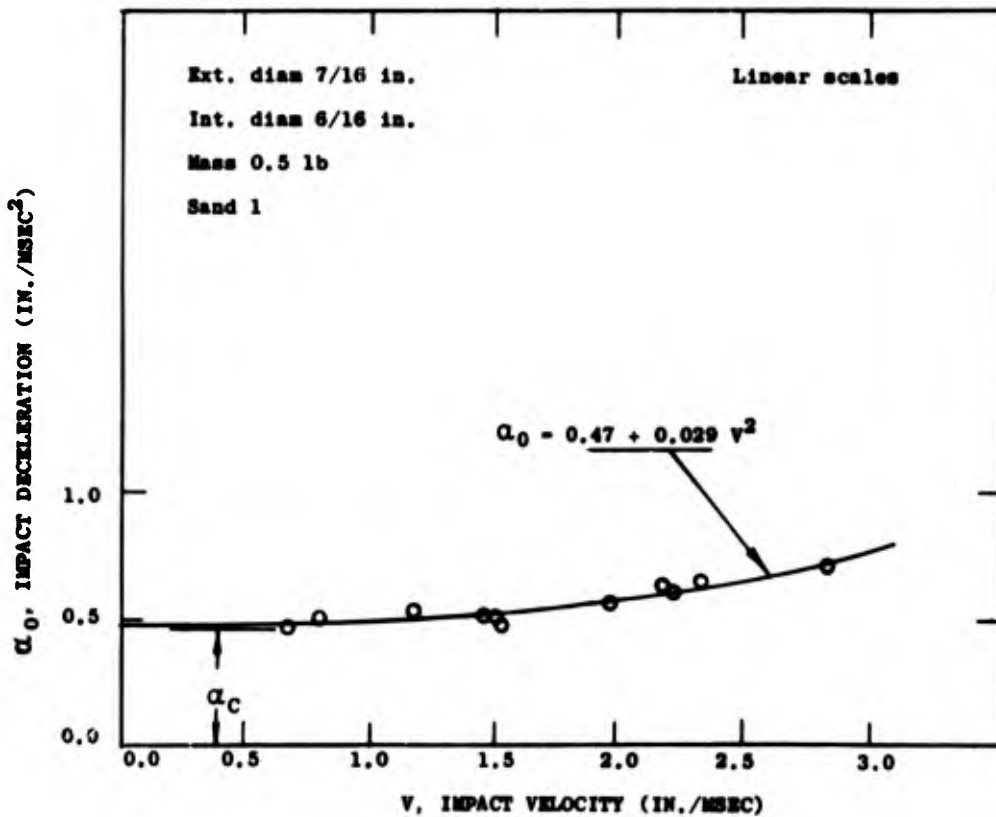


Figure 25. Impact deceleration vs impact velocity.

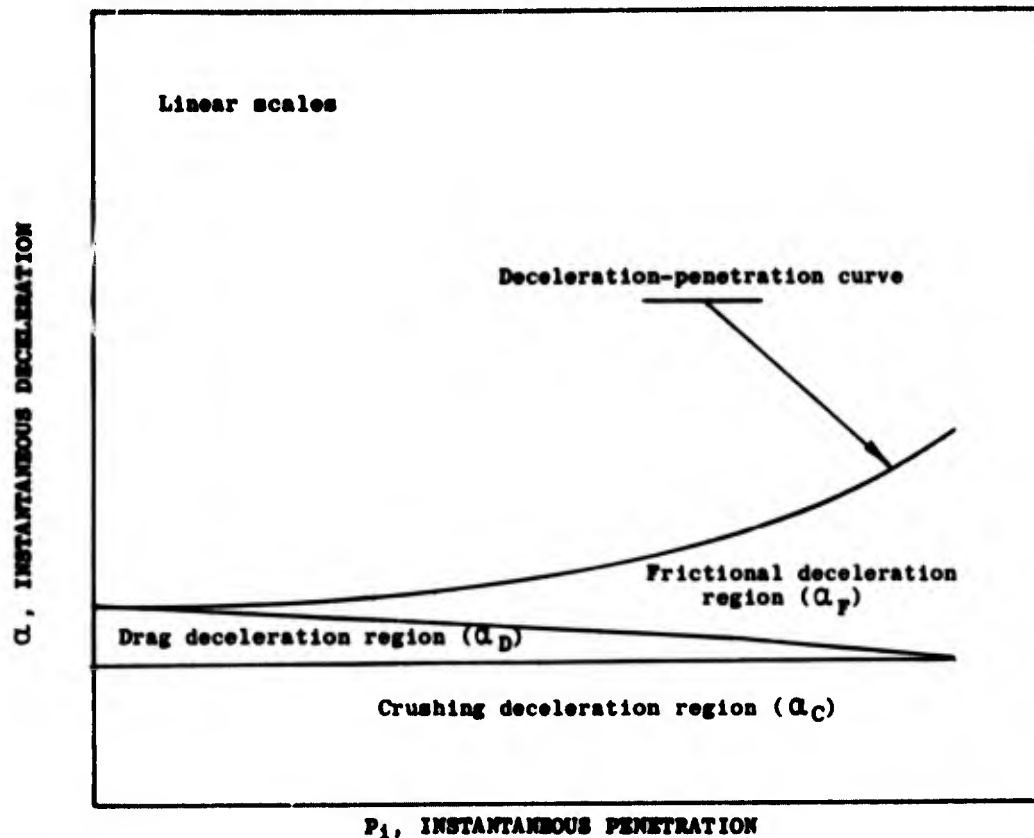


Figure 26. Total deceleration as the sum of three individual decelerations.

Using the data of Figure 25 and eq 23, one finds by graphical solution the following significant values of a_C and C_2 :

$$a_C = 0.47 \text{ in. /msec}^2$$

$$C_2 = 0.029 \text{ in.}^{-1}$$

These values of a_C and C_2 are for the 7/16 in. ext diam and 6/16 in. int diam pile used in the series of tests given in Tables DI-DIX.

Total deceleration: friction force. All the deceleration-penetration curves show an increase of deceleration rate with an increase of penetration P_1 . This observation suggests the existence of a third type of force participating in the penetration process. This force can be visualized as a friction force acting along the walls of the pile in contact with the permafrost. The area under the deceleration-penetration curve can be divided into three regions (Fig. 26). The lower region corresponds to the fraction of total deceleration due to a constant crushing force. The middle region corresponds to the fraction of total deceleration due to drag force. The height of the middle region is maximum at penetration zero, since the maximum velocity of the pile is at the beginning of the penetration. The upper region corresponds to friction force. The total deceleration can, therefore, be written

$$a = a_C + a_D + a_F \quad (25)$$

where a is total deceleration, a_C is crushing deceleration, a_D is drag deceleration, and a_F is frictional deceleration. a_F corresponds to the height of the upper region of the curve shown in Figure 26

$$a_F = a - (a_C + a_D). \quad (26)$$

It is seen that frictional deceleration increases non-linearly with penetration. One may then write:

$$a_F = f_1 (P_i, v) \quad (27)$$

where $f_1 (P_i, v)$ is a function of instantaneous penetration and instantaneous velocity.

Since, by the nature of the experiments, there were no particular indications of the behavior of the friction force, the following assumption was made. Using again the analogy of fluid dynamics (Rouse, 1946), the friction force was assumed to be proportional to the surface of the pile in contact with permafrost, therefore proportional to instantaneous penetration. Equation 27 may be written as follows:

$$a_F = P_i f_2 (P_i, v) \quad (28)$$

$f_2 (P_i, v)$ is a friction factor which is a function of instantaneous penetration P_i and instantaneous velocity v . Assuming the friction factor to be independent of penetration, eq 28 reduced to:

$$a_F = P_i f_3 (v) \quad (29)$$

where $f_3 (v)$ is a friction-factor function of instantaneous velocity.

Figure 27, from the data of Table II, shows the numerical values of the frictional deceleration region. The upper curve of Figure 27 is the deceleration-penetration curve and the lower curve is calculated from $(a_C + C_2 v^2)$ where $a_C = 0.512$ in./msec² and $C_2 = 0.029$ in.⁻¹. The numerical difference of the two curves gives frictional deceleration a_F as a function of penetration P_i (Fig. 28). The numerical values a_F/P_i plotted on a semi-log scale as a function of the velocity of the pile give Figure 29. Since a straight line of negative slope fits the points very well, one can write:

$$a_F/P_i = C_3 e^{-kv} \quad (30)$$

or

$$a_F = C_3 P_i e^{-kv} \quad (31)$$

where C_3 is a friction constant and k is a constant.

From Figure 29,

$$a_F = 0.156 P_i e^{-0.24v}.$$

Equation 31 means that frictional deceleration, or friction force, is proportional to instantaneous penetration and proportional to a friction factor decreasing exponentially with velocity. The decrease of friction force with velocity is a common phenomenon (Palmer, 1949).

Semi-empirical equation. Combining eq 25, 24 and 31,

$$a = a_C + C_2 v^2 + C_3 P_i e^{-kv} \quad (32)$$

where a is total instantaneous deceleration, a_C is deceleration due to crushing force, C_2 is a drag coefficient, v is instantaneous velocity, P_i is instantaneous penetration, and C_3 a constant of friction.

Inserting the experimental values derived from the series of tests used in this chapter, one obtains

$$a = 0.47 + 0.029 v^2 + 0.156 P_i e^{-0.24v} \quad (33)$$

where a is in in./msec², v is in in./msec, and P_i is in in. Multiplying both sides of eq 33 by \underline{M} , one obtains:

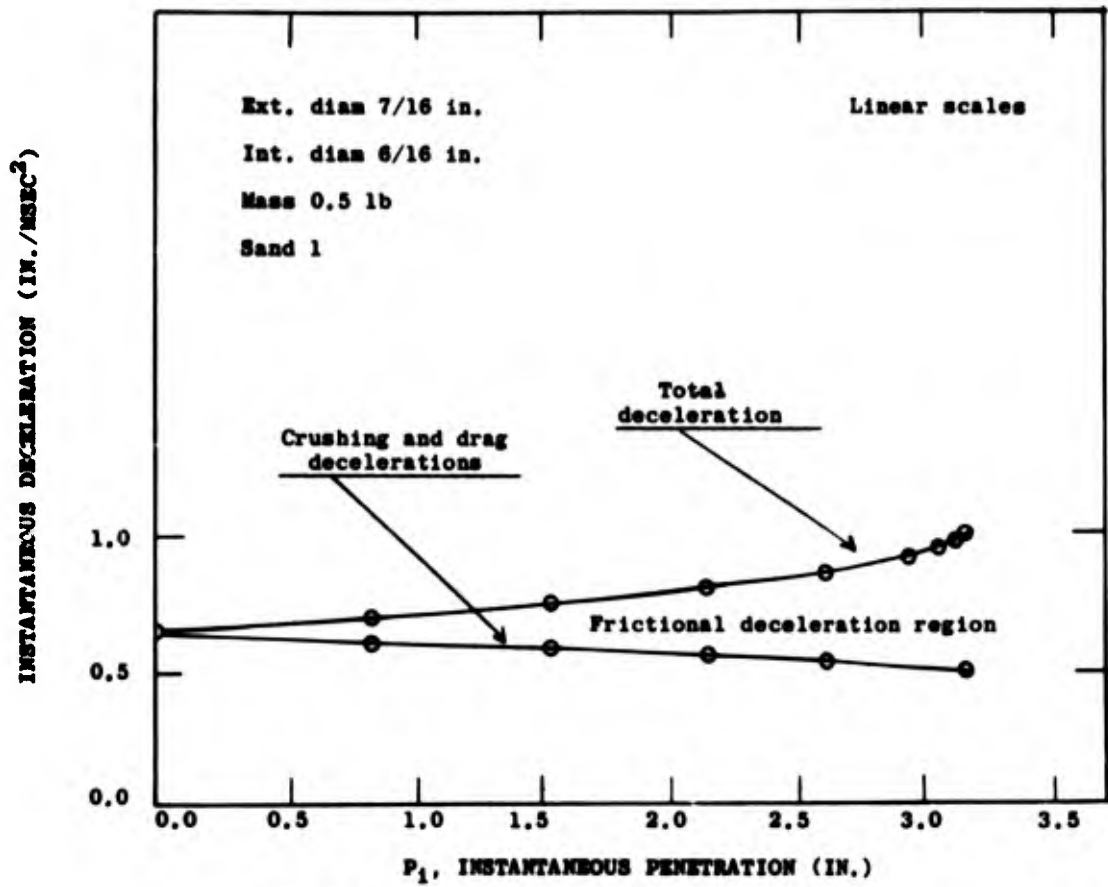


Figure 27. Frictional deceleration region.

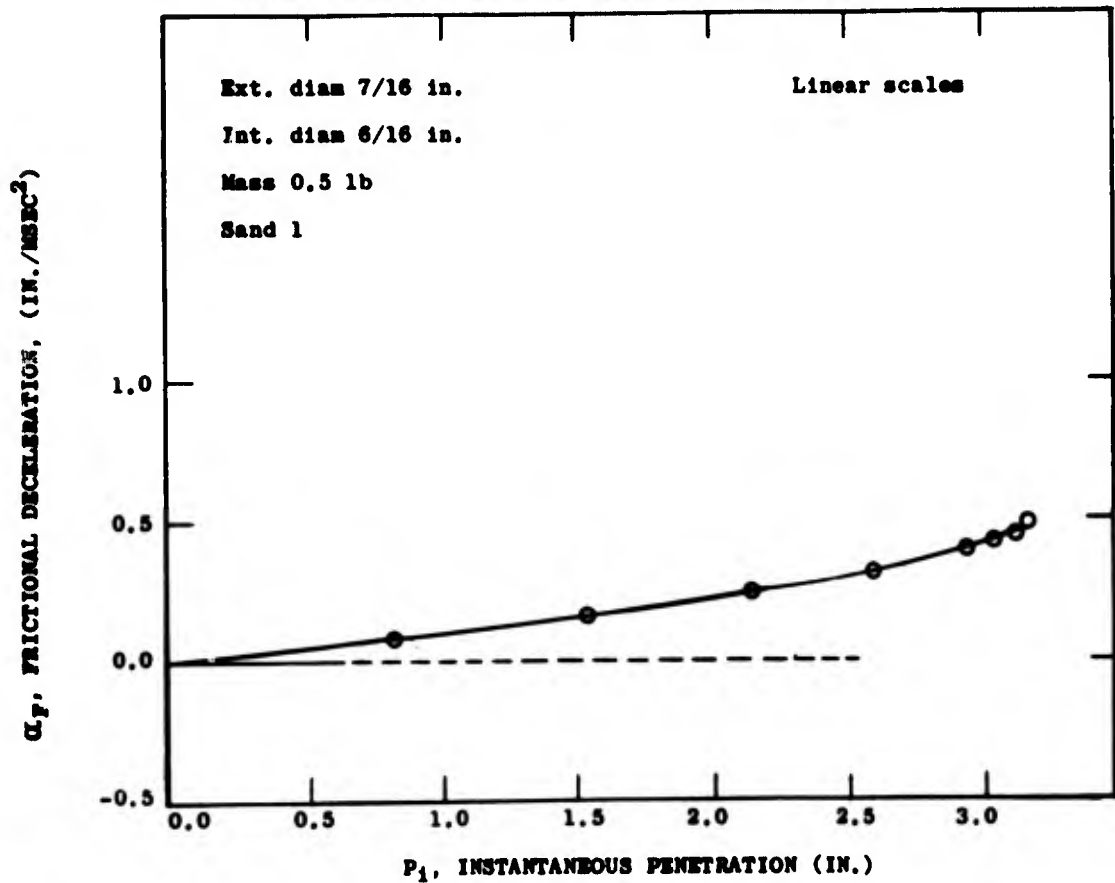


Figure 28. Frictional deceleration vs instantaneous penetration.

$$Ma = M(0.47 + 0.029 v^2 + 0.156 P_i e^{-0.24v}) \quad (34)$$

where M is the mass of the pile. Since eq 34 has the dimensions of force, using the principle of equivalence of lost kinetic energy and work done, one can write:

$$-d\left(\frac{1}{2} Mv^2\right) = (Ma) dP_i \quad (35)$$

or

$$-d\left(\frac{1}{2} Mv^2\right) = M(0.47 + 0.029 v^2 + 0.156 P_i e^{-0.24v}) dP_i \quad (36)$$

Equation 36 becomes, after simplifications,

$$-vdv = (0.47 + 0.029 v^2 + 0.156 P_i e^{-0.24v}) dP_i \quad (37)$$

Numerically integrating eq 37 by using steps of penetration of 0.1 in. and comparing the calculated results with the experimental results, one obtains the graph of Figure 30.

The upper curve is the calculated curve for a 7/16 in. ext diam and 6/16 in. int diam pile having a mass of 0.5 lb. The lower calculated curve is for the same type of pile having a mass of 0.287 lb. Both calculated curves show a good agreement with experimental data obtained during laboratory work. Table III gives the calculated penetrations.

Discussion of the physical model

The physical model mathematically represented by eq 37 is in very good agreement with experimental results. Within the range of penetration studied, it closely reproduces an average 1.5-velocity power dependence of the penetration given by eq 11. It is not surprising to obtain the 1.5-velocity power dependence, since three different forces participate in the penetration process. Any other value of velocity power dependence would also have a physical meaning, since the velocity power dependence is affected by the relative importance of each force present in the process. It can be shown that an increase of the friction force, keeping the crushing and drag forces constant, will decrease the value of the exponent of the velocity power dependence of the penetration. By the same argument, a decrease in friction will increase the velocity power dependence. This fact was confirmed by special experiments.

The first set of experiments consisted of firing a brass and a steel pile of the same mass and projected area into the same sample of permafrost. Figure 31 shows that the penetration-velocity curve has a greater slope for the brass pile, as expected since the coefficient of friction between brass and permafrost is less than that between steel and permafrost. Moreover, it was much easier to withdraw the brass pile from the permafrost than the steel pile.

The second set of experiments consisted of firing two steel piles having the same mass but different wall thicknesses (Fig. 32). The reduction of one pile wall reduced the friction between the pile and the permafrost. As expected, the penetration curve for the thinner-walled pile shows a greater slope (Fig. 33).

The calculated penetration at 200 ft/sec is 3.78 in. for a pile having a 0.5-lb mass and 2.41 in. for a pile having a 0.287-lb mass (Table III). Those values of penetration represent the range covered by the experiments. The mass power dependence of penetration at 200 ft/sec is obtained from

$$(P_2 / P_1) = (M_2 / M_1)^\mu \quad (38)$$

where μ is the mass power dependence of penetration, by inserting the numerical values:

$$(3.78/2.41) = (0.500/0.287)^\mu$$

$\mu = 0.812$. This calculated value is close to the average mass power dependence given by eq 11.

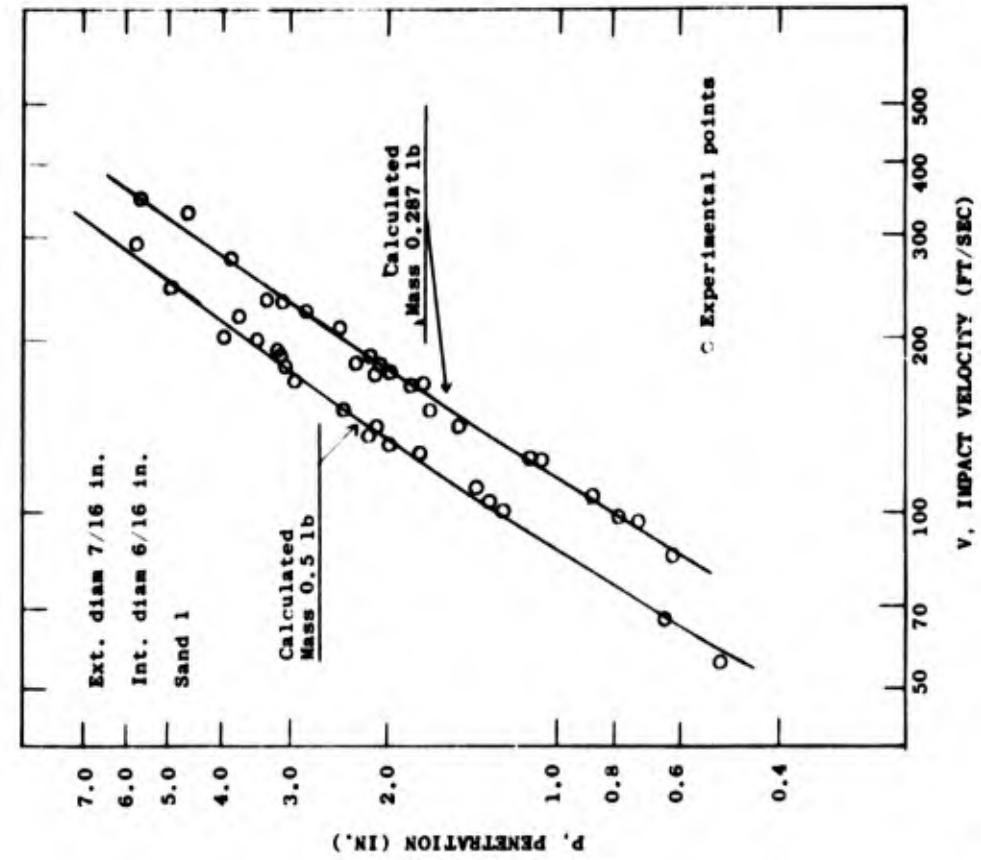


Figure 30. Experimental and calculated values of penetration for two masses.

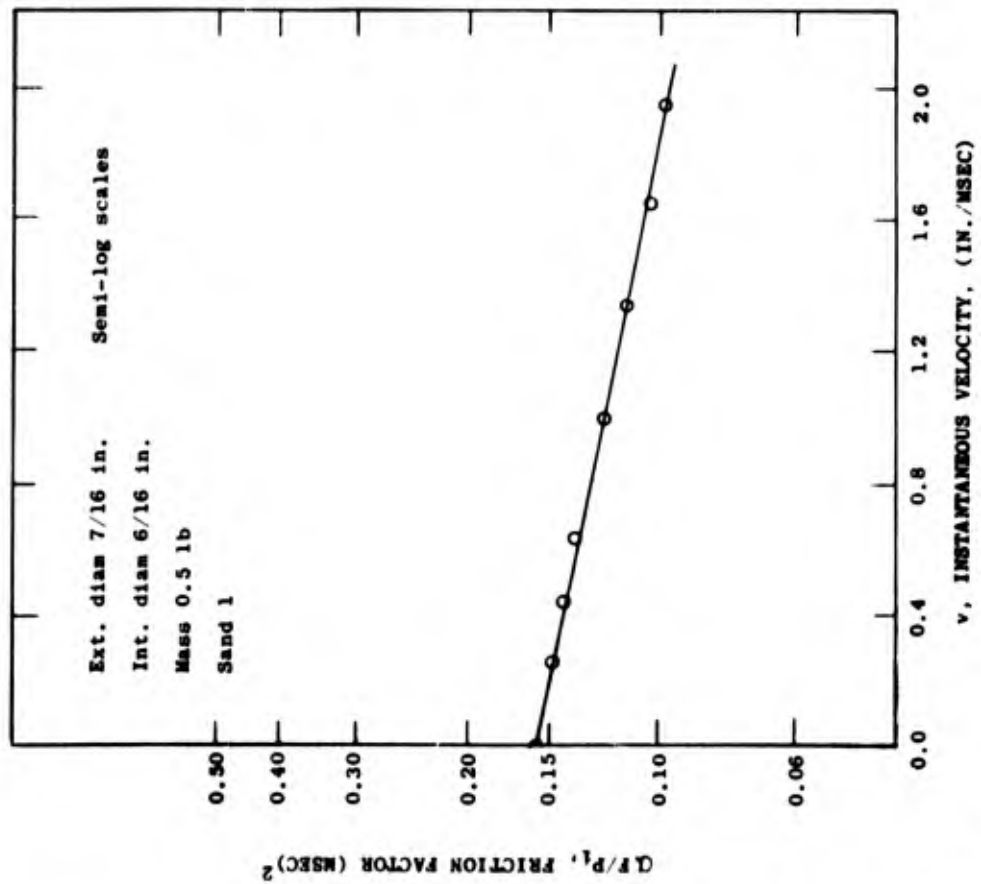


Figure 29. Friction factor vs instantaneous velocity.

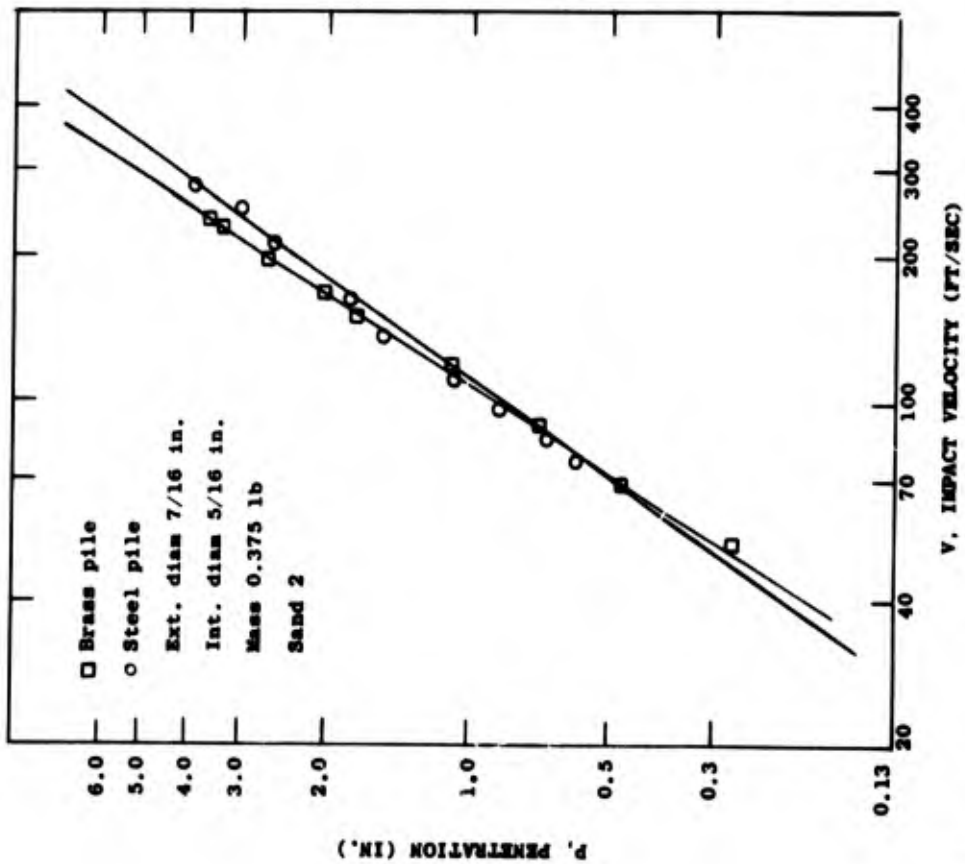


Figure 31. Penetration vs impact velocity for piles made of different materials.

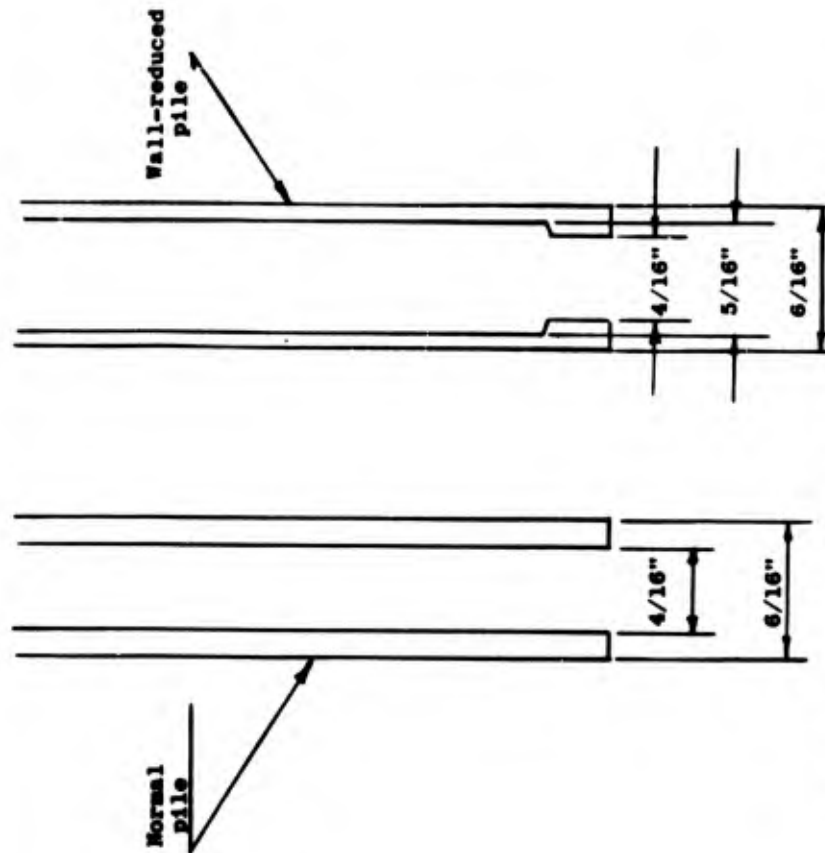


Figure 32. Normal pile and wall-reduced pile.

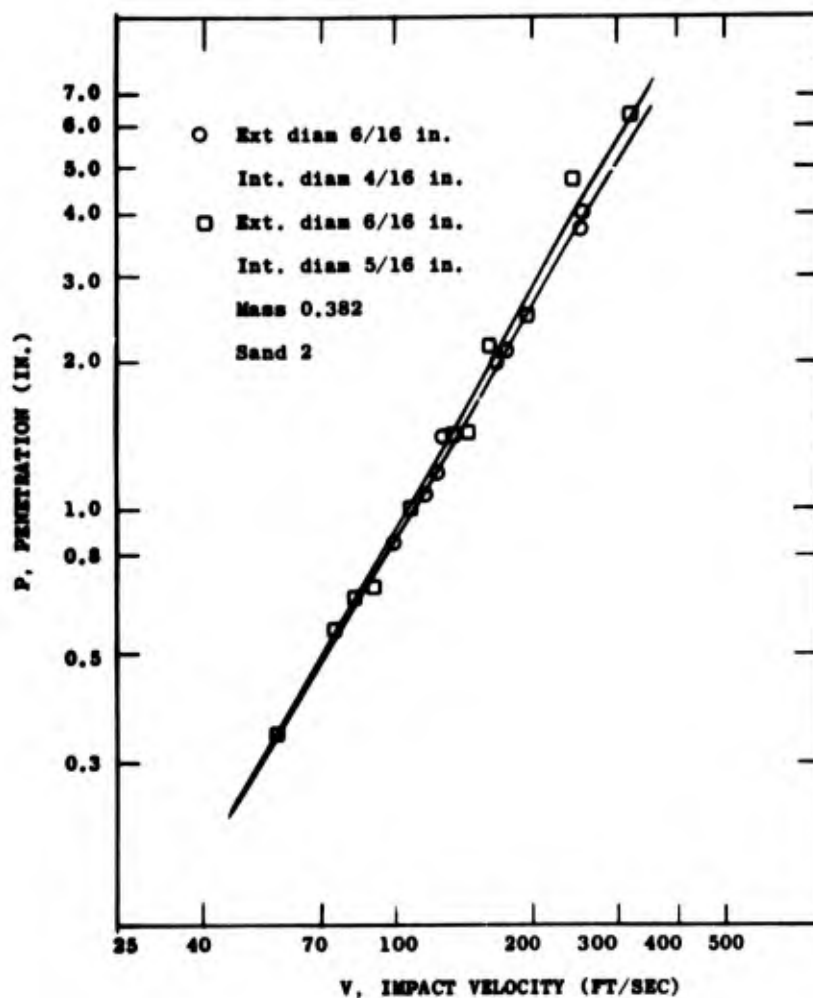


Figure 33. Penetration vs impact velocity for piles having different wall characteristics.

Table III. Calculated penetrations (eq 37).

Penetration P (in.)	Impact velocity V (in./msec)	Mass M (lb)
0.52	0.72	0.500
1.27	1.20	0.500
3.78	2.40	0.500
6.61	3.60	0.500
0.76	1.20	0.287
2.41	2.40	0.287
4.33	3.60	0.287

The calculated values for 100 ft/sec give $\mu = 0.925$. At this velocity, penetration is close to the low range of penetration, where good agreement with a 1.0-mass power dependence would be expected. Figures 34a and 34b show plots of reduced penetration $PM = P(M_0/M)$ and $P_M = P(M_0/M)^{0.8}$ for piles of different masses. There is better agreement of the experimental data with $P(M_0/M)$ in the low penetration range and with $P(M_0/M)^{0.8}$ at high penetration.

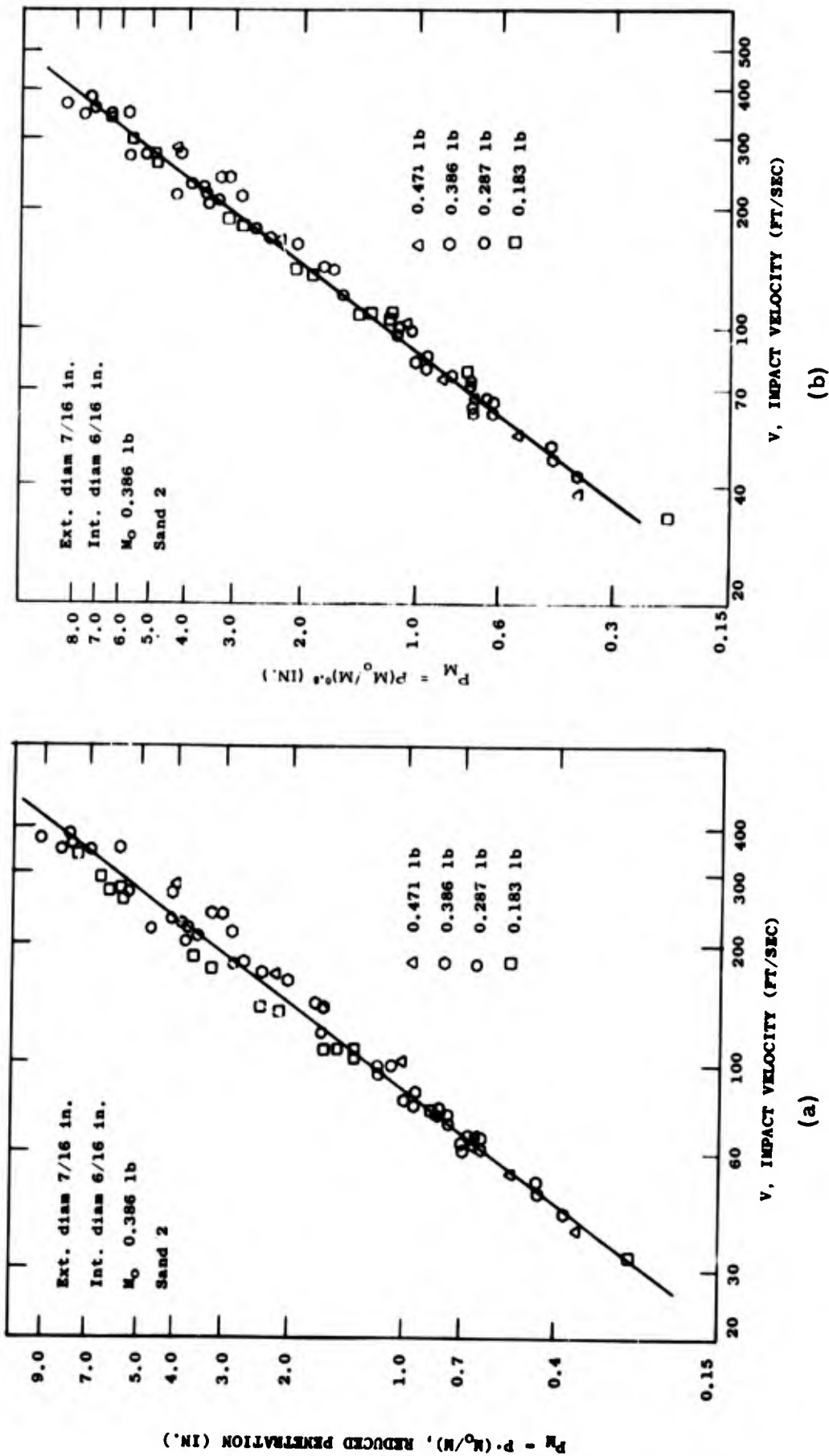


Figure 34. Reduced penetration vs impact velocity for piles having various masses.

SECOND INVESTIGATION, PHASE II

The physical model of penetration developed in the previous chapter was derived for only one thin, hollow, circular pile. The purpose of this second investigation was to study the influence of pile shape on pile penetration. The main objectives were to find parameters related to the shape of the piles and to relate these parameters to the penetrations of variously shaped piles. These piles were designated by a letter symbol and their characteristics are given in Appendix B. The firing data are given in Appendix E.

Piles of the same projected area

A useful aerodynamic concept is the projected area, the maximum cross sectional area perpendicular to the line of displacement of a penetrating object. Figures 35a to 37d were obtained by using six piles of different shapes having a mass of 0.322 lb and a projected area of approximately 0.048 in.². To compare the penetrations, a reference pile and a reference permafrost were needed, since various samples and various types of permafrost were tested. Circular pile S₄, described in Appendix B, was used as the reference pile for this series of tests; the reference sample of permafrost is the sample for which the data are plotted in Figure 35c. The correction factor λ is defined as follows:

$$\lambda = \frac{\text{penetration of reference pile in reference sample}}{\text{penetration of reference pile in the sample tested}}$$

Multiplying the ordinates of Figures 35a to 37d by the correction factor λ gives Figure 38. Because of practical difficulties in machining the piles, a 5% variation of the projected area of the piles was found. Since the penetration of a pile varies at most as the inverse of the first power of its projected area (as shown later), the maximum expected variation of penetration (the variation between the lowest and the highest curve on Figure 38) cannot be attributed only to this 5% variation of the projected area.

An examination of Figure 38 clearly indicates that the projected area is not the only significant parameter involved during the penetration of variously shaped piles. An attempt to study the penetrations of piles as a function of the perimeter of their cross section alone also proved unsatisfactory. However, the well-defined decrease of penetration when the perimeter is increased indicates that the perimeter is a controlling factor, although it does not completely explain the different penetrations obtained with various piles having the same projected area.

Effective projected area

It is the purpose of this section to define a useful quantity by which the penetrations of variously shaped piles can be expressed in simple analytical form. This useful quantity, Z , called the effective projected area, is defined as follows:

$$Z = p^m \tau^n \quad (39)$$

where p is the perimeter of the cross section of the piles, τ is the effective thickness, and m and n are empirical exponents.

The choice of quantity Z is based on the following considerations. When a pile penetrates a viscoelastic material such as permafrost, three types of forces act against the pile: frictional forces on the sides of the pile and crushing and drag forces on the tip of the pile. The frictional forces are directly related to the area of the pile in contact with the permafrost, hence to the perimeter of its cross section. The crushing and drag forces, which are related to a large extent to the lateral displacement of particles of permafrost during pile penetration, are assumed to be connected to the effective thickness, τ , which is defined now.

Effective thickness. Considering a one-dimensional situation, the total movement of displaced permafrost can easily be defined as a function of the displacement X_{\max} of particles of permafrost undergoing the greatest displacement. For any other shape of projectile, the sum of the displacements of individual particles is no longer a function of maximum displacement alone. This total displacement will now be a function of the

various dimensions of the cross section of the pile. To reduce the various possible cases to the simple case seen above, a shape factor \underline{Q} was introduced:

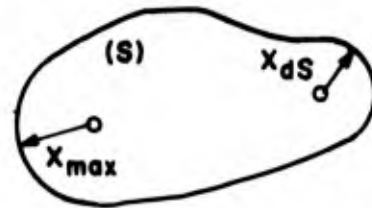
$$Q = X_{av} / X_{max} \quad (40)$$

where X_{av} is average displacement \underline{X} per particle and X_{max} the displacement of particles of permafrost undergoing the greatest displacement. See sketch below:

Now the average displacement per particle is defined as an average of the various displacements of area elements dS , the variable defining the average being \underline{S} :

$$X_{av} = \int_{(S)} X dS / \int_{(S)} dS. \quad (41)$$

In this formula, the integrals are extended on dS to the total cross section surface \underline{S} and \underline{X} is taken along the paths of flow of the material.



Since defining the paths of flow by experimental work was impossible, the assumption was made that, at any point of the surface \underline{S} , the material will flow towards the nearest edge of penetrating surface \underline{S} . This assumption is believed satisfactory for circular, square, or rectangular piles. For cross-shaped piles the assumption is not easy to apply. For a simple geometrical shape of pile, it is possible to define different areas in which displacement has the same direction for the various points of the area. In this fashion, \underline{Q} can be calculated for the piles which were studied. By applying shape factor \underline{Q} to the actual wall thickness \underline{T} of the pile, effective thickness τ is obtained:

$$\tau = T Q. \quad (42)$$

Finally, because of the symmetry of piles used for practical purposes, the maximum displacement X_{max} for these piles is always equal to half their wall thickness \underline{T} . Therefore, the effective thickness τ is equal to twice the average displacement per particle X_{av} .

Shape factors \underline{Q} are determined in Appendix F for the various piles used in this study. By calculating effective thickness τ from eq 42 and relating \underline{p} and τ to penetrations of the piles, exponents \underline{m} and \underline{n} of eq 39 can be determined.

Experimental results showed that exponents \underline{m} and \underline{n} of eq 39 had constant values for $p/\tau < 50$ and $p/\tau > 70$. From those observations, thick piles are defined by $p/\tau < 50$ and thin piles by $p/\tau > 70$.

Thick piles

The experimental results reported for piles of constant projected area (Fig. 35-37), and results of other tests (Fig. 39a-42b) are discussed. The characteristics of the piles used in this section are given in Table IV.

Determination of a relationship. To determine how penetration \underline{P} is related to \underline{p} and τ , a simple mathematical relationship was tried:

$$P = K_{16} / Z = K_{16} / p^m \tau^n. \quad (43)$$

To determine the value of exponent \underline{m} of eq 43, a rectangular pile, S_2 , and a cross-shaped pile, S_6 , of the same effective thickness were compared. From Figures 35c and 37c, the ratio, P_{S_2} / P_{S_6} , of their respective penetrations at 100 ft/sec is 1.35. From eq 43 the ratio of respective penetrations at a given velocity can be written

$$P_{S_2} / P_{S_6} = (P_{S_6} / P_{S_2})^m (\tau_{S_6} / \tau_{S_2})^n. \quad (44)$$

Since τ_{S_6} equals τ_{S_2} , for any value of \underline{n} ,

$$P_{S_2} / P_{S_6} = (P_{S_6} / P_{S_2})^m. \quad (45)$$

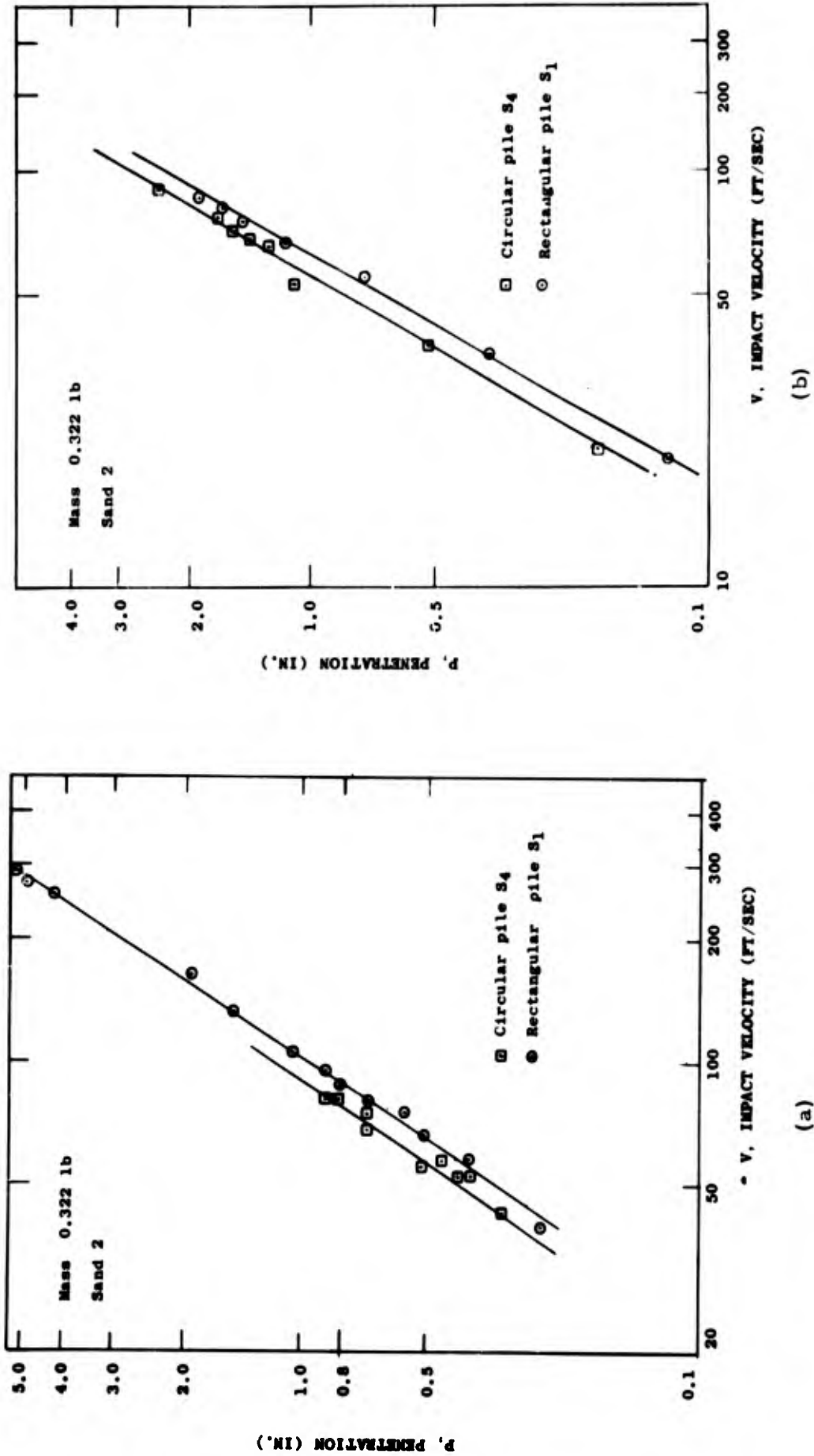


Figure 35. Penetration vs impact velocity for a circular and rectangular pile having the same projected area.

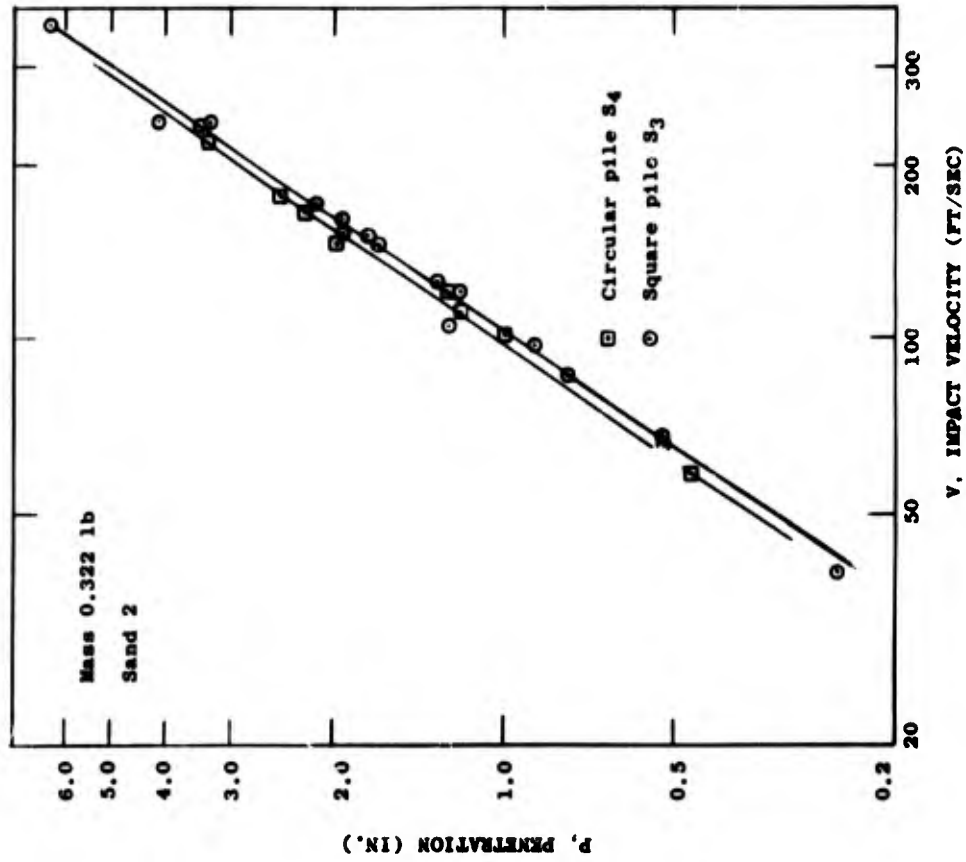


Figure 36. Penetration vs impact velocity for a circular and a square pile having the same projected area.

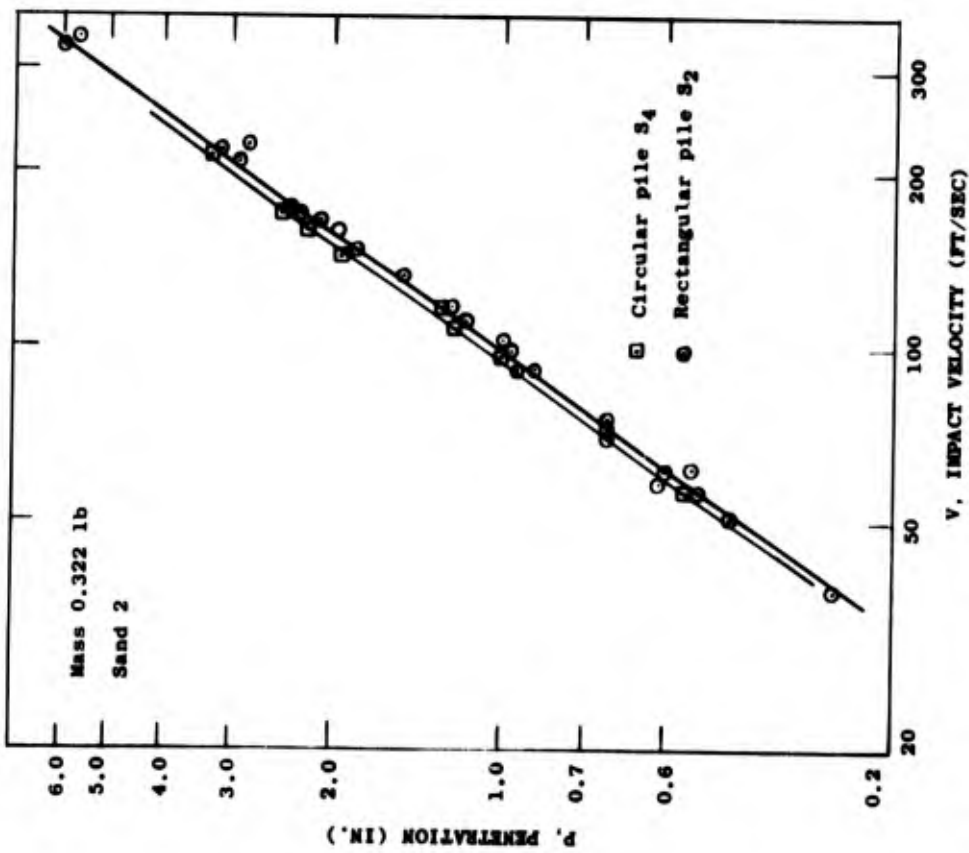


Figure 35c. Penetration vs impact velocity for a circular and rectangular pile having the same projected area.

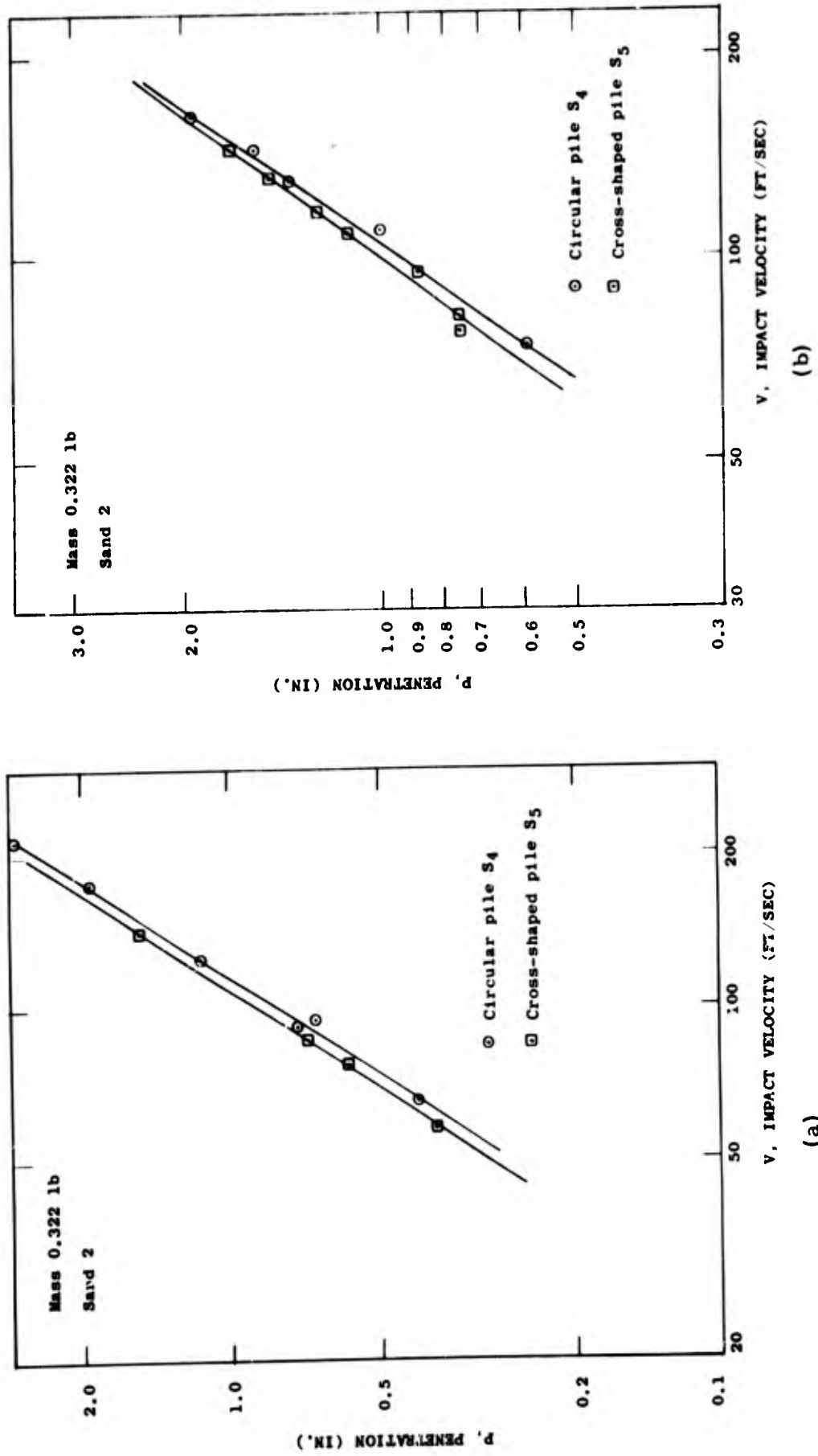


Figure 37. Penetration vs impact velocity for a circular and a cross-shaped pile having the same projected area.

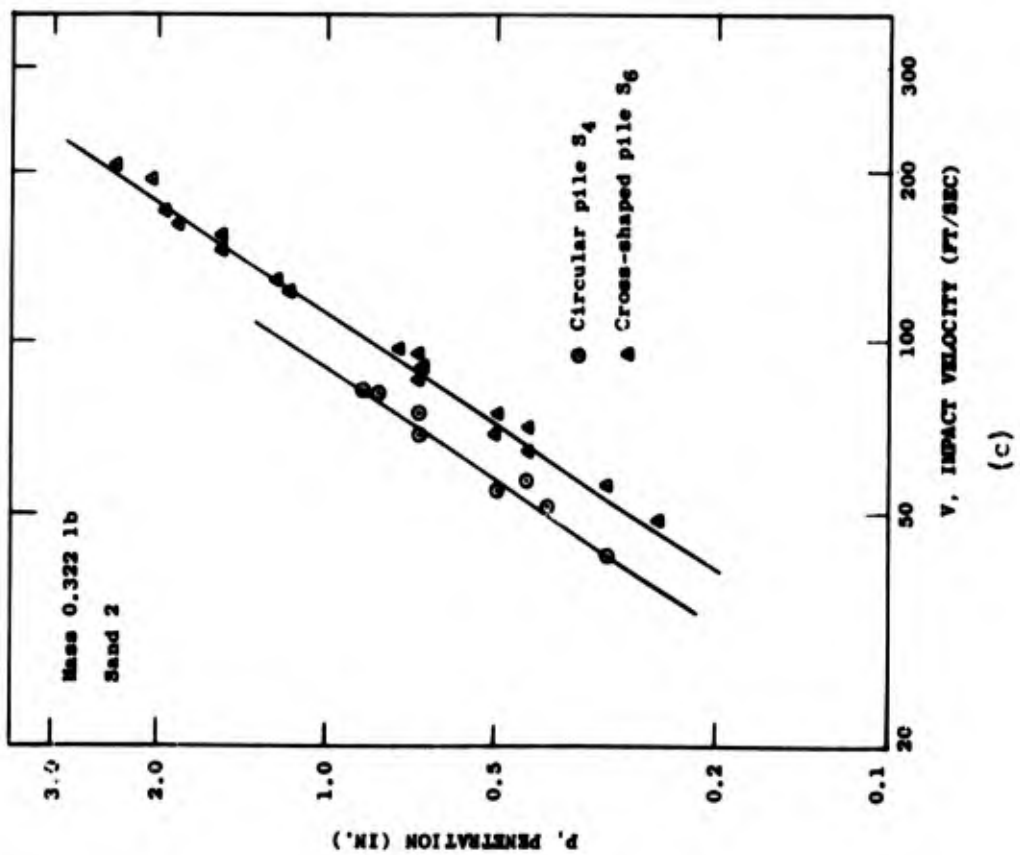
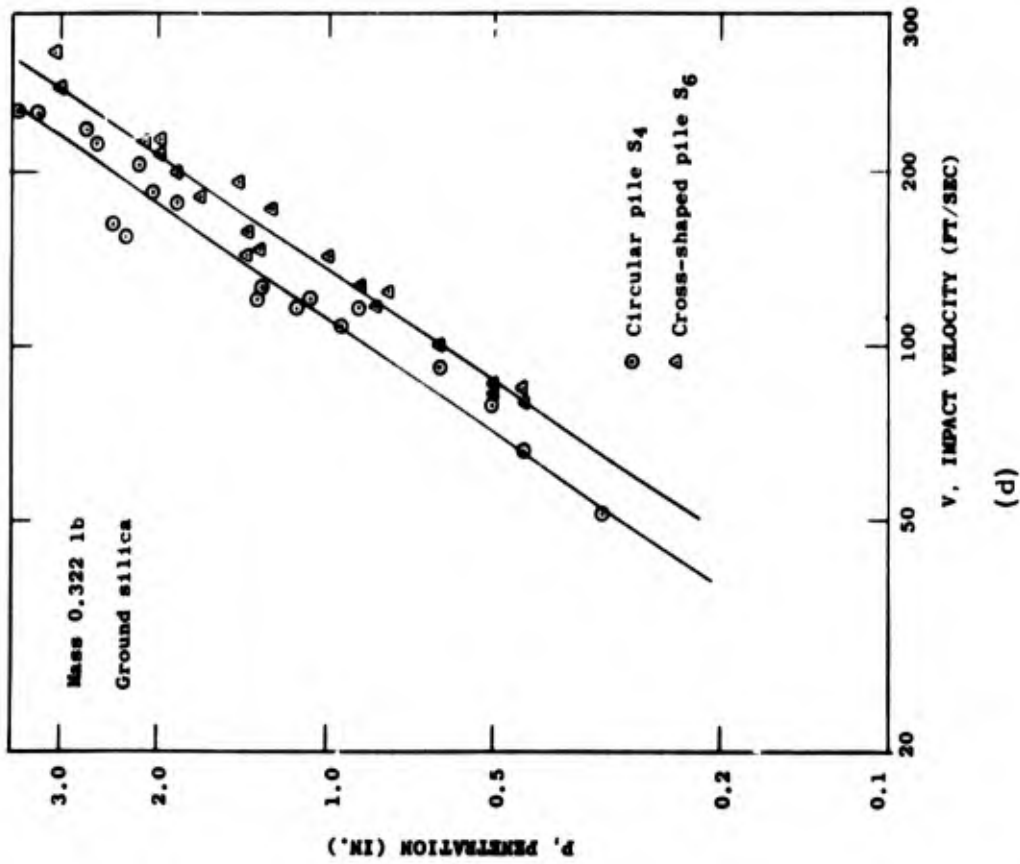


Figure 37 (Cont'd). Penetration vs impact velocity for a circular and a cross-shaped pile having the same projected area.

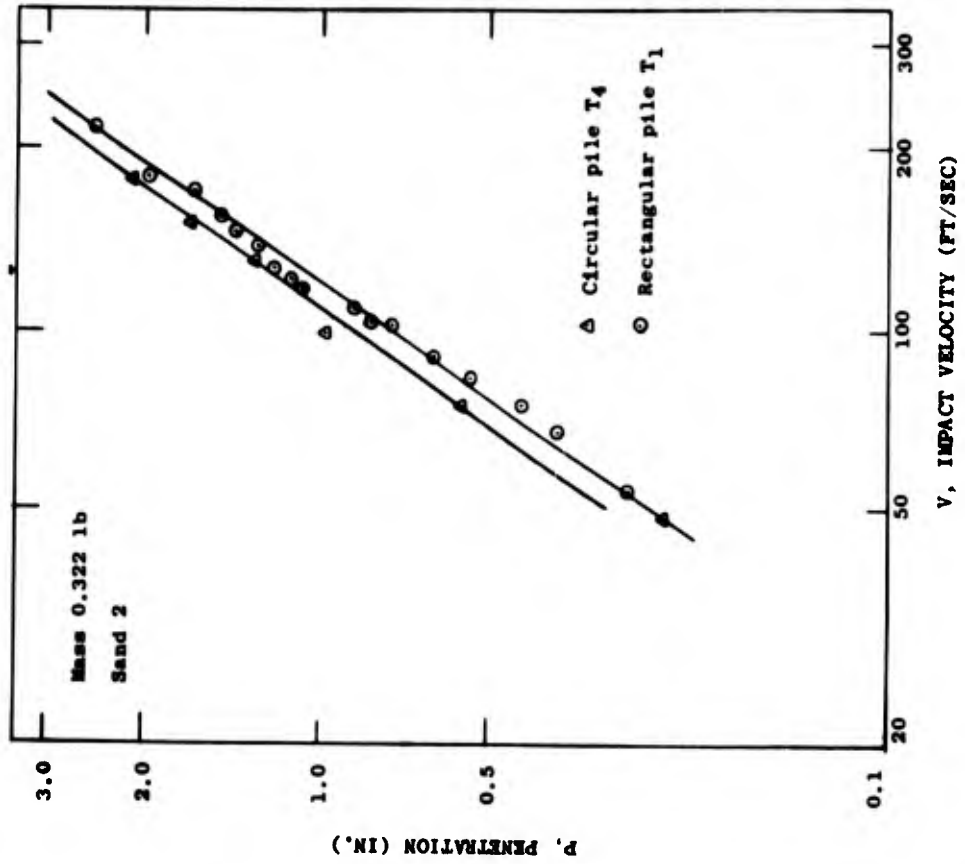


Figure 39a. Penetration vs impact velocity for a circular and a rectangular pile having the same projected area.

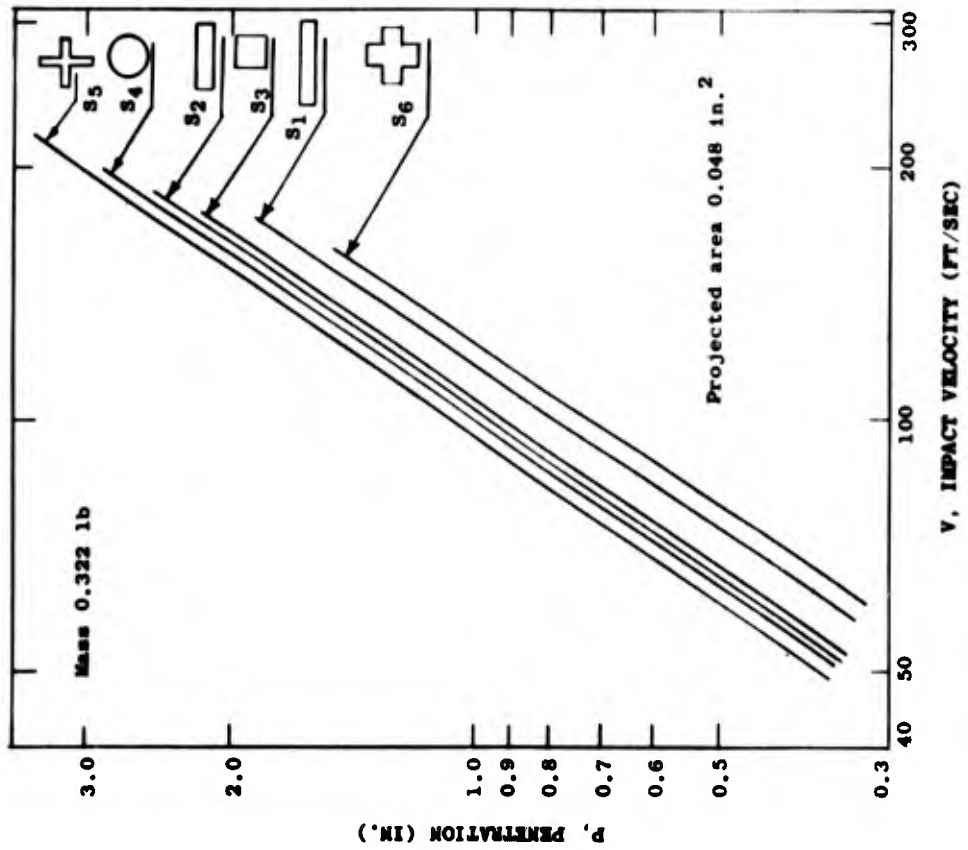


Figure 38. Penetration vs impact velocity for various piles having the same projected area.

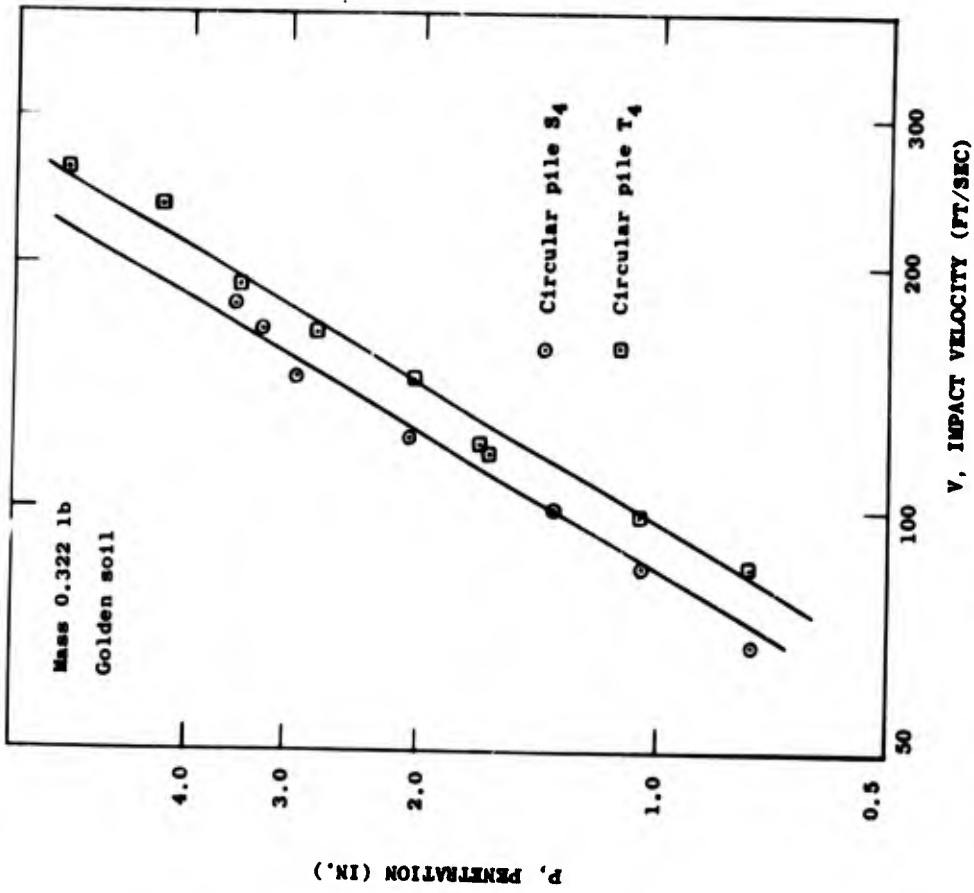


Figure 40a. Penetration vs impact velocity for circular piles having various projected areas.

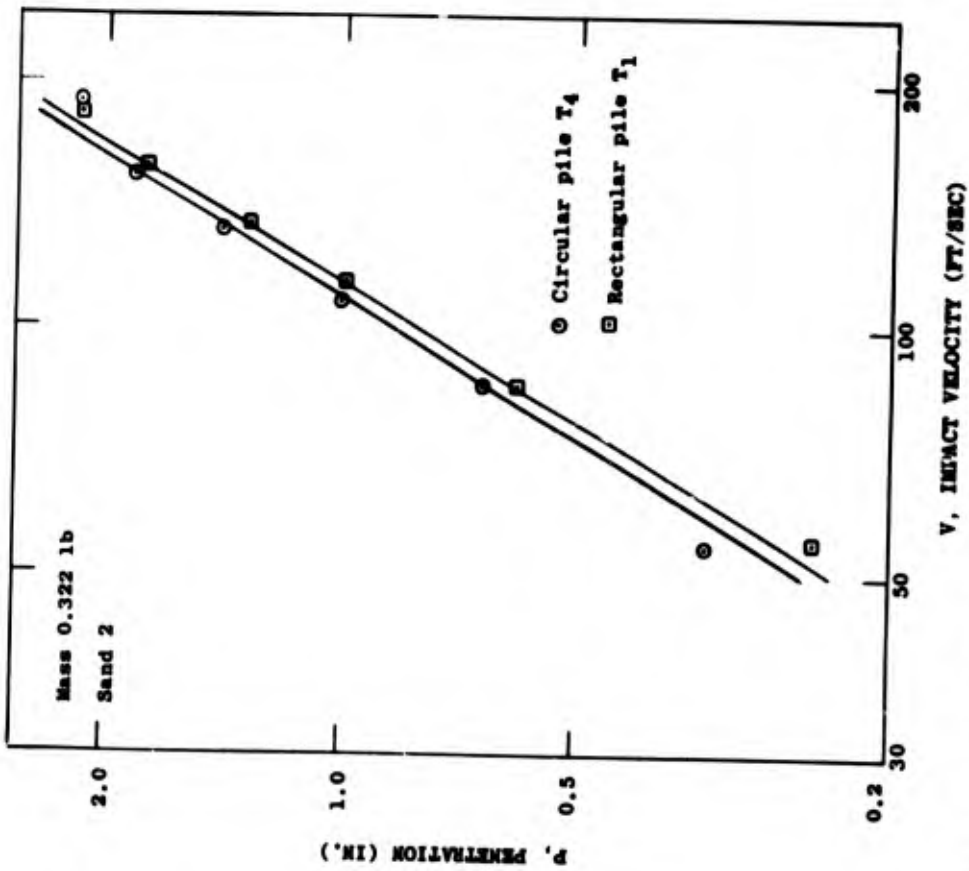
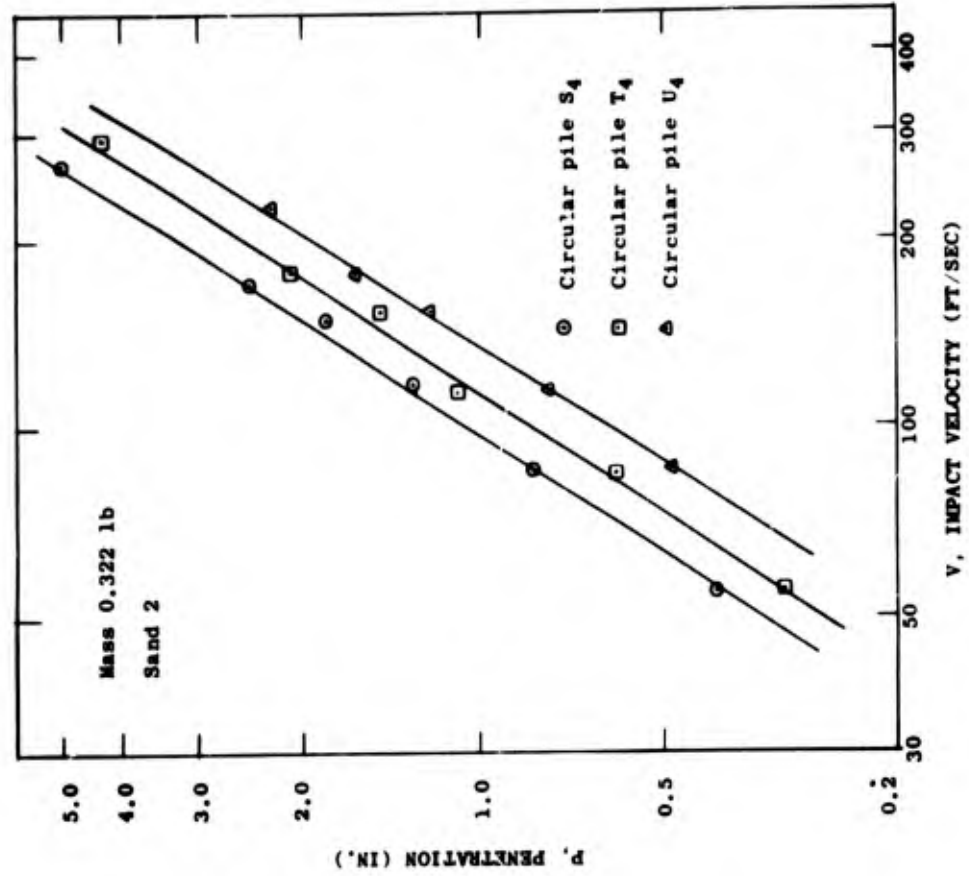
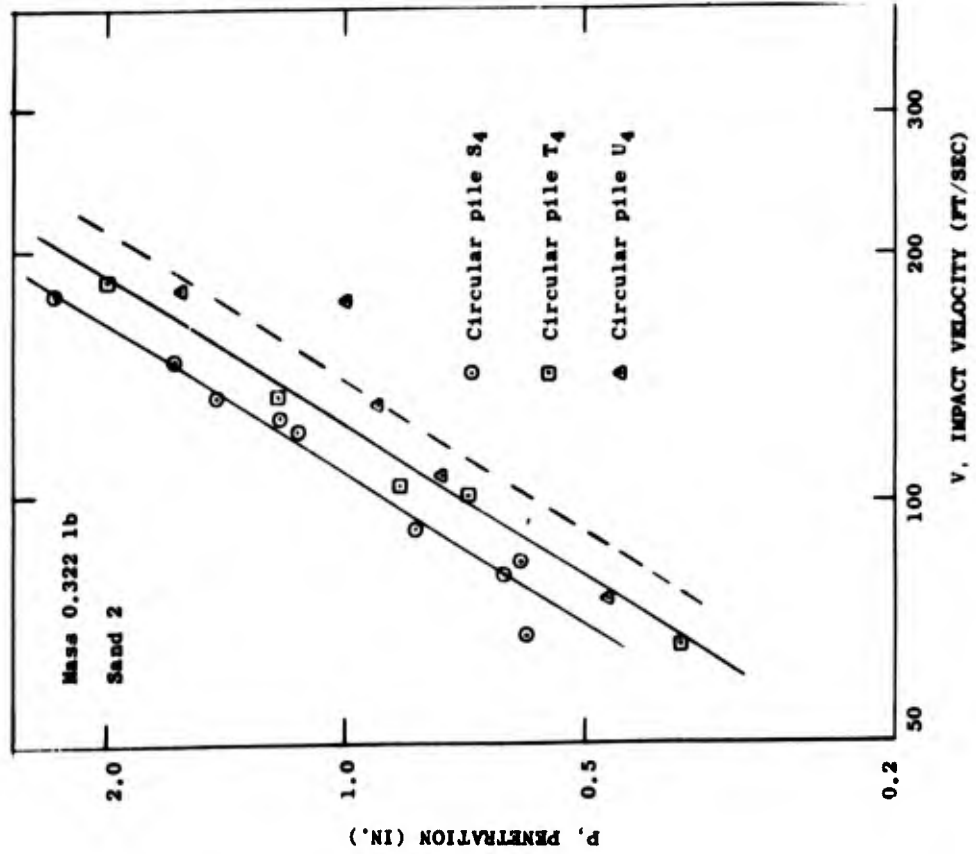


Figure 39b. Penetration vs impact velocity for a circular and a rectangular pile having the same projected area.



(c)



(b)

Figure 40 (Cont'd). Penetration vs impact velocity for circular piles having various projected areas.

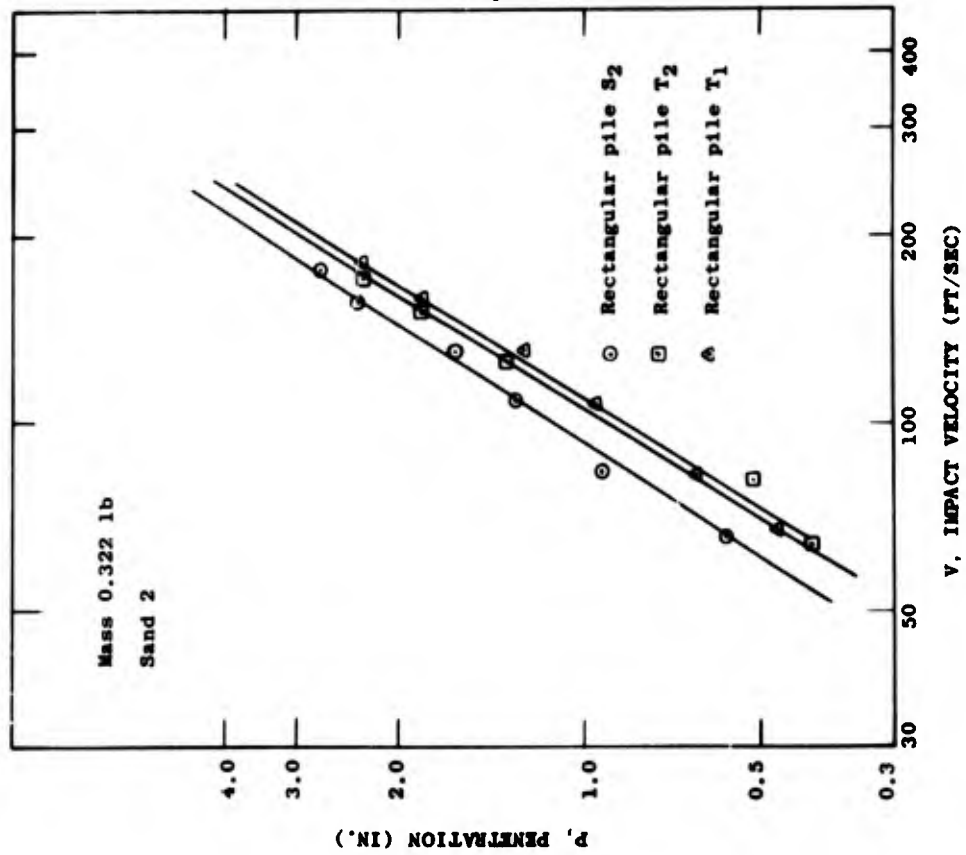


Figure 42a. Penetration vs impact velocity for rectangular piles having various cross section areas.

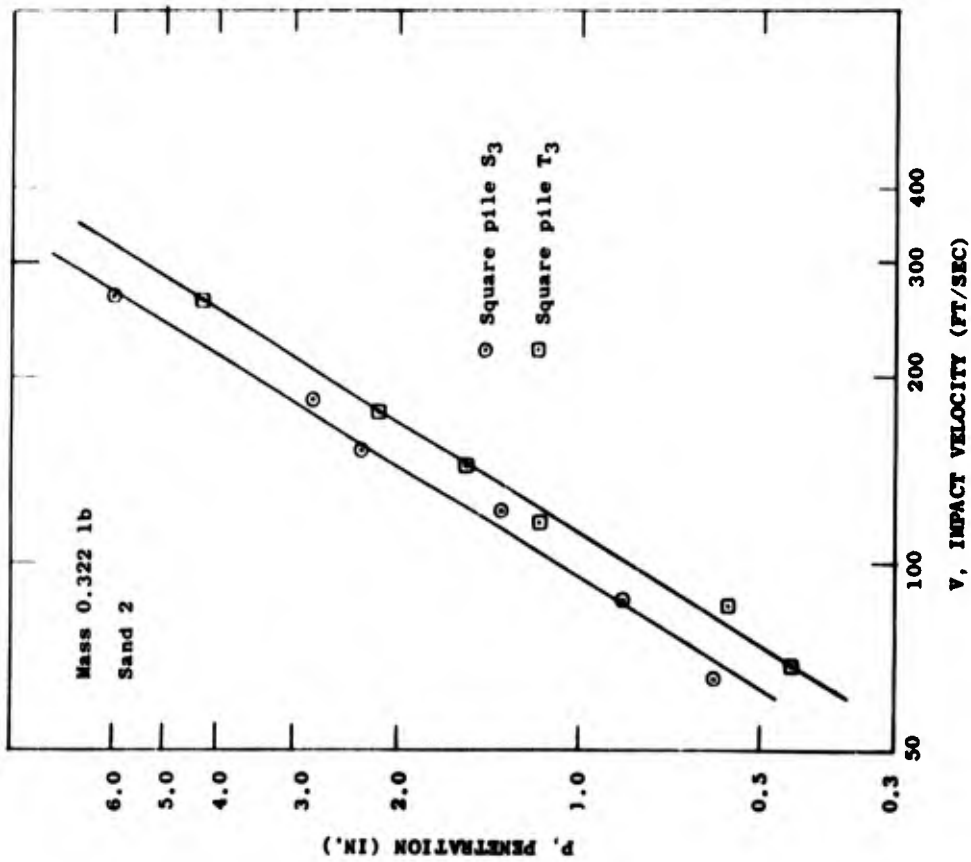


Figure 41. Penetration vs impact velocity for square piles having various projected areas.

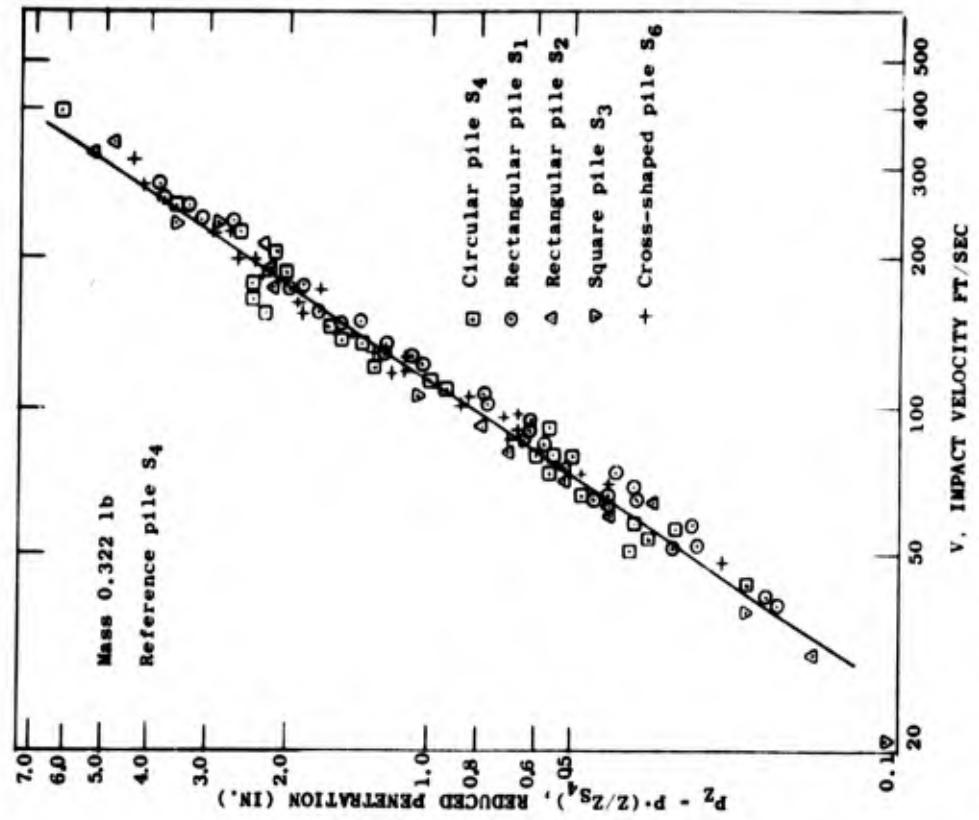


Figure 43. Reduced penetration vs impact velocity for thick piles having the same projected area.

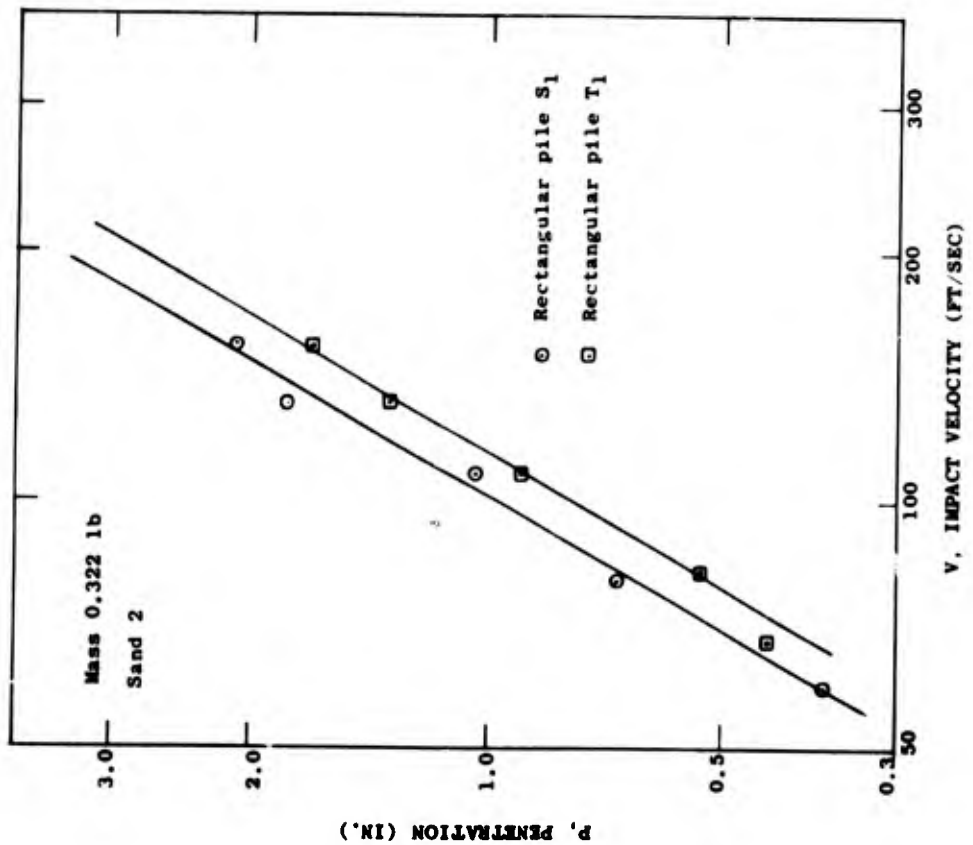


Figure 42b. Penetration vs impact velocity for rectangular piles having different projected areas.

Inserting the corresponding numerical values in eq 45, $1.35 = (1.216/0.888)^m$, from which $m = 1$. To determine the value of n , a solid circular pile T_4 and a square pile S_3 were used (Fig. 36, 40c). The ratio of their perimeters is 1.025 and the ratio of their penetrations at 100 ft/sec is 1.20. For these piles eq 44 then becomes: $1.20 = (1.025)^{1.0} \cdot (95/73)^n$ from which $n = 0.6$. From those calculated values of \underline{m} and \underline{n} , eq 43 can be written

$$P = K_{17} / p \tau^{0.6}. \quad (46)$$

The experimental results for piles of the same projected area, given in Figures 35a to 37d, reduced according to eq 46 are shown in Figure 43. Good agreement with eq 46 is seen. The pile of reference for this series of tests was circular pile S_4 and the permafrost of reference was the one corresponding to Figure 35b. The correction factor λ was applied to these calculations.

Table IV. Characteristics of thick piles.

Pile	Perimeter	Effective thickness	p/τ
	p (in.)	τ (in.)	
S_1	0.980	0.060	16.4
S_2	0.888	0.067	13.3
S_3	0.872	0.073	12.0
S_4	0.772	0.082	9.5
S_6	1.216	0.067	18.0
T_1	1.234	0.062	20.0
T_2	1.096	0.071	15.4
T_3	1.016	0.085	12.0
T_4	0.898	0.095	9.5
T_5	1.710	0.046	37.0
U_4	1.038	0.110	9.5
B_1	3.920	0.110	35.7

Experimental data for Figures 39a to 42b reduced according to eq 46 are plotted on Figure 44. The pile of reference for this series of tests was the one corresponding to Figure 42b. Both figures show good agreement with eq 46.

Piles of same shape. Equation 43 can be simplified for piles having identical cross-sectional shapes. In this case, perimeter p and the effective τ are both proportional to the same linear quantity l defining the size of the cross section. Equation 43 then becomes:

$$P = K_{18} / l^{m+n}. \quad (47)$$

As projected area S is proportional to the square of this linear quantity l ,

$$P = K_{19} / S^{m+n/2}. \quad (48)$$

Since $m = 1.0$ and $n = 0.6$, for thick piles of identical cross sectional shape,

$$P = K_{20} / S^{0.8}. \quad (49)$$

In this investigation circular, square, and cross-shaped piles were studied. The experimental results for the circular and square piles are given in Figures 40a, 40b, 40c, and 41; those for cross-shaped piles T_5 and B_1 are given in Figures 45 and 46. Since pile T_5 was tested in Sand 1 and B_1 was tested in Golden soil, corrections were necessary. First, penetration of pile T_5 was increased by 15% to make it comparable to results with Sand 2 (found experimentally to be 15% higher). An additional correction was made to compare piles tested in Golden soil with those tested in Sand 2.

This was found by comparing the penetration of pile T_4 in Golden soil and in Sand 2, as given in Figures 39b, 40a, 40b, and 40c. Finally, a mass correction was applied according to the 0.8 mass power dependence found in Phase I. The total correction factor necessary to adjust the penetration of pile T_5 to the conditions of pile B_1 was 8.2. The penetration of pile B_1 in Golden soil was 2.20 in. for an impact velocity of 100 ft/sec (Fig. 45). The corrected penetration of pile T_5 for the same conditions is $0.90 \times 8.2 = 7.38$ in. The lines passing through the different sets of experimental points show an average slope of -0.8 (Fig. 47), indicating a good agreement of experimental results with eq 49.

Thin piles

Thin piles are defined by the ratio $p/\tau > 70$. Since it is difficult to machine solid piles having a p/τ ratio larger than 70, this section is primarily concerned with thin, hollow, circular piles. The results used are presented in Figures 16e and 11. An attempt was made to use the results for the cross-shaped pile S_5 , but there was some indication that the results of this pile would follow a relationship intermediate to those for thin and thick piles.

From the penetration at 100 ft/sec of piles R_1 , R_2 , and R_3 , which all have the same effective thickness (Table V), three values of \underline{m} are obtained by eq 43. Their average value is close to 0.5. Using piles R_2 and R_6 , which have the same cross-sectional perimeter, one obtains from eq 43.

$$P_{R_2} / P_{R_6} = (\tau_{R_6} / \tau_{R_2})^n. \quad (50)$$

Inserting the values given in Table V gives a value close to 0.5 for \underline{n} . Therefore, eq 43 reduces to:

$$P = K_{21} / (p\tau)^m = K_{21} / (p\tau)^{0.5}. \quad (51)$$

Use of the projected area. It can be shown that effective thickness τ approaches half the thickness \underline{T} of the pile when p/τ exceeds 60. Then, for thin piles,

$$P = K_{22} / (pT)^m. \quad (52)$$

Since for circular piles the projected area is $(\pi/4)(D_1^2 - D_2^2)$, or $(\pi/2)(D_1 + D_2)T$, or $pT/2$ where $\pi(D_1 + D_2)$ is the total perimeter \underline{p} and \underline{T} is the thickness, eq 52 can be written:

$$P = K_{23} / (D_1^2 - D_2^2)^m = K_{24} / S^m. \quad (53)$$

Figure 48, which gives the penetration (from Table V) as a function of projected area S , clearly indicates that the power dependence of penetration is different on the projected area for thin and thick piles. The slope of the curve corresponding to thin piles is close to -0.4, which is believed more accurate than the result found in the first attempt to determine a relationship for thin piles. Equations 51 and 53 can be written, respectively,

$$P = K_{25} / (p\tau)^{0.4} \quad (54)$$

and

$$P = K_{26} / (S)^{0.4} \quad (55)$$

and become useful relationships for thin piles, relating their penetration to their perimeter, to their effective thickness, and to their projected area.

Solid circular piles with conical and ogival tips

Results have indicated that the velocity power dependence of the penetration for conical and ogival-tipped piles is very close to that for flat-tipped piles. Thus the penetrations can be compared to find the function of the shape.

Table V. Penetration of circular piles at 100 ft/sec.

Pile	Penetration	Perimeter	Effective thickness	p/τ
	P (in.)	P (in.)	τ (in.)	
R ₁	1.50	1.768	0.015	117.0
R ₂	1.32	2.160	0.015	143.0
R ₃	1.24	2.555	0.015	170.0
R ₄	1.20	1.570	0.029	55.0
R ₅	1.10	1.963	0.031	63.0
R ₆	1.02	2.360	0.031	77.0
R ₆	0.75	2.160	0.046	47.0
R ₇	0.65	1.374	0.145	9.5

Table VI. Penetration ratios of conical-tipped piles.

Pile	Apex angle $2\beta^\circ$	Penetration ratio $P/P\pi_1$	$\cos \beta$
π_1	180	1.00	0.00
π_2	135	1.07	0.38
π_3	110	1.22	0.57
π_4	80	1.56	0.77
π_5	45	1.95	0.92

Conical-tipped piles. Table VI gives the penetration ratio of 100 ft/sec for various conical-tipped piles; the values were obtained from Figures 49a-e. The diameter of the piles was 7/16 in. and their mass was 0.5 lb; their apex angle 2β varied from 180° to 45° . The penetration ratio for pile π_2 is the average of three series of tests (49a-c). The penetration ratio plotted against the cosine of angle β (Fig. 50, 51) showed that, for the range of penetration studied, the penetration ratio varies as the cube of $\cos \beta$.

Ogival-tipped piles. Conical- and ogival-tipped piles with apex angles 2β of 100° and 80° were tested. The piles were 5/16 in. in diam and their mass was 0.5 lb. Penetration was 17% and 31% higher, respectively, for the 110° and 80° ogival-tipped piles than for the conical-tipped piles having the same apex angles (Fig. 52a, b). The small crater formed at the surface of the permafrost, a phenomenon observed during most of the tests conducted with thick piles, was not as large in the case of ogival-tipped piles as in the case of conical-tipped piles.

Discussion

The relationships developed in this chapter give a very good approximation for a first step of calculation. Because of the natural scatter of experimental data and variations in the properties of permafrost samples, this approach is quite satisfactory.

Penetration ratios given by the experiments with thick piles are compared with ratios computed from eq 46 and 51 (Table VII). This shows a better agreement of the experimental results with eq 46.

Equation 46, $P = K_{17}/p\tau^{0.6}$, indicates why piles of the same projected area may give different penetrations. It also holds for piles of different shapes and different projected areas. Equation 49, $P = K_{20}/S^{0.8}$, which was derived for thick piles of the same shape, is also in good agreement with experimental results.

MECHANICS OF PENETRATION OF PILES INTO PERMAFROST

Table VII. Comparison between two relationships for thick piles.

Piles	Penetration ratio	Experimental	Calculated $P \propto 1/\rho r^{0.6}$	Calculated $P \propto 1/\rho r^{0.5}$
$S_1 : S_4$	P_{S_1} / P_{S_4}	0.81	0.94	0.92
$S_2 : S_4$	P_{S_2} / P_{S_4}	0.96	0.98	0.96
$S_4 : S_3$	P_{S_4} / P_{S_3}	1.06	1.06	0.96
$S_6 : S_4$	P_{S_6} / P_{S_4}	0.72	0.72	0.71
$T_1 : T_4$	P_{T_1} / P_{T_4}	0.92	0.92	0.90
$S_4 : T_4$	P_{S_4} / P_{T_4}	1.27	1.27	1.25
$S_3 : T_3$	P_{S_3} / P_{T_3}	1.27	1.27	1.25
$S_4 : U_4$	P_{S_4} / P_{U_4}	1.63	1.61	1.55
$S_2 : T_2$	P_{S_2} / P_{T_2}	1.28	1.28	1.27
$T_2 : T_1$	P_{T_2} / P_{T_1}	1.04	1.02	1.03
$S_1 : T_1$	P_{S_1} / P_{T_1}	1.27	1.27	1.26

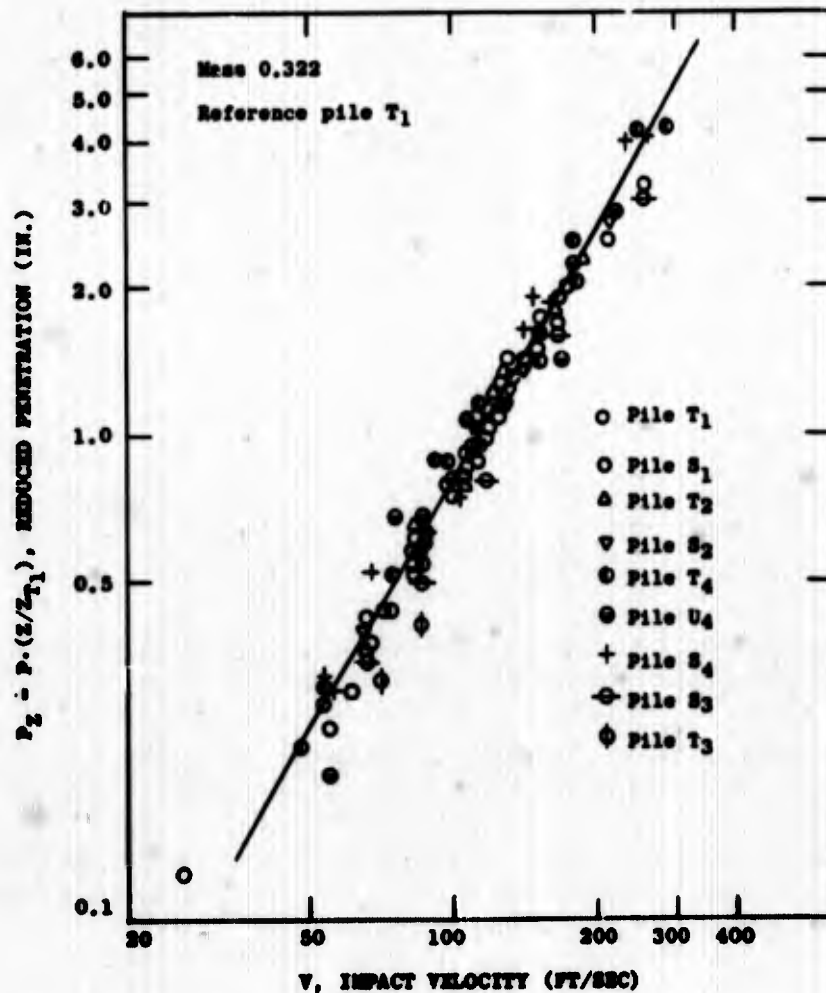


Figure 44. Reduced penetration vs impact velocity for thick piles having various projected areas.

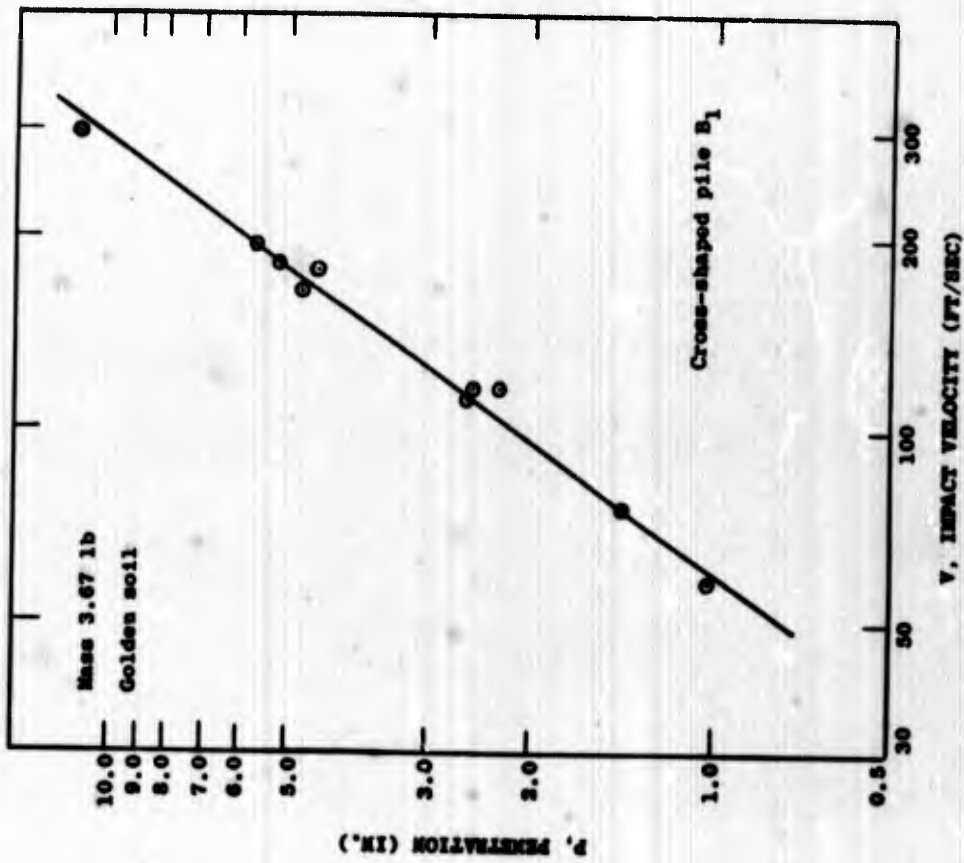


Figure 45. Penetration vs impact velocity for a 1.0-in.-diam cross-shaped pile.

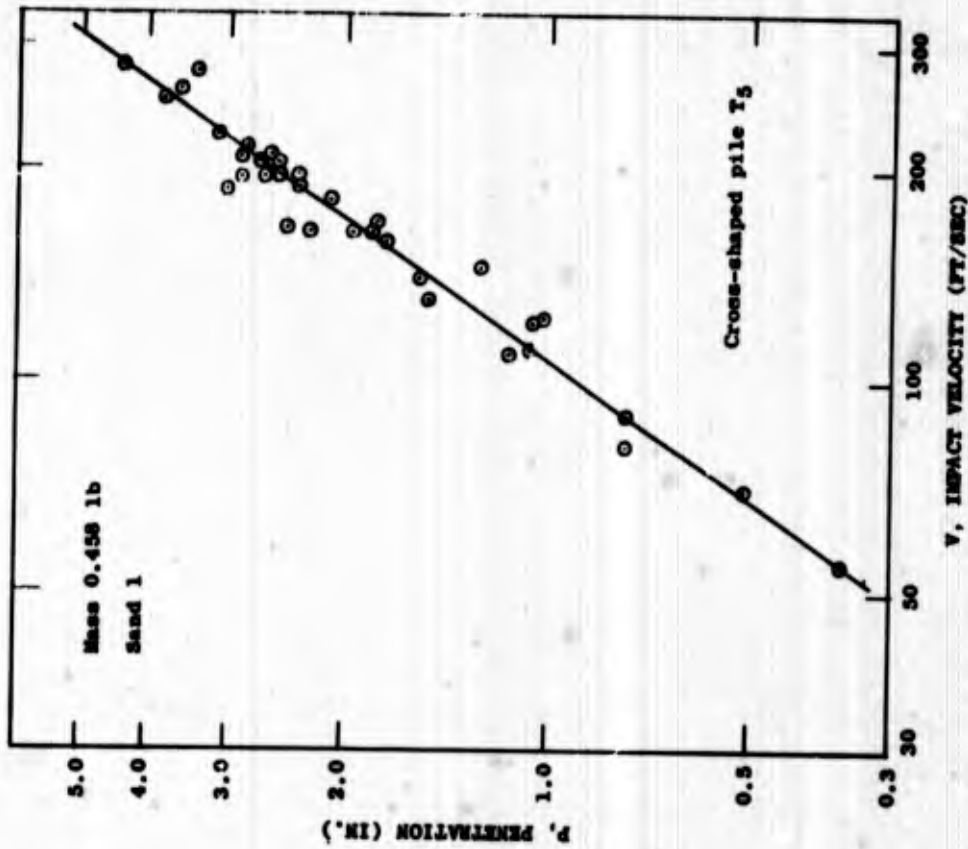


Figure 46. Penetration vs impact velocity for a 7/16-in.-diam cross-shaped pile.

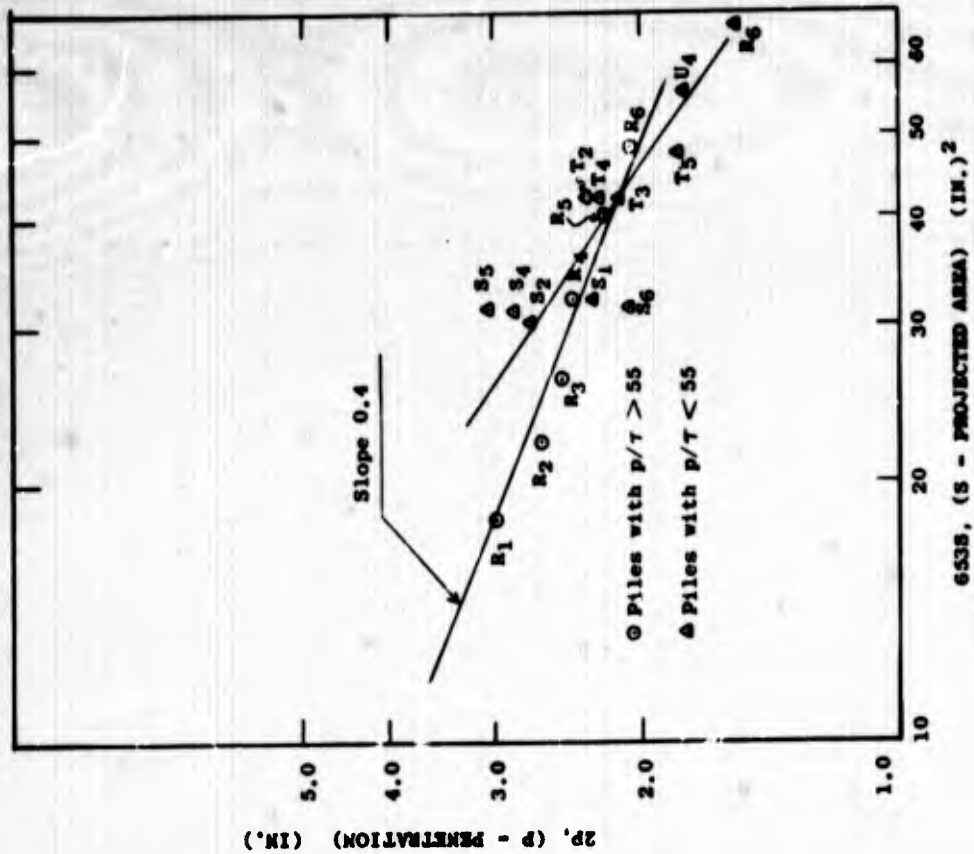


Figure 47. Penetration at impact velocity of 100 ft/sec vs projected area for thick piles having the same shape.

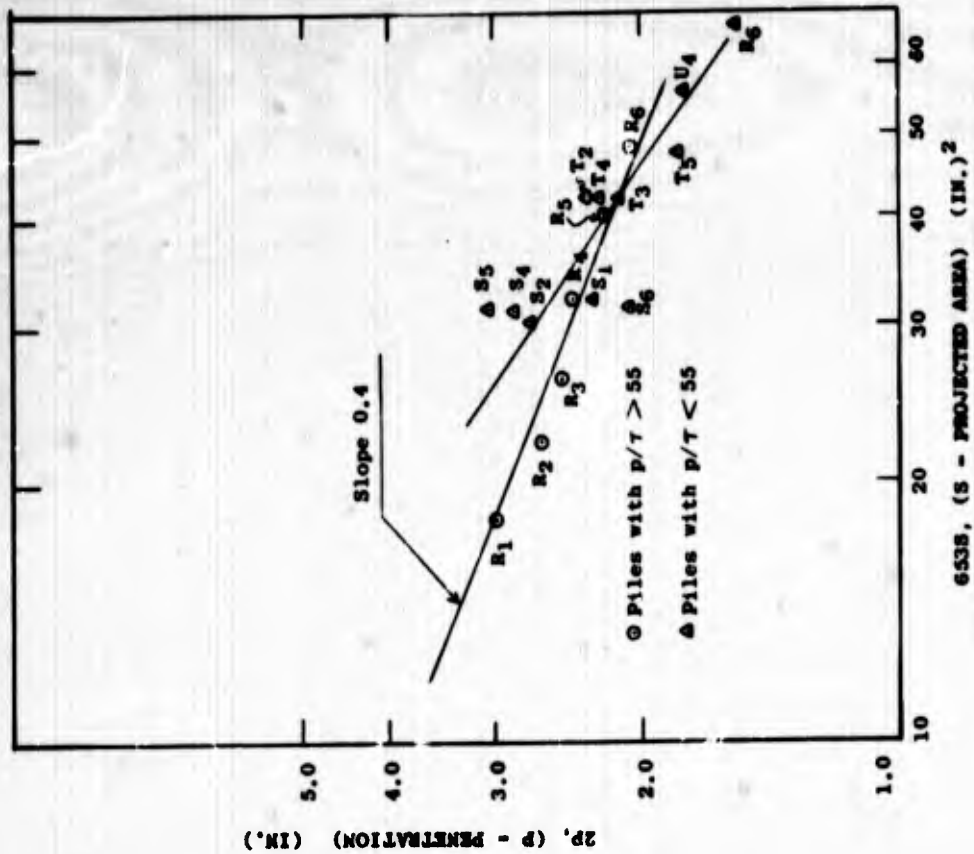
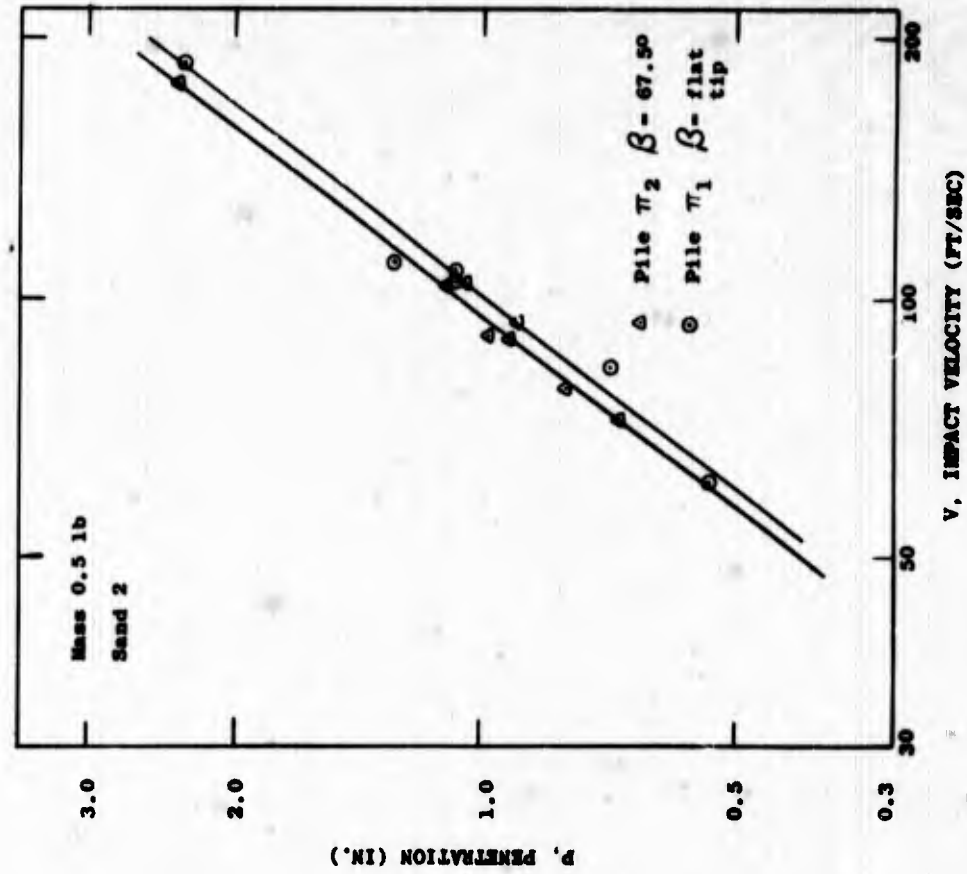
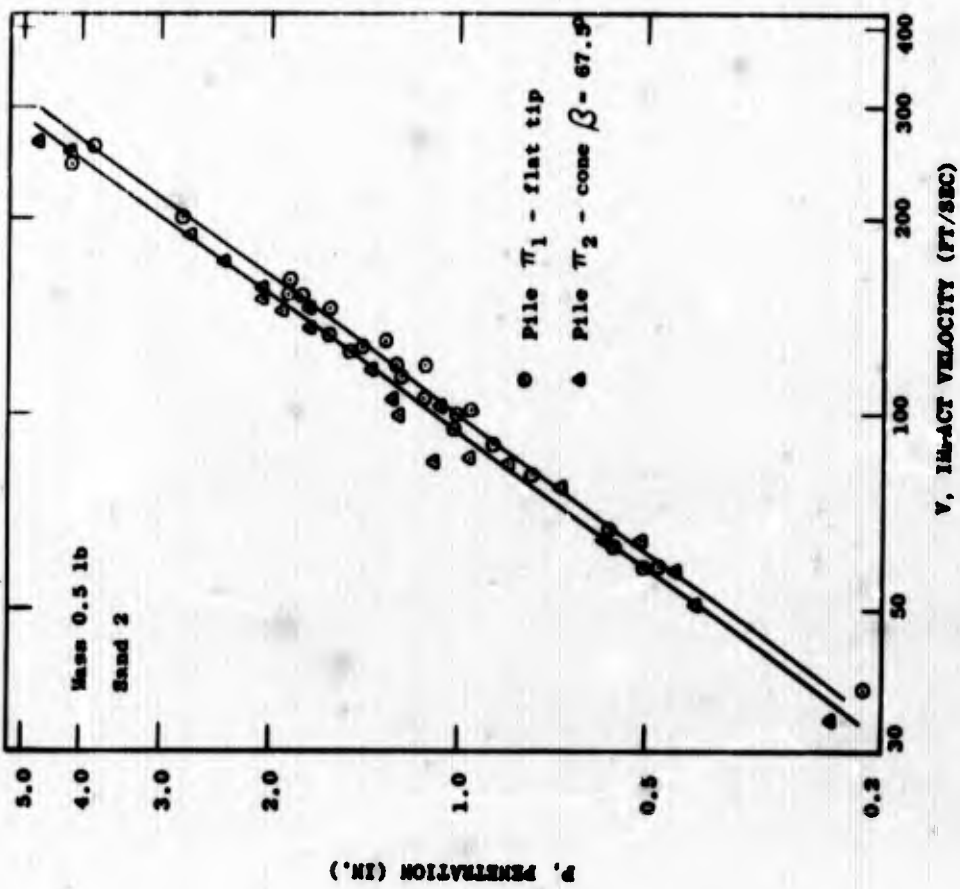


Figure 48. Penetration vs projected area for various piles.



(a)



(b)

Figure 49. Penetration vs impact velocity for piles having various tips.

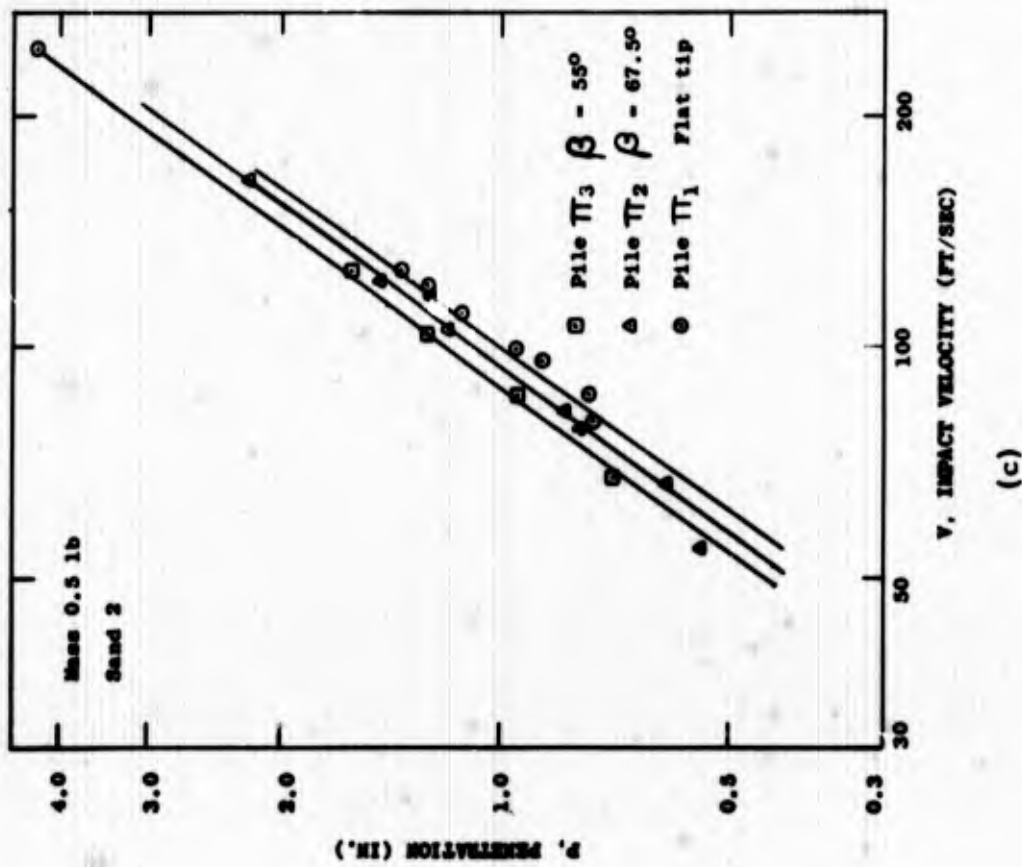
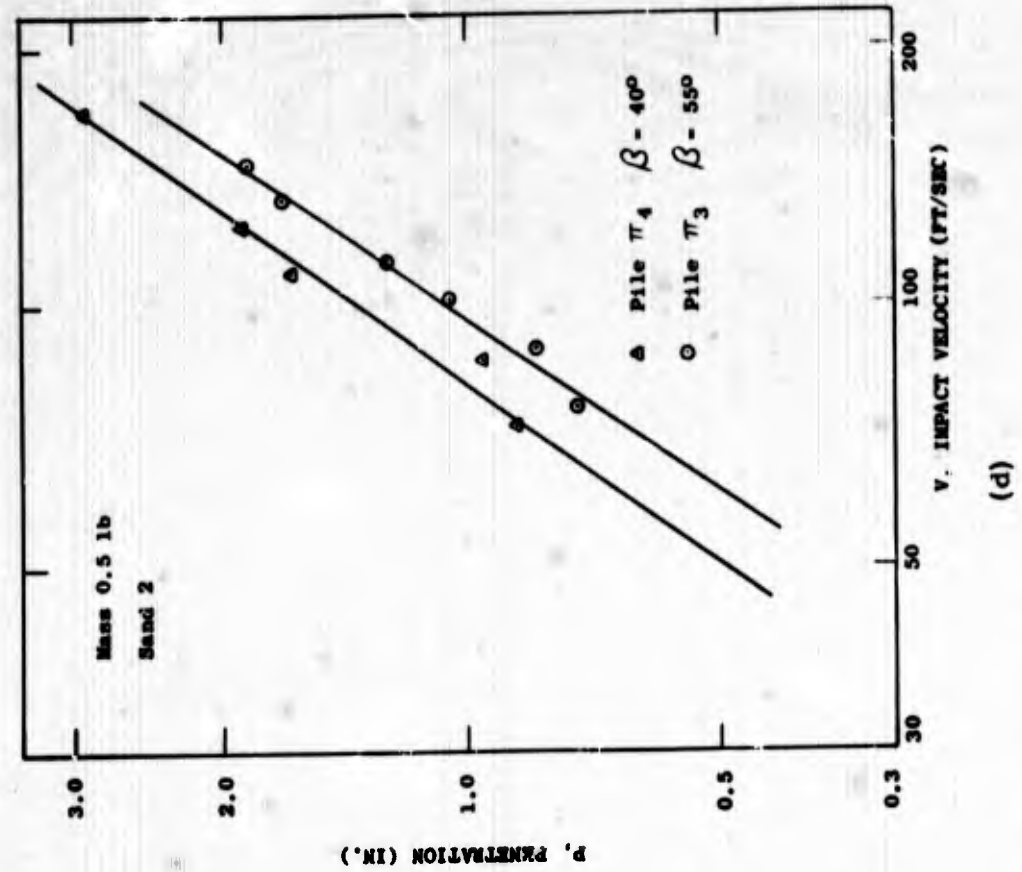


Figure 49 (Cont'd). Penetration vs impact velocity for piles having various tips.

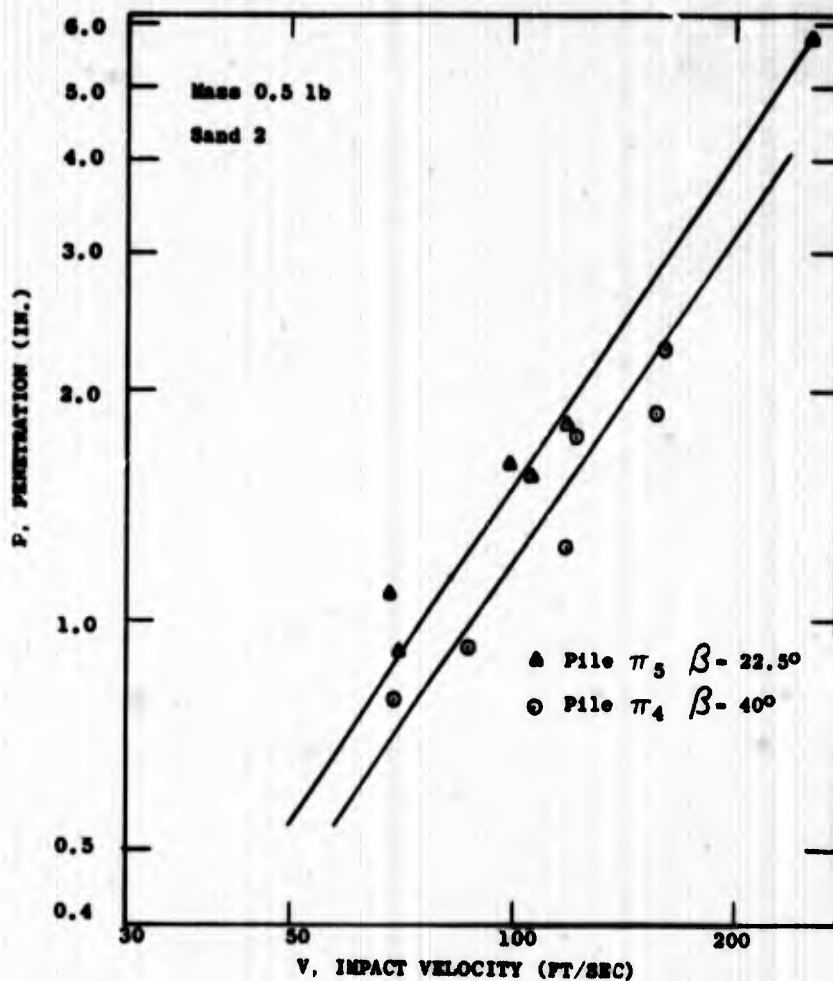


Figure 49e. Penetration vs impact velocity for piles having various tips.

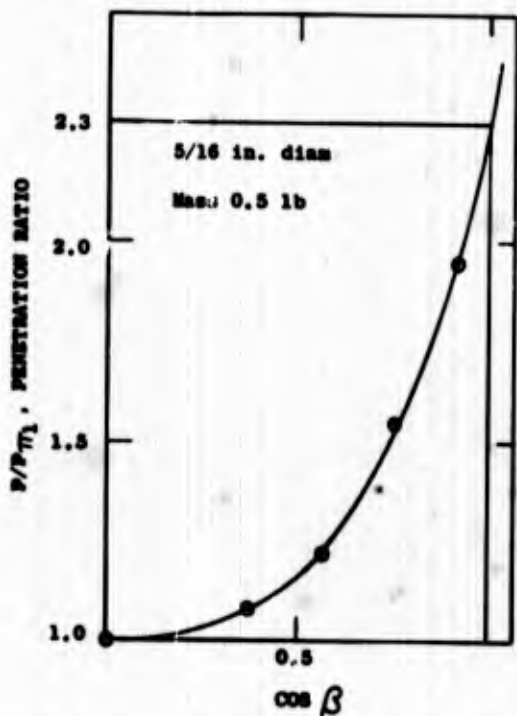


Figure 50. Penetration ratio vs cosine β (Linear scales). Conical-tipped piles.

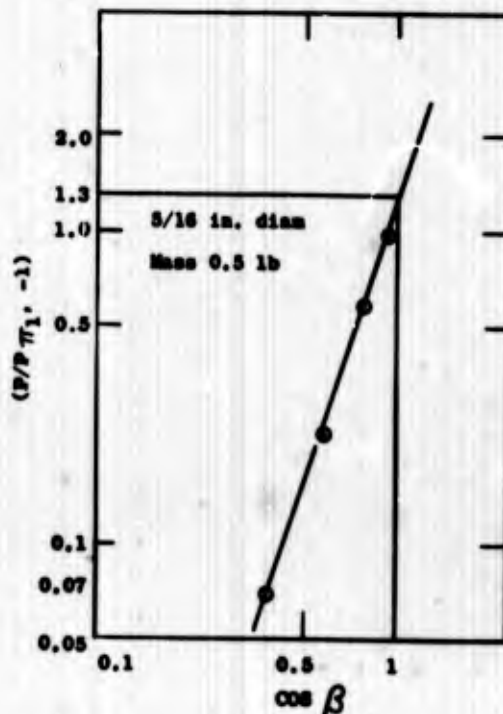


Figure 51. Penetration ratio vs cosine β (Log scales). Conical-tipped piles.

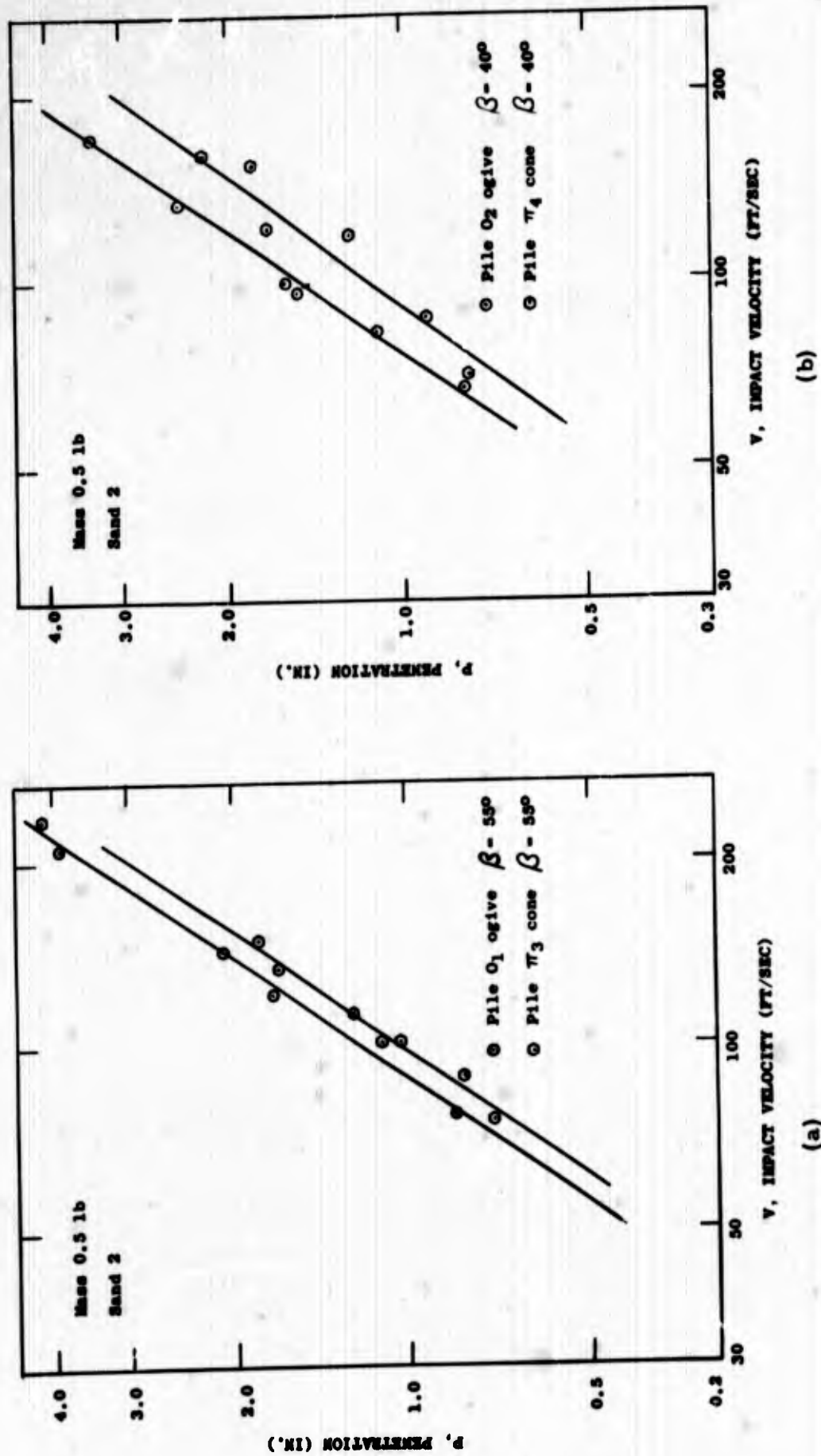


Figure 52. Penetration vs impact velocity for piles having conical and ogival tips.

It is interesting to note that a pure crushing of the material would give a resistance to penetration which is about proportional to $1/S$. This result was found in the case of spherical projectiles impacting solid media like rock (Maurer and Rinehart, 1960). The fact that a relationship $1/S^{0.8}$ is found strongly indicates that the process of penetration is intermediate between a pure crushing and a pure friction, as seen in the section on theoretical considerations.

The same comments hold for the relationships $P = K_{25} / (p\tau)^{0.4}$ and $P = K_{26} / S^{0.4}$ developed for thin piles. The lower values of these exponents are explained by the greater relative importance of the frictional forces during the penetrations of thin piles. As expected, greater penetrations were found for conically tipped piles of the same diameter having a smaller apex angle. For piles having the same diameter and apex angle, the ogival-tipped pile gave larger penetration than the conical-tipped pile.

FIELD TESTS

Experimental

Location of the tests. Field tests of rapid pile driving into permafrost were conducted at USA CRREL's Alaska Field Station, located approximately 6 miles north-northeast of Fairbanks, Alaska. The tests were conducted from 2 March through 20 March 1961. The air temperature was never above freezing during this period. The weather was cold, still, and sunny. On warmer days, minor thawing was observed on the surrounding ridges and slopes facing south, but no significant thawing occurred in the test area.

The test area was previously stripped of trees and the moss-peat mantle. The exposed frozen soil, mapped as Q.S.U. (Péwé and Faige, 1963), is undifferentiated silt of Quaternary Age occurring on lower slopes and valley bottoms physically and stratigraphically above the flood plain and in terrace deposits of the Chena-Tanana River system. These perennially frozen silt deposits are gray to black in color, unconsolidated, well sorted, containing some clay and abundant carbonaceous materials in bands, lenses, and flecks. Ice is abundant as horizontal bands, vertical veinlets, and scattered isolated masses.

Two holes were drilled in the test area to obtain core samples of permafrost. Descriptions of the cores and ground temperatures are given in Tables VIII and IX. The temperature measurements of the upper part of the holes were obtained by placing a standard alcohol thermometer in a small horizontal hole made in the wall of each drilled hole. The temperatures at the bottom of the holes were obtained by simply hanging the thermometer in a vertical position. In each case the hole was covered and the thermometer left a sufficient time to obtain a constant reading.

Table X shows the results of laboratory tests on the permafrost samples. Available information (Kitze, personal communication) indicates that the active layer of permafrost in the Fairbanks area ranges from 2 to 3.5 ft thick.

Launching stand. The launching stand used for the field tests consisted essentially of a 10.5 ft high stand and a 15 ft long launching tube (Fig. 53). The whole arrangement was skid-mounted for easy and rapid movement over the test area, and the launching tube could be tilted horizontally for easy loading of the pile-rocket assembly.

Pile-rocket assembly. The pile-rocket assembly used is illustrated in Figure 3. The same driving head was used for each series of tests on piles of the same diameter. The driving head consisted of a steel case which exactly fitted the internal diameter of a given size of piles. The rocket, in turn, exactly fitted the internal diameter of the driving head and was loosely loaded in it.

Table VIII. Description of drill hole 1. Air temperature: 12F.

<u>Depth (in.)</u>	<u>Description</u>	<u>Ground temperature (°F)</u>
0-8	Silts, gray-black, with abundant carbonaceous matter, few thin horizontal ice bands.	
12		28.0
8-12.5	Silts, gray, with some carbonaceous matter, no noticeable ice.	
12.5-19.5	Silts, gray, no carbonaceous matter, with vertical ice veinlets.	
24		29.5
19.5-25	Silts, gray-black, with abundant horizontal ice bands.	
25-29	Silts, gray, no noticeable ice.	
29-38	Silts, gray, with few thin horizontal ice bands.	
38-43	Silts, gray-black, with abundant horizontal ice bands $\frac{1}{4}$ in. to $\frac{1}{8}$ in. thick.	
43-53	Silts, gray, with few thin ice bands.	
53-59	Silts, light gray, no noticeable ice.	
59		31.5

Table IX. Description of drill hole 2. Air temperature: 10F.

<u>Depth (in.)</u>	<u>Description</u>	<u>Ground temperature (°F)</u>
0-10	Silts, gray-black, with abundant carbonaceous matter. No noticeable ice.	
12		27.5
10-18	Silts, gray, with some carbonaceous matter, few scattered ice masses.	
24		30.0
18-33	Silts, light gray, with abundant horizontal ice bands.	
33-57	Silts, gray, no noticeable ice.	
57		31.0

Table X. Analyses of permafrost samples from drill holes 1 and 2.

	Drill hole					
	2	1	1	1	2	2
	31-37"	43-49"	4½-10½"	19½-25½"	18-24"	3-9"
Unit wt (wt/cm ³ of permafrost in natural state as received)	1.41 g/cm ³	1.45 g/cm ³	1.03 g/cm ³	1.25 g/cm ³	1.29 g/cm ³	0.75 g/cm ³
Moisture content (% of total original weight)	43.87	42.78	85.57	63.80	58.21	92.88
Unit wt of soil skeleton (wt of dried solids/cm ³ permafrost in natural state)	0.79 g/cm ³	0.83 g/cm ³	0.13 g/cm ³	0.45 g/cm ³	0.54 g/cm ³	0.59 g/cm ³
Specific gravity						
Trial 1	2.33	2.43	0.58	1.88	1.95	0.48
Trial 2	2.56	2.52	0.57	1.93	2.14	0.33
Trial 3	2.47	2.49	0.61	1.84	2.01	0.41
Trial 4	2.39	-----	-----	-----	-----	-----
Average specific gravity	2.43	2.48	0.62	1.88	2.03	0.41
Organic material (percentage of wt of dried solids)	-----	-----	44.23	7.37	-----	-----

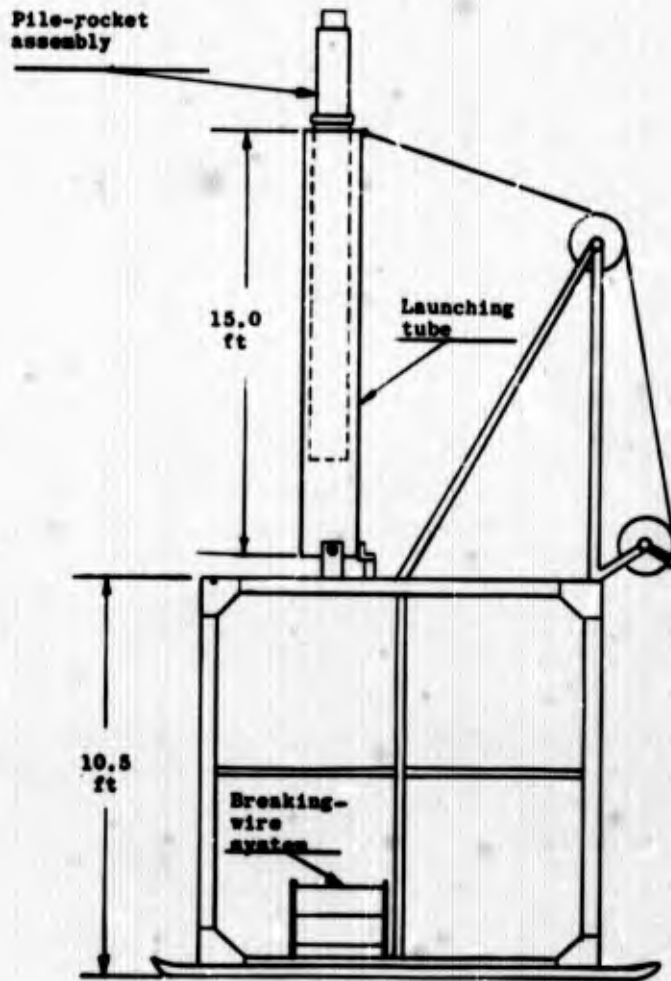


Figure 53. Arrangement of the launching stand.

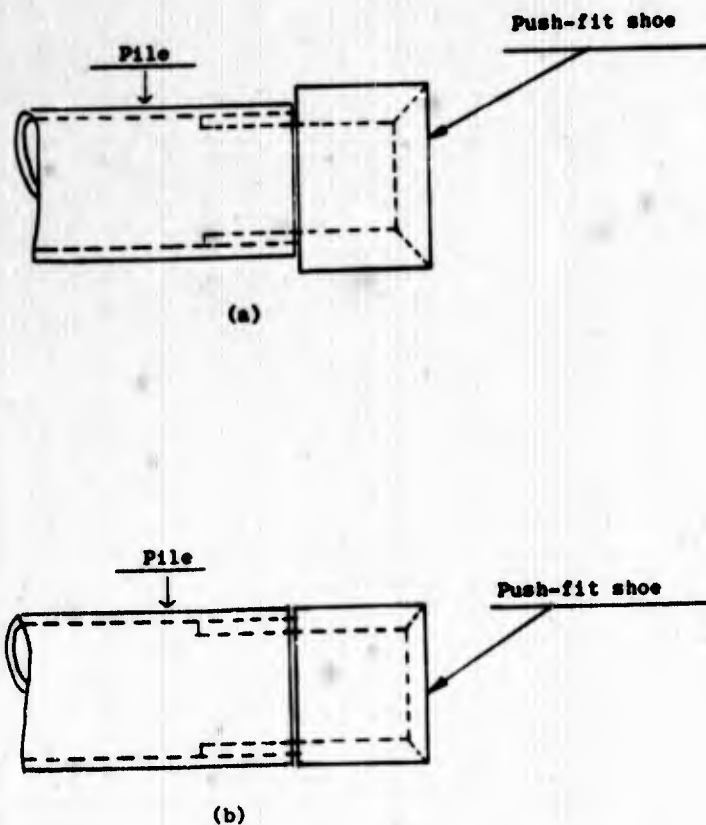


Figure 54. Reinforcement shoes.

An inert-loaded M-17-A1 rocket with the following characteristics (U. S. Army, 1950) was used in the tests:

Length unfused	27.8 in.
Mass	40.1 lb
Maximum velocity	940 ft/sec
Temperature limits of operation	-20F to 120F
Burning time at -25F	0.34 sec
Burning time at 120F	0.10 sec
Mass of propellant	4.81 lb

A double-base propellant having a linear rate of burning was used in the rocket.

Velocity measurement system. The impact velocities of the piles were measured by a breaking-wire system, similar to that used in the laboratory. Figure 53 shows the position of the system. Glass tubes, each 1 ft apart and containing a tiny strip of aluminum foil, played the role of breaking wires. Hewlett-Packard counters, type 523-B, were used to measure the time interval between each successive electrical impulse given by the velocity measurement system.

Results

Sixty-nine piles were driven into the permafrost during the field tests; Appendix G gives the complete firing record. The piles used were 2, 4, 6, and 8 in. in normal diameters, and the wall thickness varied from 0.22 to 0.43 in. Most of the piles were 5.0 or 5.5 ft long but a few of the 2 in. diam piles were longer.

Some of the 8 in. diam piles collapsed upon impact with permafrost because of wall thinness. This could be avoided by using piles with thicker walls or by using reinforcement shoes. A reinforcement shoe used during some of the field tests (Fig. 54a) did not give satisfactory results because bond with the permafrost was insufficient. Figure 54b shows a corrected type of reinforcement shoe which should give better results.

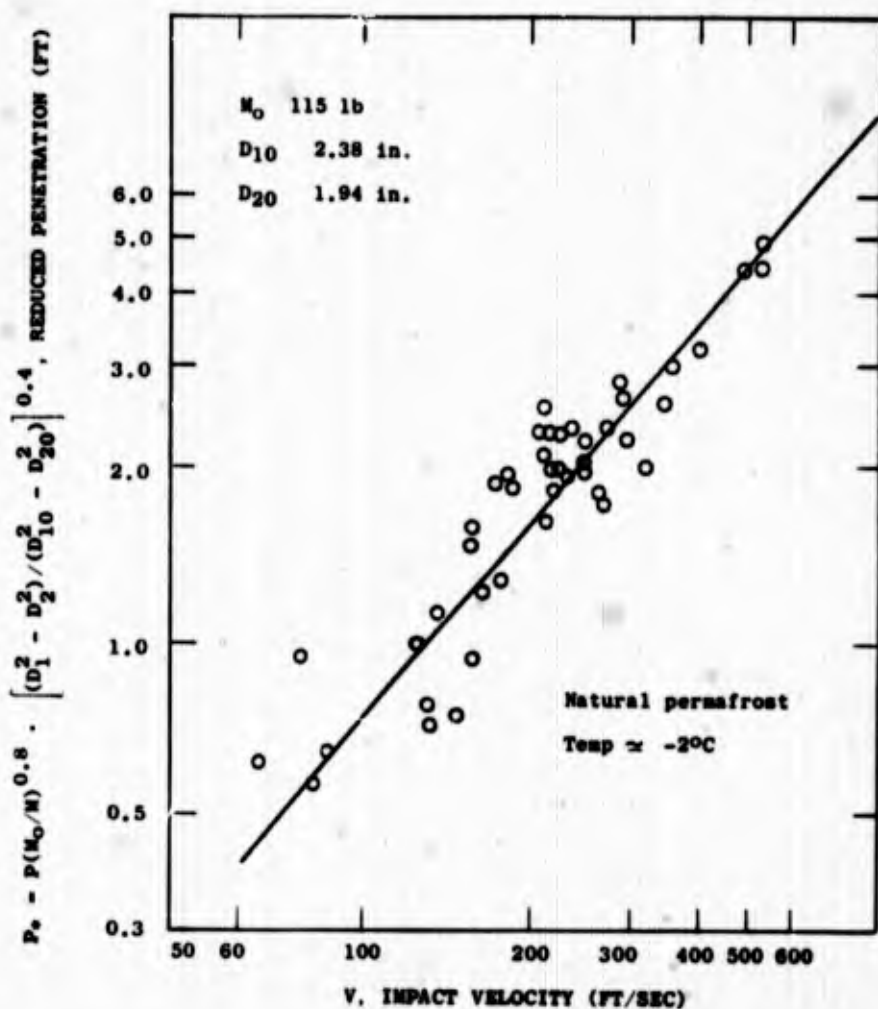


Figure 55. Reduced penetration vs impact velocity for field test results.

An attempt was made to extract the piles to check end damage, but they were so firmly bonded that a 25-ton mobile crane could not extract them. Successful pile extraction was possible only by digging a hole around the pile.

The penetrations reduced according to eq 10 are plotted in Figure 55 versus impact velocity. The use of eq 10 was found quite satisfactory for reducing the penetrations of the various piles tested in the natural permafrost. The penetrations obtained during the field tests were also reduced with a more commonly encountered relationship of the type,

$$P^* = P (M_0/M) [(D_1^2 - D_2^2)/(D_{10}^2 - D_{20}^2)] \quad (56)$$

and plotted versus the impact velocity. The graph obtained with the penetrations reduced according to eq 56 indicated no power dependence between reduced penetration and impact velocity. Figure 55 shows that the velocity power dependence of the reduced penetration is close to 1.2 for the field test results. The difference from the average value of 1.5 found in Phase I of laboratory work can be explained in the following way. As pointed out before, the mass power dependence of penetration approaches unity for small penetrations. For thin, hollow, circular piles, the average value of P/D_1 , the ratio of penetration to external diameter, is about twice as large for the laboratory tests as for the field tests. Reduction of field-test penetrations according to a mass power dependence close to unity would increase the slope of the line in Figure 55 to give a velocity power dependence closer to what was found in

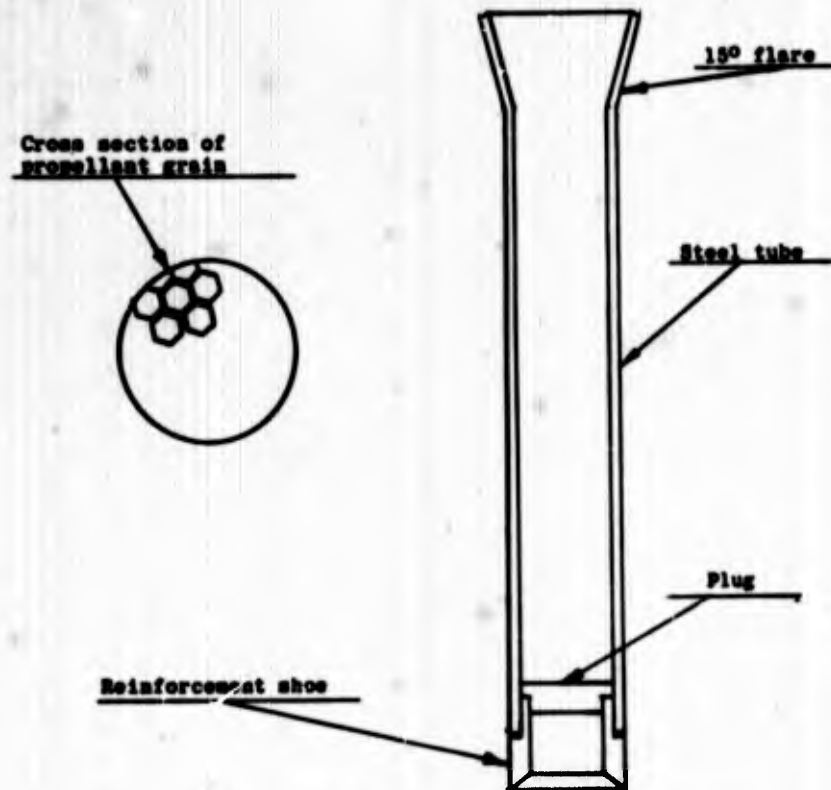


Figure 56. Integrated pile-rocket assembly.

Phase I. Slopes smaller than 1.5 were found in some of the laboratory tests as well. As was pointed out in the theoretical considerations, the slope is largely controlled by the relative magnitude of various forces acting on the pile during the penetration process.

Proposal for an integrated pile-rocket

It is believed that piles should be driven at least 6 to 8 ft into permafrost to avoid heaving caused by thawing and freezing of the active layer. A 6 in. nominal diameter pile is considered to be a reasonable size for a foundation pile. From these considerations and from field-test results, it was found that the M-17-A1 rocket had insufficient thrust characteristics. To avoid the collapsing of piles, as had happened during the field tests, a pile having the following characteristics was believed satisfactory for practical operations. The pile should be 10 ft long; its external and internal diameters should be, respectively, 6.63 and 5.5 in.; its approximate mass should be 400 lb, including the extra mass of the rocket. On the basis of field test results reduced by eq 10, the rocket should have about a 100,000-lb thrust and an 80-msec burning duration to achieve 6 to 8 ft of penetration with the above pile. To drive a 10-ft pile would require a 6 ft long rocket. Considering the 16-ft length of such a pile-rocket assembly and a necessary standoff position of about 25 ft, various technical difficulties are anticipated for the launching operations. Moreover, a rocket having 100,000-lb thrust and 80-msec burning duration was not commercially available.

Consequently, a study was made which led to the design of an integrated pile-rocket assembly (Reliance Rocket Corporation, 1962). The essential features are given in Figure 56. This self-powered pile consists, primarily, of a steel tube filled with a solid propellant. To obtain a short burning duration, the propellant can be thinly coated on a honeycomb matrix. At one end of the steel tube, the penetrating end of the pile, a reinforcement shoe, similar to the one shown in Figure 54b, is fixed. A plug, free to move upward inside the tube, is held in place by the reinforcement shoe. This plug prevents the combustion gases from escaping in the direction of pile movement. Because of the short burning duration, no constricted nozzle is necessary to obtain the proper thrust.

Upon ignition of the propellant, a high thrust of short duration is imparted to the pile. If all the propellant is burned at the time of impact with permafrost and the proper impulse is given to the arrangement, the integrated pile-rocket assembly behaves as a hollow pile penetrating permafrost under its own kinetic energy. This type of arrangement can be used to obtain a 100,000-lb thrust and a burning duration of 80 msec.

CONCLUSIONS AND RECOMMENDATIONS

This investigation indicates that the use of rockets for driving of piles is technically feasible. It is estimated that a 6 in. nominal diameter pile of 0.56 in. wall thickness could be driven 6 to 8 ft into permafrost by a 100,000 lb thrust rocket having 80 msec burning duration. To resist collapse upon impact with the permafrost, the pile should have either a reinforcement shoe or a minimum wall thickness of 0.56 in.

A design of an integrated pile-rocket assembly meeting the above requirements is proposed. Its estimated cost in small lots is \$1200. The interesting features of this pile-rocket assembly are the following: The length of the pile is reduced, thus facilitating field operations. The shoe, which is an integral part of the pile-rocket assembly, serves as reinforcement against pile collapse. However, the design of this pile-rocket assembly should be completely developed and a series of field tests conducted. The field tests would provide technical information for further development.

The laboratory program in which model piles were driven into artificial permafrost gave a good picture of the mechanics of penetration of piles into permafrost and the relationships developed proved useful for reducing field-test results. Direct and detailed application of these relationships to predict field-test performance was not expected. The laboratory results do, however, form a good basis for a future extensive program of field tests, during which the various parameters could be studied over a wider range. This program would show whether laboratory relationships are directly applicable to field test results or in what way they should be modified.

LITERATURE CITED

- Charest, J., Duler, P., and Rinehart, J. S. (1961) Experimental model studies of pile driving into permafrost, Colorado School of Mines Research Foundation, Inc., Technical Report.
- Comings, E. W. (1940) English engineering units and their dimensions, Ind. Eng. Chem., vol. 32, p. 984-987.
- Kitze, F. F., Personal communication, Project engineer, USA CRREL Alaska Field Station, Fairbanks, Alaska.
- Maurer, W. C. and Rinehart, J. S. (1960) Impact crater formation in rock, Journal of Applied Physics, vol. 31, no. 7, p. 1247-1252.
- Palmer, F. (1949) What about friction?, American Journal of Physics, vol. 17, no. 4, p. 181-187, 327-342.
- Péwé, T. L. and Paige, R. A. (1963) Frost heaving of piles with an example from Fairbanks Alaska, U. S. Geological Survey, Bulletin-J, p. 333-407.
- Reliance Rocket Corporation (1962) The feasibility of rocket propulsion systems for driving steel piles in permafrost, Report No. RRC 62-2.
- Rouse, H. (1946) Elementary mechanics of fluids. New York: Wiley.
- U. S. Army, Headquarters (1950), TM9-1950.

BLANK PAGE

Table AIII. Screen analysis of Fine Ottawa Sand

Mesh	Aperture (μ)	Tyler #	Direct % Weight Retained	Cumulative % Weight Finer
	840	+ 20	0.6	100.0
	589	- 20 + 28	1.6	99.4
	420	- 28 + 35	29.0	97.8
	297	- 35 + 48	42.2	68.8
	246	- 48 + 60	11.8	26.6
	210	- 60 + 65	6.2	14.8
	177	- 65 + 80	3.9	8.6
	105	- 80 + 150	4.5	4.7
		-150	0.2	0.2
			100.0	

APPENDIX A

Data on artificial permafrost

Table AI. Screen analysis of Mausau Sand 3/O, Sand 1

Mesh	Aperture (μ)	Tyler #	Direct % Weight Retained	Cumulative % Weight Finer
	177	+ 80	.7	100
	105	- 80 + 150	3.5	99.2
	74	-150 + 200	23.3	95.6
	62	-200 + 250	8.7	72.5
	53	-250 + 270	17.7	63.8
	43	-270 + 325	17.7	46.2
		-325	28.4	28.4
			100.0	

Table AII. Screen analysis of Vausau Sand 3/O, Sand 2

Mesh	Aperture (μ)	Tyler #	Direct % Weight Retained	Cumulative % Weight Finer
	177	+ 80	0	100.0
	105	- 80 + 150	4.6	95.6
	74	-150 + 200	22.7	72.9
	62	-200 + 250	9.8	63.1
	53	-250 + 270	14.0	49.1
	43	-270 + 325	17.4	31.7
		-325	31.7	31.7
			100.2	

Table AIV. Screen analysis of Ground Silica

Mesh	Aperture (μ)	Tyler #	Direct % Weight Retained	Cumulative % Weight Finer
	177	+ 80	0	100.0
	105	- 80 + 150	3.0	97.0
	74	-150 + 200	12.8	84.0
	62	-200 + 250	11.3	73.0
	53	-250 + 270	45.8	27.0
	43	-270 + 325	21.6	5.5
		-325	5.5	5.5
			100.0	

Because of the difficulty of screening samples of Bauxite and Golden soil, the results of their screen analyses are omitted.

Table AV. Average water content of the permafrost obtained with various materials at saturation

Material	Water content Weight percent (%)
Wausau Sand, Sand 1	22
Wausau Sand, Sand 2	24
Fine Ottawa Sand	21
Ground Silica	19
Golden Soil	20
Bauxite	28

Table AVI. Average density of the permafrost obtained with various materials at saturation

Material	Density (g/cm ³)
Wausau Sand, Sand 1	1.79
Wausau Sand, Sand 2	1.75
Fine Ottawa Sand	1.89
Ground Silica	1.92
Golden Soil	1.95
Bauxite	1.73

Measurements of dilatational wave velocity were made with permafrost obtained from Sand 1 and gave an average value of 12,700 ft./sec. From these measurements, an estimated value of Young's modulus was found to be 2.9×10^6 psi for this artificial permafrost.

APPENDIX B

Characteristic of piles used in laboratory and field work

Table BI. Piles used during Phase I and during the first investigation of Phase II. Steel piles

External diameter D ₁ (in.)	Internal diameter D ₂ (in.)	Shape of the tip
*7/16	6/16	flat
*7/16	5/16	"
7/16	4/16	"
7/16	0	"
*6/16	5/16	"
*6/16	4/16	"
5/16	4/16	"
5/16	3/16	"
1.0	0.83	"

During the first investigation of Phase II, a brass pile, 7/16 in. and 5/16 in. in external and internal diameter was used also.

*Used during 1st investigation of Phase II.

Table III. Steel piles used during the second investigation of Phase II. a and b are defined at the right. D₁ and D₂ are defined in Table II. p is perimeter of the cross section of the pile.

Pile	Mass M (lb)	Shape of pile	2a (in.)	2b (in.)	D ₁ (in.)	D ₂ (in.)	p (in.)	Shape of the tip
S1	0.322	rect.	0.137	0.359			0.960	flat
S2	"	"	0.168	0.376			0.898	"
S3	"	square	0.218	0.218			0.872	"
S4	"	circ.			0.246		0.772	"
S5	"	cross shape	0.036	0.444			1.776	"
S6	"	cross shape	0.094	0.304			1.216	"
T1	"	rect.	0.137	0.460			1.234	"
T2	"	"	0.167	0.381			1.066	"
T3	"	square	0.254	0.254			1.016	"
T4	"	circ.			0.296		0.896	"
U4	"	circ.			0.330		1.038	"
R1	0.500	hollow circ.			5/16	4/16	1.768	"
R2	"	"			6/16	5/16	2.160	"
R3	"	"			7/16	6/16	2.555	"
R4	"	"			5/16	3/16	1.570	"
R5	"	"			6/16	4/16	1.963	"
R6	"	"			7/16	5/16	2.360	"
R6	"	"			7/16	4/16	2.155	"
R7	"	circ.			7/16	4/16	1.374	"
T71	0.500	circ.			5/16		0.982	conical
T72	"	"			"		"	"
T73	"	"			"		"	"
T74	"	"			"		"	"
T75	"	"			"		"	"
O1	"	"			"		"	ogival
O2	"	"			"		"	"
D1	3.670	cross shape	0.222	0.994			3.636	flat
T5	0.460	"	0.693	0.436			1.744	"
R2	3.100	hollow circ.			1.000	0.83	5.750	"

The quantity 2a is the side of the cross section of a square pile. The quantities 2a and 2b are the sides of the cross section of a rectangular pile. The quantities 2a and 2b are also used for a cross-shaped pile. See sketch below.

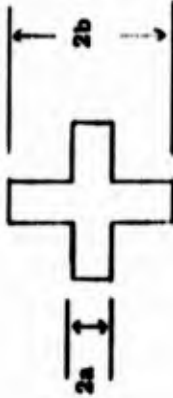


TABLE IIII. Piles used in field tests. Steel piles.

External diameter D ₁ (in.)	Internal diameter D ₂ (in.)	Shape of the tip
2.37	1.93	flat
4.50	4.02	"
4.50	3.82	"
6.62	6.06	"
6.62	5.76	"
8.62	8.18	"
8.62	8.05	"

APPENDIX C

Firing data of Phase I

Table CI. Steel circular pile, ext. diam 7/16 in.,
int. diam 5/16 in. Fine Ottawa Sand

Mass M (lb)	Penetration P (in.)	Impact velocity V (ft/sec)
0.500	5.00	392
"	3.56	326
"	2.75	245
"	2.50	259
"	2.50	282
"	2.50	262
"	2.13	224
"	2.00	237
"	2.00	225
"	1.88	185
"	1.63	187
"	1.44	171
"	1.19	155

Table CII. Steel circular pile, ext. diam 7/16 in.,
int. diam 5/16 in. Pure ice.

Mass M (lb)	Penetration P (in.)	Impact velocity V (ft/sec)
0.500	8.13	203
"	6.75	173
"	4.75	150
"	4.50	138
"	4.25	131
"	3.37	118
"	3.13	105
"	2.60	97
"	2.38	89
"	2.31	95

(continued)

Table CII
(continued)

Mass M (lb)	Penetration P (in.)	Impact velocity V (ft/sec)
0.500	2.19	82
"	1.25	60
"	0.94	50
"	0.90	51
"	0.85	49

Table CIII. Steel circular pile, ext. diam 7/16 in.,
int. diam 5/16 in. Baunitz

Mass M (lb)	Penetration P (in.)	Impact velocity V (ft/sec)
0.500	5.50	283
"	5.25	277
"	4.62	246
"	2.94	172
"	2.90	186
"	1.94	141
"	1.31	108

Table CIV. Steel circular pile, ext. diam 7/16 in.,
int. diam 5/16 in. Unsaturated Sand 1

Mass M (lb)	Penetration P (in.)	Impact velocity V (ft/sec)	Mass M (lb)	Penetration P (in.)	Impact velocity V (ft/sec)
0.500	4.75	345	3.05	11.75	250
"	4.75	333	"	6.12	155
"	3.75	303	"	3.00	90
"	3.13	250	1.65	5.75	224
"	3.06	240	"	3.88	175
"	2.13	212	"	2.63	128
"	1.75	177			
"	1.13	124			

Table CV
(continued)

Table CVI. Steel circular pile, ext. diam 7/16 in.,
int. diam 6/16 in. Sand 1

Mass M (lb)	Penetration P (in.)	Impact velocity V (ft/sec)	Mass M (lb)	Penetration P (in.)	Impact velocity V (ft/sec)
5.22	13.38	241	0.500	5.90	290
"	10.88	196	"	5.00	240
"	8.00	155	"	4.00	198
4.25	15.50	282	"	3.75	218
"	8.13	169	"	3.50	200
"	2.88	75	"	3.22	188
3.10	17.00	355	"	3.15	185
"	14.88	305	"	3.10	179
"	10.50	215	"	2.98	170
"	9.75	218	"	2.43	150
"	8.75	183	"	2.12	140
"	8.00	187	"	2.18	135
"	6.00	151	"	2.00	128
"	5.00	130	"	1.78	126
"	3.75	113	"	1.38	110
"	1.50	62	"	1.32	103
			"	1.23	96
			"	0.64	66
			"	0.50	56

(continued)

(continued)

Table CVI
(continued)

Mass M (lb)	Penetration P (in.)	Impact velocity V (ft/sec)	Mass M (lb)	Penetration P (in.)	Impact velocity V (ft/sec)
0.430	7.25	366	0.287	1.75	166
"	2.82	193	"	1.69	150
"	2.75	190	"	1.50	141
"	2.13	161	"	1.13	125
0.362	5.38	348	"	1.09	123
"	2.63	213	"	0.88	109
"	1.38	128	"	0.78	99
"	1.25	123	"	0.71	97
0.347	8.00	433	"	0.61	85
"	5.25	347	0.214	3.96	290
"	4.75	300	"	3.44	263
"	4.00	238	"	3.25	256
"	3.81	247	"	3.25	328
"	2.50	173	"	2.69	224
"	1.63	138	"	2.06	190
"	1.19	110	"	2.00	183
"	0.63	75	"	1.88	198
"	0.44	62	"	1.63	188
0.287	5.63	350	"	1.00	122
"	4.63	332	"	0.69	90
"	4.09	316			
"	3.90	277			
"	3.38	233			
"	3.13	230			
"	2.82	223			
"	2.38	207			
"	2.31	181			
"	2.45	206			
"	2.14	187			
"	2.13	174			
"	2.06	183			
"	2.00	176			
"	1.81	169			

(continued)

Table CVII. Steel circular pile, ext. diam 7/16.,
int. diam 5/16 in. Sand 1

Mass M (lb)	Penetration P (in.)	Impact velocity V (ft./sec)	Mass M (lb)	Penetration P (in.)	Impact velocity V (ft./sec)
0.597	4.78	260	0.500	3.05	210
"	4.03	236	"	2.96	205
"	3.97	212	"	2.80	209
"	2.78	217	"	2.75	195
"	2.78	166	"	2.72	190
"	0.32	46	"	2.63	188
0.550	4.34	240	"	2.60	197
"	3.27	191	"	2.57	183
"	0.40	46	"	2.52	188
0.500	6.90	368	"	2.51	198
"	6.00	340	"	2.39	184
"	5.95	332	"	2.36	170
"	5.85	330	"	2.31	169
"	5.25	300	"	2.13	164
"	5.05	315	"	2.00	156
"	5.00	300	"	1.95	150
"	4.89	305	"	1.97	152
"	4.87	280	"	1.92	143
"	4.45	268	"	1.87	150
"	4.16	282	"	1.75	141
"	4.00	260	"	1.67	140
"	4.00	256	"	1.56	136
"	3.97	241	"	1.57	133
"	4.00	237	"	1.50	130
"	4.00	229	"	1.43	129
"	3.95	229	"	1.32	126
"	3.85	258	"	1.21	109
"	3.75	252	"	1.13	117
"	3.75	255	"	1.12	108
"	3.75	239	"	1.13	103
"	3.68	240	"	1.07	102
"	3.63	247	"	0.89	100
"	3.50	230	"	0.86	90
"	3.38	212	"	0.85	86
"	3.32	215	"	0.87	82
"	3.25	207	"	0.75	76
"	3.20	226	"	0.74	84
				0.60	69

(continued)

Table CVII
(continued)

Mass M (lb)	Penetration P (in.)	Impact velocity V (ft./sec)
0.460	4.37	307
"	3.23	220
"	2.15	168
"	2.34	202
"	1.84	160
"	1.49	147
"	1.03	103
"	0.96	115
"	0.78	78
0.370	5.75	350
"	4.70	325
"	4.50	307
"	3.96	313
"	3.41	296
"	2.25	220
"	2.16	202
"	2.13	197
"	2.06	184
"	1.84	183
"	1.71	179
"	1.49	158
"	1.25	135
"	1.21	144
"	1.19	143
"	0.96	118
"	0.60	87
"	0.41	70
"	0.41	61
0.205	2.94	327
"	2.97	340
"	1.57	204
"	1.38	196
"	1.34	200
"	1.13	172
"	0.88	139
"	0.60	120
"	0.50	100

Table CVIII. Steel circular pile, ext. diam 7/16 in.,
int. diam 4/16 in. Sand 1.

Mass M (lb)	Penetration P (in.)	Impact velocity V (ft./sec)
0.500	5.00	350
"	4.35	305
"	4.00	290
"	3.90	320
"	3.20	282
"	3.00	270
"	2.50	242
"	2.50	220
"	2.08	200
"	2.08	192
"	1.95	183
"	1.88	190
"	1.77	191
"	1.67	189
"	1.38	145
"	1.37	138
"	1.31	141
"	1.20	142
"	1.14	138
"	1.07	127
"	1.00	133
"	1.00	128
"	0.89	116
"	0.75	100
"	0.76	99
Steel pile, ext. diam 7/16 in., int. diam 0 in.		
"	1.33	151
"	2.25	250
"	3.70	310

Table CIX. Steel circular pile, ext. diam 6/16 in.,
int. diam 5/16 in. Sand 1.

Mass M (lb)	Penetration P (in.)	Impact velocity V (ft./sec)	Mass M (lb)	Penetration P (in.)	Impact velocity V (ft./sec)
0.500	7.00	302	0.280	5.90	366
"	5.71	255	"	3.00	257
"	5.56	263	"	2.75	233
"	5.35	264	"	2.27	210
"	5.10	248	"	2.16	190
"	5.00	241	"	1.88	176
"	4.81	234	"	1.46	138
"	4.45	228	0.190	4.50	375
"	3.70	205	"	2.74	289
"	3.55	191	"	2.30	244
"	3.38	186	"	2.18	250
"	3.00	180	"	1.72	195
"	2.83	167	"	1.66	201
"	2.26	134	0.100	3.00	436
"	2.19	138	"	1.82	300
"	2.18	139	"	1.72	289
"	1.75	125	"	1.68	284
"	1.75	120	"	1.59	274
"	1.61	114	"	1.58	266
"	1.50	113	"	1.09	209
"	1.50	108	0.050	1.90	403
"	1.14	95	"	1.23	302
0.380	5.50	295	Steel pile, ext. diam 6/16 in., int. diam 4/16 in.		
"	5.31	289	0.500	5.20	290
"	4.25	250	"	3.50	230
"	3.65	220	"	3.00	200
"	3.25	200	"	2.30	160
"	3.00	205	"	1.51	120
"	2.45	174	"	0.83	93
"	2.40	179	"	0.58	62
"	2.25	162			
"	2.06	152			
"	2.04	157			
"	1.74	141			
"	1.73	136			
"	1.44	123			

(continued)

Table CX. Steel circular pile, ext. diam 5/16 in.,
int. diam 4/16 in. Sand 1.

Mass M (lb)	Penetration P (in.)	Impact velocity V (ft./sec)
0.500	6.50	265
"	5.00	225
"	3.90	193
"	3.00	153
"	2.70	148
"	2.12	131
"	1.93	118
"	1.75	110
"	1.03	82
"	0.92	73
"	0.69	60
0.395	4.25	242
"	2.78	188
"	2.25	165
"	1.69	128
0.310	3.00	214
"	2.70	212
"	2.25	179
"	1.87	154
"	1.38	138
0.225	3.45	286
"	2.62	234
"	2.63	235
"	2.06	192
"	1.70	165
0.161	3.00	300
"	2.82	299
"	2.00	240
"	1.50	186
"	0.87	123

Table CXI. Steel circular pile, ext. diam 5/16 in.,
int. diam 3/16 in. Sand 1.

Mass M (lb)	Penetration P (in.)	Impact velocity V (ft./sec)
0.500	6.40	285
"	4.10	225
"	3.80	210
"	3.45	207
"	2.63	175
"	1.55	120
"	1.50	115
"	1.46	108

APPENDIX D

Firing data of the first investigation of Phase II.

Table DI. Steel circular pile, ext. diam 7/16 in., int. diam 6/16 in., mass 0.5 lb. Sand 1. Impact velocity, 240 ft./sec.

Penetration P_1 (in.)	Time t (msec)
0.000	0.0
0.278	0.1
0.557	0.2
0.820	0.3
1.080	0.4
1.340	0.5
1.585	0.6
1.825	0.7
2.060	0.8
2.285	0.9
2.490	1.0
2.690	1.1
2.885	1.2
3.075	1.3
3.245	1.4
3.420	1.5
3.575	1.6
3.725	1.7
3.870	1.8
4.005	1.9
4.140	2.0
4.260	2.1
4.370	2.2
4.465	2.3
4.565	2.4
4.650	2.5
4.730	2.6
4.790	2.7
4.845	2.8
4.890	2.9
4.930	3.0
4.960	3.1
4.980	3.2
4.990	3.3
5.000	3.4

Table DII. Steel circular pile, ext. diam 7/16 in., int. diam 6/16 in., mass 0.5 lb. Sand 1. Impact velocity, 198 ft./sec.

Penetration P_1 (in.)	Time t (msec)
0.000	0.0
0.230	0.1
0.455	0.2
0.680	0.3
0.900	0.4
1.105	0.5
1.300	0.6
1.505	0.7
1.695	0.8
1.870	0.9
2.045	1.0
2.200	1.1
2.360	1.2
2.505	1.3
2.650	1.4
2.780	1.5
2.910	1.6
3.030	1.7
3.140	1.8
3.240	1.9
3.340	2.0
3.425	2.1
3.505	2.2
3.575	2.3
3.640	2.4
3.703	2.5
3.760	2.6
3.810	2.7
3.855	2.8
3.895	2.9
3.925	3.0
3.955	3.1
3.975	3.2
3.985	3.3
4.000	3.4

Table DIII. Steel circular pile, ext. diam 7/16 in., int. diam 6/16 in., mass 0.5 lb. Sand 1. Impact velocity, 188 ft/sec.

Penetration P_1 (in.)	Time t (msec)
0.000	0.0
0.225	0.1
0.440	0.2
0.650	0.3
0.855	0.4
1.055	0.5
1.250	0.6
1.425	0.7
1.600	0.8
1.760	0.9
1.920	1.0
2.065	1.1
2.205	1.2
2.335	1.3
2.455	1.4
2.565	1.5
2.670	1.6
2.765	1.7
2.855	1.8
2.930	1.9
3.000	2.0
3.060	2.1
3.115	2.2
3.150	2.3
3.185	2.4
3.205	2.5
3.220	2.6

Table DIV. Steel circular pile, ext. diam 7/16 in., int. diam 6/16 in., mass 0.5 lb. Sand 1. Impact velocity, 184 ft/sec.

Penetration P_1 (in.)	Time t (msec)
0.000	0.0
0.220	0.1
0.420	0.2
0.620	0.3
0.820	0.4
1.010	0.5
1.200	0.6
1.375	0.7
1.540	0.8
1.705	0.9
1.861	1.0
2.000	1.1
2.140	1.2
2.265	1.3
2.380	1.4
2.495	1.5
2.600	1.6
2.690	1.7
2.775	1.8
2.855	1.9
2.936	2.0
2.990	2.1
3.040	2.2
3.085	2.3
3.115	2.4
3.140	2.5
3.150	2.6

Table DV. Steel circular pile, ext. diam 7/16 in., int. diam 6/16 in., mass 0.5 lb. Sand 1. Impact velocity, 167 ft/sec.

Penetration P_i (in.)	Time t (msec)
0.000	0.0
0.193	0.1
0.385	0.2
0.570	0.3
0.750	0.4
0.925	0.5
1.096	0.6
1.256	0.7
1.416	0.8
1.561	0.9
1.710	1.0
1.840	1.1
1.970	1.2
2.090	1.3
2.203	1.4
2.305	1.5
2.404	1.6
2.496	1.7
2.580	1.8
2.650	1.9
2.730	2.0
2.785	2.1
2.840	2.2
2.890	2.3
2.930	2.4
2.970	2.5
2.995	2.6
3.018	2.7
3.028	2.8

Table DVI. Steel circular pile, ext. diam 7/16 in., int. diam 6/16 in., mass 0.5 lb. Sand 1. Impact velocity, 128 ft/sec.

Penetration P_i (in.)	Time t (msec)
0.000	0.0
0.150	0.1
0.300	0.2
0.441	0.3
0.580	0.4
0.710	0.5
0.840	0.6
0.960	0.7
1.065	0.8
1.170	0.9
1.270	1.0
1.365	1.1
1.450	1.2
1.530	1.3
1.600	1.4
1.670	1.5
1.725	1.6
1.780	1.7
1.825	1.8
1.865	1.9
1.900	2.0
1.925	2.1
1.945	2.2
1.965	2.3

Table DVII. Steel circular pile, ext. diam 7/16 in., int. diam 6/16 in., mass 0.5 lb. Sand 1. Impact velocity, 126 ft/sec.

Penetration P_1 (in.)	Time t (msec)
0.000	0.0
0.155	0.1
0.300	0.2
0.435	0.3
0.565	0.4
	0.5
0.690	0.6
0.810	0.7
0.925	0.8
1.030	0.9
1.130	
	1.0
1.225	1.1
1.305	1.2
1.380	1.3
1.450	1.4
1.515	
	1.5
1.570	1.6
1.620	1.7
1.663	1.8
1.703	1.9
1.735	
	2.0
1.760	2.1
1.775	2.2
1.780	

Table DVIII. Steel circular pile, ext. diam 7/16 in., int. diam 6/16 in., mass 0.5 lb. Sand 1. Impact velocity, 122 ft/sec.

Penetration P_1 (in.)	Time t (msec)
0.000	0.0
0.142	0.1
0.280	0.2
0.415	0.3
0.545	0.4
	0.5
0.670	0.6
0.788	0.7
0.892	0.8
1.000	0.9
1.095	
	1.0
1.185	1.1
1.270	1.2
1.345	1.3
1.420	1.4
1.480	
	1.5
1.540	1.6
1.590	1.7
1.635	1.8
1.670	1.9
1.703	
	2.0
1.735	2.1
1.760	2.2
1.770	2.3
1.780	

Table DX. Steel circular pile, ext. diam 7/16 in.,
int. diam 5/16 in., mass 0.375 lb. Sand 2

Mass M (lb)	Penetration P (in.)	Impact velocity V (ft/sec)
0.375	3.84	275
"	2.97	248
"	2.53	210
"	1.78	161
"	1.53	136
"	1.10	111
"	0.88	97
"	0.69	84
"	0.60	76
"	0.28	51

Table DIX. Steel circular pile, ext. diam 7/16 in., int. diam
6/16 in., mass 0.5 lb. Sand 1. Impact velocity, 98 ft/sec.

Penetration P ₁ (in.)	Time t (msec)
0.000	0.0
0.120	0.1
0.230	0.2
0.335	0.3
0.435	0.4
0.520	0.5
0.610	0.6
0.690	0.7
0.765	0.8
0.830	0.9
0.893	1.0
0.955	1.1
1.000	1.2
1.045	1.3
1.080	1.4
1.115	1.5
1.140	1.6
1.165	1.7
1.185	1.8
1.200	1.9
1.210	2.0
1.215	2.1
1.220	2.2

Table DXI. Brass circular pile, ext. diam 7/16 in.,
int. diam 5/16 in., mass 0.375 lb. Sand 2.

Mass M (lb)	Penetration P (in.)	Impact velocity V (ft/sec)
0.375	3.53	234
"	3.31	226
"	2.63	195
"	2.03	166
"	1.72	148
"	1.09	118
"	0.97	100
"	0.72	90
"	0.47	69
"	0.28	51

Table DXII. Steel "wall reduced pile", ext. diam 6/16 in.,
int. diam 5/16 in., mass 0.382 lb. Sand 2.

Mass M (lb)	Penetration P (in.)	Impact velocity V (ft/sec)
0.382	6.16	312
"	4.84	241
"	2.47	190
"	2.13	158
"	1.41	143
"	1.41	130
"	1.03	106
"	0.69	90
"	0.66	81
"	0.56	75
"	0.34	56

Table DXIII. Steel circular pile, ext. diam 6/16 in., int. diam
4/16 in., mass 0.382 lb. Sand 2

Mass M (lb)	Penetration P (in.)	Impact velocity V (ft/sec)
0.382	4.03	251
"	3.72	253
"	3.72	247
"	2.10	171
"	2.00	161
"	1.40	124
"	1.19	121
"	1.06	114
"	0.85	98
"	0.72	90
"	0.66	83
"	0.47	65

Table DXIV. Steel circular pile, ext. diam 7/16 in.,
int. diam 6/16 in. Sand 2.

Mass M (lb)	Penetration P (in.)	Impact velocity V (ft/sec)
0.471	4.94	276
"	2.70	166
"	1.25	101
"	1.00	74
"	0.82	66
"	0.82	62
"	0.63	53
"	0.43	38
0.386	5.75	347
"	4.13	272
"	3.25	239
"	3.06	237
"	2.88	214
"	2.75	180
"	2.43	168
"	2.06	162
"	1.75	142
"	1.70	140
"	1.00	81
"	0.95	78
"	0.94	85
"	0.82	76
"	0.70	63
"	0.70	61
"	0.63	65
"	0.63	61
"	0.44	50
"	0.44	47
"	0.38	42
0.287	6.87	366
"	6.07	348
"	5.80	375
"	5.63	356
"	5.08	341

Table DXIV.
(continued)

APPENDIX E

Firing data of the second investigation of Phase II.
Table E1. Steel rectangular pile, S₁, mass 0.322 lbs.
Sand 2.

Mass M (lb)	Penetration P (in.)	Impact velocity V (ft/sec)	Figure	Penetration P (in.)	Impact velocity V (ft/sec)
0.287	4.50	270	35a	0.50	65
"	3.50	216	"	0.56	73
"	3.07	226	"	0.69	78
"	2.87	225	"	0.88	93
"	2.80	219	"	0.38	52
"	2.80	203	"	0.81	84
"	2.62	207	"	0.25	39
"	2.13	177	"	0.38	58
"	1.25	119	"	1.06	102
"	0.88	96	"	1.50	127
"	0.88	98	"	1.94	154
"	0.88	96	"	4.38	242
"	0.80	99	"	5.44	275
"	0.57	75	"	5.19	258
"	0.57	71	"	0.12	40
"	0.50	66	"	0.34	70
0.153	3.53	334	35b	0.72	107
"	3.09	293	"	1.12	128
"	2.65	268	"	1.44	147
"	2.65	262	"	1.66	158
"	1.72	186	"	1.88	171
"	1.53	173	"	0.38	60
"	1.15	139	"	0.69	80
"	1.03	134	"	1.03	106
"	0.78	107	"	1.81	129
"	0.72	109	"	2.12	154
"	0.72	108	42b		
"	0.65	109	"		
"	0.65	108	"		
"	0.65	107	"		
"	0.12	33	"		

Table III. Steel rectangular pile, S₂, mass 0.322 lb.
Sand 2.

Figure	Penetration P (in.)	Impact velocity V (ft/sec)
35c	0.44	64
"	1.00	106
"	0.94	90
"	0.38	52
"	0.25	39
"	0.50	58
"	0.69	75
"	1.50	135
"	1.88	150
"	2.44	177
"	2.12	168
"	0.88	94
"	0.62	75
"	0.50	63
"	2.00	163
"	2.88	231
"	3.25	195
"	2.75	214
"	0.38	52
"	0.18	31
"	0.50	63
"	0.62	77
"	5.69	332
"	2.00	156
"	3.00	219
"	6.18	318
"	0.50	60
"	1.00	105
42a	0.56	65
"	0.91	82
"	1.28	107
"	1.625	130
"	2.375	155
"	2.75	182

Table EIII. Steel square pile, S₃, mass 0.322 lbs.
Sand 2.

Figure	Penetration P (in.)	Impact velocity V (ft/sec)
41	0.59	65
"	0.84	86
"	1.38	118
"	2.03	147
"	2.78	177
"	5.16	257

Table EIV. Steel circular pile, S₄, mass 0.322 lb
Sand 2, Ground silica, Golden soil.

Table EIV
(continued)

Figure	Penetration P (in.)	Impact velocity V (ft./sec)	Figure	Penetration P (in.)	Impact velocity V (ft./sec)
35a and 37c	0.31	43	37b	0.59	87
"	0.40	51	"	1.00	109
"	0.44	57	"	1.41	129
"	0.88	78	"	1.59	145
"	0.81	79	"	1.97	162
"	0.50	54	"	0.59	74
"	0.81	73	"	0.41	54
"	0.69	66	40c	0.81	84
35b	1.22	127	"	1.28	117
"	1.38	133	"	1.81	148
"	1.53	137	"	2.47	168
"	2.38	175	"	5.16	261
"	1.00	102	"	0.84	102
"	0.50	72	40b	1.16	117
"	0.18	42	"	1.22	123
35c and 36	2.25	164	"	1.66	144
"	3.25	222	"	1.47	131
"	1.94	147	"	2.34	176
"	1.25	122	"	0.59	67
"	0.97	101	"	0.62	80
"	2.44	175	"	2.06	183
"	1.94	147	37d	2.62	223
"	1.19	112	"	1.88	175
"	1.88	149	"	1.06	121
"	0.44	58	"	1.12	120
37a	1.91	174	"	2.69	234
"	0.66	93	"	6.19	396
"	1.12	122	"	0.31	52
"	0.72	90	"	1.06	118
"	0.41	64	"	1.31	118
"	2.78	214	"	2.44	161
			"	1.31	123
			"	0.94	107
			"	2.31	152
			"	3.62	252

(continued)

Table EIV
(continued)Table EVI. Steel cross shape, S6, mass 0.322 lb
Sand 2, Ground silica.

Figure	Penetration P (in.)	Impact velocity V (ft./sec)
37c	0.75	94
"	0.50	73
"	0.50	67
"	0.44	69
"	0.44	62
"	0.31	56
"	0.25	48
"	0.69	91
"	0.69	92
"	0.69	86
"	2.12	184
"	1.12	122
"	1.19	117
"	1.56	140
"	2.00	161
"	2.00	160
"	1.88	152
"	1.56	148
"	2.50	194
37d	1.00	138
"	2.00	220
"	1.31	148
"	2.12	219
"	1.38	142
"	0.78	124
"	0.44	80
"	0.88	116
"	1.88	196
"	1.69	181
"	1.38	154
"	0.88	123
"	0.62	98
"	0.81	115
"	3.00	271

(continued)

Table EV. Steel cross-shaped pile, S5, mass 0.322 lb
Sand 2.

Figure	Penetration P (in.)	Impact velocity V (ft./sec)
37b	0.75	77
"	0.88	95
"	1.25	117
"	1.50	132
"	1.69	146
"	2.00	166
"	1.12	108
"	0.75	80
37a	1.50	141
"	0.69	86
"	0.38	57
"	0.57	77

Table EVII. Steel rectangular pile, T₁, mass 0.322 lb
Sand 2.

Figure	Penetration P (in.)	Impact velocity V (ft./sec)
39a	0.12	26
"	0.28	52
"	0.37	65
"	0.44	73
"	0.62	87
"	0.53	81
"	0.75	97
"	0.81	100
"	0.88	106
"	1.09	114
"	1.22	121
"	1.31	133
"	1.41	140
"	1.50	149
"	1.12	119
"	1.66	162
"	2.00	175
"	2.50	214
39b	0.25	54
"	0.59	82
"	1.00	107
"	1.34	124
"	1.81	152
"	2.23	181
42b	0.44	67
"	0.53	82
"	0.91	105
"	1.31	130
"	1.69	152
42a	0.47	66
"	0.62	80
"	0.94	106
"	1.22	129
"	1.88	153
"	2.38	175

Table EVI
(continued)

Figure	Penetration P (in.)	Impact velocity V (ft./sec)
37d	0.50	84
"	0.50	82
"	1.25	172
"	1.44	190

Table EX. Steel circular pile, T₄, mass 0.322 lb
Sand 2, Golden soil.

Figure	Penetration P (in.)	Impact velocity V (ft/sec)
39a	0.25	48
"	0.56	73
"	0.97	97
"	1.31	126
"	1.66	147
"	2.12	174
39b	0.34	51
"	0.66	83
"	1.00	107
"	1.44	128
"	1.84	152
"	2.34	182
40b	0.69	100
"	0.38	65
"	0.81	91
"	0.60	82
"	1.22	128
"	2.00	177
40c	0.31	54
"	0.59	84
"	1.06	113
"	1.47	152
"	2.09	178
"	4.38	291
40a	0.75	83
"	1.03	95
"	1.66	115
"	2.00	140
"	2.72	159
"	3.47	176
"	1.62	113
"	5.81	247

Table EVIII. Steel rectangular pile, T₂, mass 0.322 lb.
Sand 2

Figure	Penetration P (in.)	Impact velocity V (ft/sec)
42a	0.41	64
"	0.56	81
"	0.88	105
"	1.34	126
"	2.31	163

Table EIX. Steel square pile, T₃, mass 0.322 lb.
Sand 2.

Figure	Penetration P (in.)	Impact velocity V (ft/sec)
41	0.44	69
"	0.56	84
"	1.19	114
"	1.56	139
"	2.19	170
"	4.34	254

Table EXII. Steel circular pile, π_1 , mass 0.500 lb.
Sand 2.

Figure	Penetration P (in.)	Impact velocity V (ft/sec)
49a	1.88	149
"	1.00	93
"	1.44	123
"	0.94	101
"	1.12	119
"	1.61	152
"	0.88	88
"	1.62	144
"	2.81	200
"	1.31	127
"	1.25	117
"	4.25	238
"	3.94	258
"	1.25	112
"	0.56	65
"	1.62	129
"	0.75	79
"	2.25	140
"	0.22	38
"	0.47	58
"	0.97	83
"	1.12	104
"	1.50	122
49b	0.53	60
"	0.69	82
"	1.06	102
"	1.06	104
"	1.28	108
"	1.38	111
"	2.31	185
49c	0.75	78
"	0.88	95
"	1.12	109
"	1.25	114
"	1.38	123

Table EXI. Steel circular pile, U_4 , mass 0.322 lb.
Sand 2.

Figure	Penetration P (in.)	Impact velocity V (ft/sec)
40b	0.06	17
"	0.47	75
"	0.75	106
"	0.91	128
"	1.00	171
"	1.62	175
40c	0.16	54
"	0.47	86
"	0.75	115
"	1.19	152
"	1.62	176
"	2.25	222

Table EXII.
(continued)

Figure	Penetration P (in.)	Impact velocity V (ft/sec)
49c	0.94	97
"	0.75	86
"	1.25	115

Table EXIII. Steel circular pile, π_2 , mass 0.500 lb.
Sand 2.

Figure	Penetration P (in.)	Impact velocity V (ft/sec)
49a	2.38	169
"	1.75	144
"	1.88	158
"	2.69	185
"	2.06	153
"	1.25	98
"	2.06	149
"	4.25	240
"	1.06	102
"	1.00	98
"	1.38	116
"	0.56	63
"	0.81	82
"	4.81	260
"	0.56	68
"	0.62	75
"	0.50	63
"	0.44	57
"	0.25	34
"	0.40	51

(continued)

Table EXIII
(continued)

Figure	Penetration P (in.)	Impact velocity V (ft/sec)
49a	0.56	66
"	0.67	74
"	0.94	84
"	0.88	80
"	1.00	92
"	1.47	118
"	1.75	131
"	1.94	141
"	1.28	111
49b	0.97	89
"	0.91	92
"	0.67	71
"	0.78	77
"	0.91	88
"	1.03	96
"	1.06	102
"	2.34	172
49c	1.28	104
"	0.78	77
"	0.16	22
"	0.81	81
"	1.16	103
"	1.47	119
"	0.60	65

Table EXIV. Steel circular pile, π_3 , mass 0.500 lb.
Sand 2.

Figure	Penetration P (in.)	Impact velocity V (ft/sec)
49c	0.69	68
"	0.94	86
"	1.25	103
"	1.34	113
"	1.60	124
"	0.53	55
"	2.22	161
"	4.34	240
49d and 52a	0.81	88
"	0.72	75
"	1.03	100
"	1.25	112
"	1.69	131
"	1.85	145

Table EXV. Steel circular pile, π_4 , mass 0.500 lb.
Sand 2.

Figure	Penetration P (in.)	Impact velocity V (ft/sec)
49d	2.91	169
"	0.85	71
"	0.94	84
"	1.62	107
"	1.85	121
49e and 52b	0.91	86
"	1.22	116
"	1.72	120
"	1.85	154
"	0.78	68
"	2.25	158

Table EXVI. Steel circular pile, π_5 , mass 0.500 lb.
Sand 2.

Figure	Penetration P (in.)	Impact velocity V (ft/sec)
49c	5.78	252
"	1.78	119
"	0.91	69
"	1.09	67
"	1.53	103
"	1.59	97

Table EXVII. Steel circular pile, O_1 , mass 0.500 lb.
Sand 2.

Figure	Penetration P (in.)	Impact velocity V (ft/sec)
52a	0.85	76
"	1.09	100
"	1.72	119
"	2.09	140
"	4.22	231
"	3.97	206

Table EXVIII. Steel circular pile, O_2 , mass 0.500 lb.
Sand 2.

Figure	Penetration P (in.)	Impact velocity V (ft/sec)
52b	2.44	129
"	0.78	66
"	1.09	81
"	1.53	93
"	1.59	96
"	3.47	166

Table EXIX. Steel cross-shaped pile, T₅, mass 0.459 lb.
Sand 1.

Figure	Penetration P (in.)	Impact velocity V (ft/sec)
46	3.62	273
"	3.56	258
"	4.38	286
"	2.50	203
"	2.88	198
"	2.88	204
"	1.81	162
"	0.75	90
"	0.36	54
"	2.65	206
"	3.10	221
"	1.13	109
"	2.10	182
"	2.35	195
"	1.54	140
"	2.35	194
"	2.55	194
"	1.03	121
"	2.60	208
"	2.85	213
"	1.75	161
"	1.50	129
"	0.75	81
"	2.80	213
"	3.75	248
"	2.50	200
"	2.35	188
"	1.80	166
"	2.25	162
"	3.00	185
"	2.47	161
"	0.75	129
"	1.00	123
"	1.25	145
"	0.50	69
"	1.92	159
"	2.75	220
"	2.43	196
"	1.05	110

Table EXX. Steel cross-shaped pile, E₁, mass 3.67 lb.
Golden soil.

Figure	Penetration P (in.)	Impact velocity V (ft/sec)
45	1.38	73
"	2.50	109
"	4.50	172
"	2.25	112
"	2.50	111
"	4.75	160
"	5.25	175
"	5.75	188
"	1.00	56
"	11.50	280

APPENDIX F

Determination of the shape factor Q.

Solid circular pile

According to the assumptions made in the section "Effective Thickness", the lines of flow are the radii. In polar coordinates, the shape factor Q for a solid circular pile is then given by:

$$Q = \int_0^R 2\pi r(R-r) dr / \pi R^3 = 1/3$$

where the quantities R, r are given in the sketch below:

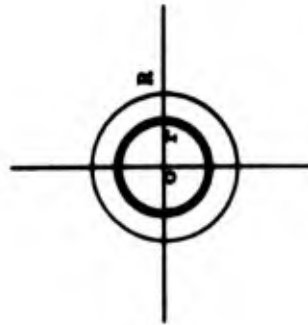


Figure F1.

Square-shaped pile

The direction of the lines of flow is indicated in the sketch below. The shape factor Q for a square-shaped pile is then given by:

$$Q = \int_0^a (a-x) \cdot x \cdot dx / a \int_0^a x \cdot dx = 1/3$$

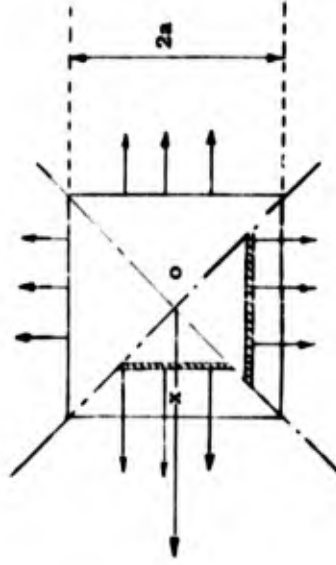


Figure F2.

Rectangular-shaped pile

The direction of the lines of flow is indicated in the sketch below. The shape factor Q for a rectangular-shaped pile is then given by:

$$Q = \left[\int_0^a (a-x)(b-a+x) dx + \int_0^a x(a-x) dx \right] / a^2 \cdot b$$

$$Q = 1/2 - a/6b$$

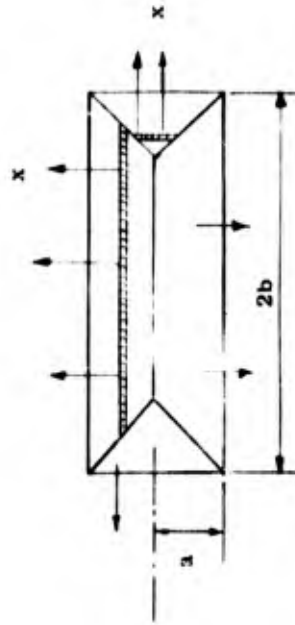


Figure F3.

Cross-shaped pile S6

The direction of the lines of flow is indicated in Figure F4a, b and c. The shape factor Q of the cross-shaped pile S6 is given by

$$Q = 4(I_1 + 2I_2 + 2I_3) / a \cdot S$$

where S is the projected area and I_1 , I_2 , and I_3 are the integrals corresponding to the various directions of the flow as shown in the sketch (c).

$$I_1 = 2 \int_0^a (a-x) \cdot x \cdot dx = a^3/6$$

$$I_2 = \int_0^a (b-3a+2x)(a-x) dx = ba^2/2 + 7a^3/6$$

$$I_3 = \sqrt{2} \int_0^{a\sqrt{2}} (a\sqrt{2}-x)^2 \cdot dx = 4a^3/3$$

$$\text{Then } Q = [b + 2a/3] / [2b-a]$$

APPENDIX G

Firing record of Alaskan tests.

Nominal diameter (in.)	Ext. diam D1 (in.)	Int. diam D2 (in.)	Mass M (lb)	Impact velocity V (ft/sec)	Penetration P (ft)	Remarks
2	2.37	1.93	115	480	4.50	Pipe driven to hilt
"	"	"	115	526	4.50	Pipe driven to hilt
"	"	"	258	72	1.42	One velocity only
"	"	"	118	515	5.00	Pipe driven to hilt
"	"	"	242	200	----	Pipe collapsed by bending
4	4.50	4.02	140	231	2.08	Extracted-End Collapsed
"	"	"	134	289	2.25	
"	"	"	139	286	2.50	Extracted-End Collapsed
"	"	"	134	269	2.00	
"	"	"	134	450	2.33	One velocity only
"	"	"	134	---	1.83	Counters did not operate
"	"	"	134	355	1.67	One velocity reading only
"	"	"	201	264	2.00	
"	"	"	240	80	0.75	Pipe pulled-no end damage
"	"	"	246	---	2.67	Counters did not operate
"	"	"	246	169	2.58	
"	"	"	252	176	2.75	
"	"	"	240	135	1.50	
"	"	"	262	80	0.67	With drive shoe
"	"	"	147	286	1.92	With drive shoe
"	"	"	251	201	1.42	With drive shoe
"	"	"	147	275	1.75	With drive shoe
4	4.50	3.82	162	203	2.00	Pipe pulled-no end damage
"	"	"	162	171	1.08	Hit timing stand-one velocity-pipe pulled-no end damage

Appendix G
(continued)

Nominal diameter (in.)	Ext. diam D1 (in.)	Int. diam D2 (in.)	Mass M (lb)	Impact velocity V (ft/sec)	Penetration P (ft)	Remarks
4	4.50	3.82	155	204	1.75	Pipe pulled-no end damage
"	"	"	155	---	1.67	Counters did not operate
"	"	"	162	213	2.00	
"	"	"	162	355	2.58	
"	"	"	155	---	2.00	Missed timing stand
"	"	"	162	342	2.25	
"	"	"	155	397	2.58	
"	"	"	274	133	3.08	
"	"	"	267	245	2.83	
"	"	"	274	336	2.16	
6	6.62	6.06	185	591	2.00	Pipe pulled - end collapsed
"	"	"	185	---	----	Pile hit timing stand
"	"	"	185	---	1.67	Fuses blew-no velocity meas.
"	"	"	185	220	2.00	
"	"	"	185	214	1.58	
"	"	"	185	213	1.75	Pipe pulled - end collapsed
"	"	"	185	224	1.67	Pipe pulled - end collapsed
"	"	"	194	---	1.75	Counters did not stop
"	"	"	185	480	1.58	
"	"	"	244	658	2.92	
"	"	"	244	745	2.92	
"	"	"	287	242	2.50	
"	"	"	300	123	1.08	With drive shoe
"	"	"	196	164	0.92	With drive shoe

Appendix G
(continued)

Nominal diameter (in.)	Ext. diam D ₁ (in.)	Int. diam D ₂ (in.)	Mass M (lb)	Impact velocity V (ft/sec)	Penetration P (ft)	Remarks
6	6.62	5.76	247	152	1.33	Pipe pulled-no end damage
"	"	"	247	148	0.67	Pipe pulled-no end damage
"	"	"	247	152	1.42	
"	"	"	305	155	1.00	
"	"	"	233	160	1.08	
"	"	"	358	203	3.16	
"	"	"	349	180	2.25	
"	"	"	335	85	0.75	Pipe pulled-no end damage
"	"	"	349	76	1.16	Pipe pulled-no end damage
"	"	"	335	124	1.16	
"	"	"	358	62	0.75	
8	8.62	8.18	---	146	---	End collapsed on impact
"	"	"	---	170	1.00	End collapsed on impact
8	8.62	8.05	215	208	1.42	Pipe pulled-no end damage
"	"	"	265	292	2.33	
"	"	"	228	220	1.83	Pipe pulled - end collapsed
"	"	"	278	315	2.16	
"	"	"	278	130	0.83	Pipe pulled - end collapsed
"	"	"	205	242	1.83	
"	"	"	270	131	0.75	Pipe pulled-no end damage
"	"	"	270	260	1.92	

APPENDIX H: BUCKLING OF PILES UNDER DECELERATION

by

Sp/4 Christopher Goetze

In the main body of this report the mechanism of penetration is studied in detail, but no design criteria are provided for the piles themselves. If improperly designed, however, piles may be expected to buckle under the tremendous decelerations encountered in penetration. This appendix is intended to provide a criterion to guard against this type of failure.

Consider a pile with physical properties,

- ρ = density
- E = Young's modulus
- I = Moment of inertia of the cross-section.

In Figure H2 the pile is shown undergoing an instantaneous deceleration \underline{a} with an exposed length \underline{l} . A small displacement from the vertical is shown with dimensions \underline{y} , \underline{x} , and \underline{u} as indicated. A horizontal deceleration, \underline{a} (\underline{a} small), has been included to take into account the possibility that the pile may be deflected slightly from the vertical during the early stages of penetration as shown in Figure H1. This could be due to an irregularity in the firing procedure or to inhomogeneity of the soil. High speed photographs of actual penetration tests will have to be consulted to obtain an idea of how large \underline{a} is in practice but theory indicates that this may be a significant variable.



Figure H1.

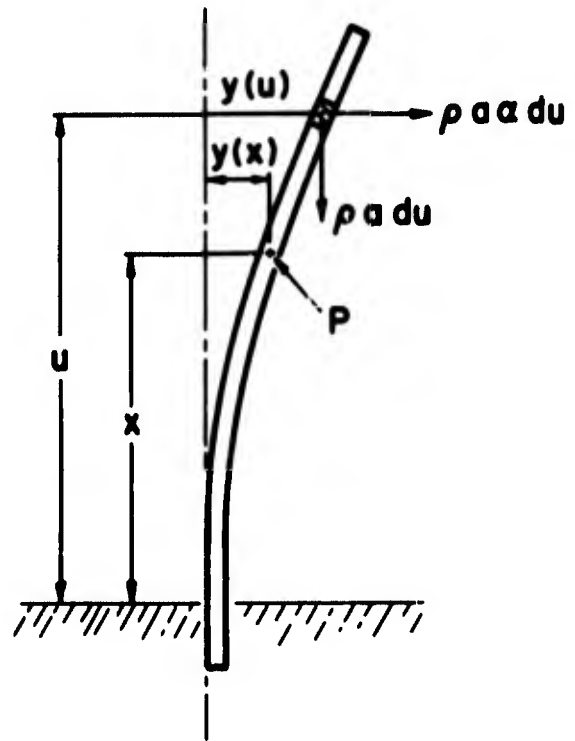


Figure H2.

Taking moments about \underline{P} we have

$$EI \frac{d^2 y}{dx^2} = \rho a \int_x^l [y(u) - y(x) + a(u-x)] du \tag{1}$$

differentiating with respect to \underline{x}

$$EI \frac{d^3 y}{dx^3} = -pa(l-x) \frac{dy}{dx} - pa^2(l-x)$$

$$\text{letting } P^2 = \frac{\rho a}{EI} \quad (2)$$

$$\frac{d^3 y}{dx^3} + P^2(l-x) \frac{dy}{dx} = -aP^2(l-x). \quad (3)$$

To solve the homogeneous equation, we perform the substitutions

$$\xi = \frac{2}{3} P(l-x)^{3/2} \quad \eta = \frac{dy}{dx} (l-x)^{-1/2}.$$

We have

$$\begin{aligned} \frac{d}{dx} &= -P \sqrt{l-x} \frac{d}{d\xi} \\ \frac{d^3 y}{dx^3} &= \frac{d^2 \eta}{dx^2} \sqrt{l-x} - \frac{1}{\sqrt{l-x}} \frac{d\eta}{dx} - \frac{1}{4} \eta (l-x)^{-3/2} = \\ &= \frac{d\eta}{d\xi} P/2 + P^2(l-x)^{3/2} \frac{d^2 \eta}{d\xi^2} + P \frac{d\eta}{d\xi} - \frac{1}{4} \eta (l-x)^{-3/2}. \end{aligned}$$

Substituting into eq 3

$$\begin{aligned} 0 &= \frac{d^2 \eta}{d\xi^2} + \frac{3}{2P} (l-x)^{-3/2} \frac{d\eta}{d\xi} + \eta \left[1 - \frac{1}{4P^2(l-x)^3} \right] \\ 0 &= \frac{d^2 \eta}{d\xi^2} + \frac{1}{\xi} \frac{d\eta}{d\xi} + \eta \left(1 - \frac{1}{9\xi^2} \right). \end{aligned} \quad (4)$$

The solution to this is known to be

$$\eta = AJ_{\frac{1}{3}}(\xi) + BJ_{-\frac{1}{3}}(\xi)$$

where A, B are undetermined constants.

$$\frac{dy}{dx} = \sqrt{l-x} [AJ_{\frac{1}{3}}(\xi) + BJ_{-\frac{1}{3}}(\xi)].$$

To this we add the obvious particular solution $dy/dx = -a$, obtaining

$$\frac{dy}{dx} = -a + \sqrt{l-x} [AJ_{\frac{1}{3}}(\xi) + BJ_{-\frac{1}{3}}(\xi)] \quad (5)$$

$$\xi = \frac{2}{3} P(l-x)^{3/2}.$$

The boundary conditions we wish to satisfy are

$$y(0) = 0 \quad (6)$$

$$\frac{dy}{dx}(0) = 0 \quad (7)$$

$$\frac{d^2 y}{dx^2}(l) = 0. \quad (8)$$

The first two express the geometry at the point of penetration and the third states that the top end is free (i. e., moment = 0).

$y(0) = 0$: To apply this boundary condition, we must first integrate eq 5

$$y = -ax + \int_0^x [AJ_{\frac{1}{3}}(\xi) + BJ_{-\frac{1}{3}}(\xi)] \sqrt{l-x} dx + C.$$

Clearly we can adjust C so that this boundary condition is met. Our further analysis does not require the value of C .

$$\frac{d^2 y}{dx^2}(l) = 0:$$

$$\frac{d^2 y}{dx^2} = \frac{-1}{2\sqrt{l-x}} [AJ_{\frac{1}{3}}(\xi) + BJ_{-\frac{1}{3}}(\xi)] - P(l-x) \left[\frac{-\frac{1}{3}J_{\frac{1}{3}}(\xi)A}{\frac{2}{3}P(l-x)^{3/2}} + \frac{-\frac{1}{3}J_{-\frac{1}{3}}(\xi)B}{\frac{2}{3}P(l-x)^{3/2}} + AJ_{-\frac{2}{3}}(\xi) + BJ_{\frac{2}{3}}(\xi) \right]$$

$$\frac{d^2 y}{dx^2}(x) = -P(l-x)[AJ_{-\frac{2}{3}}(\xi) + BJ_{\frac{2}{3}}(\xi)]$$

$$\frac{d^2 y}{dx^2}(l) = \frac{-PA(P/3)^{-\frac{2}{3}}}{\Gamma(4/3)} = 0$$

hence $A = 0$.

$$\frac{dy}{dx}(0) = 0:$$

$$\frac{dy}{dx}(x) = -a + \sqrt{l-x} BJ_{-\frac{1}{3}}(\xi)$$

$$\frac{dy}{dx}(0) = -a + \sqrt{l} BJ_{-\frac{1}{3}}(\frac{2}{3}Pl^{3/2}). \quad (9)$$

Note that if we let $a = 0$ and set $dy/dx(0) = a$ we obtain the same result.

Case I $a = 0$

This case can only be solved for specific values of $(\frac{2}{3}Pl^{3/2})$. Instability first sets in at $\frac{2}{3}Pl_0^{3/2} = \xi_0 =$ the first zero of $J_{-\frac{1}{3}}(\xi) = 1.86635$.

$$\frac{2}{3}\sqrt{\rho/EI} a^{1/2} l_0^{3/2} = 1.86635 \quad (10)$$

$$al_0^3 = 7.837 EI/\rho \quad (11)$$

$$l_0 = 1.986 [EI/\rho a]^{1/3}.$$

Here l_0 represents the greatest length of exposed pile permissible with physical properties E , I and ρ undergoing an acceleration of a when the pile points perfectly in its direction of motion.

Case II $a \neq 0$

$$\frac{dy}{dx} = a \left[\sqrt{\frac{l-x}{l}} \frac{J_{-\frac{1}{3}}(\xi)}{J_{-\frac{1}{3}}(\frac{2}{3}Pl^{3/2})} - 1 \right]. \quad (12)$$

The critical value for unlimited deformation is again $\frac{2}{3}Pl^{3/2}$ = first zero of $J_{-\frac{1}{3}}(\xi)$ as in the case of $\alpha = 0$. In this case, however, the moment may reach high values before buckling (i. e., elastic instability) sets in. These are reached as $l \rightarrow l_0$. To investigate this, let us consider the moment:

$$EI \frac{d^2 y}{dx^2} = \frac{-PEI(l-x)\alpha J_{\frac{2}{3}}\left[\frac{2}{3}P(l-x)^{3/2}\right]}{\sqrt{l} J_{-\frac{1}{3}}\left(\frac{2}{3}Pl^{3/2}\right)}$$

To simplify this expand $J_{-\frac{1}{3}}\left(\frac{2}{3}Pl^{3/2}\right)$ about $l = l_0$ to obtain

$$EI \frac{d^2 y}{dx^2} = \frac{EIP(l-x)\alpha J_{\frac{2}{3}}\left[\frac{2}{3}P(l-x)^{3/2}\right]}{\sqrt{l}(\xi_0 - \xi) J_{\frac{2}{3}}(\xi_0)}$$

Since $J_{\frac{2}{3}}(\xi)$ is a monotonically increasing function of ξ for $0 < \xi < \xi_0$ we may safely assume that the maximum moment occurs at $x = 0$ or

$$\text{Max. moment} = M_0 = \frac{EI \sqrt{l} \alpha}{\frac{2}{3}(l_0^{3/2} - l^{3/2})}$$

or

$$M_0 = \frac{3EI\alpha}{2l[1 - (l/l_0)^{3/2}]} \quad (13)$$

To solve exactly for l requires the solution of a cubic but we can obtain an approximate expression for $l_0 - l \ll l_0$ as follows:

$$\frac{2M_0}{3} (\sqrt{l_0} - \sqrt{l}) (l + \sqrt{l l_0} - l_0) = EI\alpha \sqrt{l}$$

or approximately

$$\sqrt{l_0} - \sqrt{l} = \frac{\alpha EI}{2M_0 \sqrt{l_0}}$$

$$\sqrt{\frac{l}{l_0}} = 1 - \frac{\alpha EI}{2M_0 l_0}$$

Again making approximations, we obtain

$$l = l_0 - \frac{\alpha EI}{M_0} \quad (14)$$

We cannot use relationships 11 and 14 directly as design criteria since l_0 refers only to the portion which has not yet penetrated the ground. With reference to eq 10 we can see that the greatest buckling danger occurs when αl^3 is a maximum.

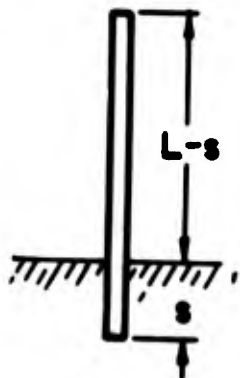


Figure H3.

$$\text{let } f = (L-s)^3 \frac{d^2 s}{dt^2}$$

Only a maximum in the range $0 \leq s \leq L$ is of interest, of course. The exact form of $d^2 s/dt^2 (s)$ is quite complicated but the strong dependence of \bar{f} on $L-s$ allows us to concentrate our attention only on the very earliest stages of penetration. If $d^2 s/dt^2$ were known to be constant throughout the penetration, then \bar{f} would achieve its highest value at $s = 0$. This is not in fact the case, but $d^2 s/dt^2$ increases only slightly with penetration (see Fig. 24, 26, 27, 28) and for the purposes of this discussion we may approximate it by $d^2 s/dt^2 = a + a's$

$$\bar{f} = (L-s)^3 (a + a's) \quad (15)$$

$$\frac{d\bar{f}}{ds} = 0 \text{ at } s = \frac{L}{4} - \frac{3a}{4a'}, \text{ and } s = L.$$

The form of eq 15 is sketched in Figure H4.

Clearly, as long as $3a/a' \geq L$, \bar{f} reaches its maximum in $0 \leq s \leq L$ at $s = 0$. From the somewhat limited data available, it appears reasonable to assume $3a/a' \sim 5L_0 - 10L_0$ where L_0 is the total penetration. Thus, as long as a significant portion of the pile penetrates the ground we may assume that \bar{f} is maximized at $s = 0$.

Lastly, in view of the previous result, we need a short discussion of the boundary condition $dy/dx(0) = 0$. The fact that buckling is most likely to occur at zero penetration implies that the bottom end of the pile cannot be considered fixed during buckling. If the bottom end is left free, however (i. e., $d^2 y/dx^2(0) = 0$), we obtain as before a series of discrete solutions. The first, $\frac{2}{3}Pl^{3/2} = 0$, corresponds to the pile falling over. From experience we know that this does not occur. Higher order solutions lead to permissible lengths much larger than l_0 . Thus buckling cannot be expected to occur until the boundary condition $dy/dx(0) = 0$ is established. We may conclude then that

$$L = 1.986 \left[\frac{EI}{\rho a} \right]^{1/3} - \frac{aEI}{M_0}$$

represents the greatest permissible length for a pile with physical constants E , I , ρ . The value of \underline{a} is to be taken from the "impact deceleration" data in the report.

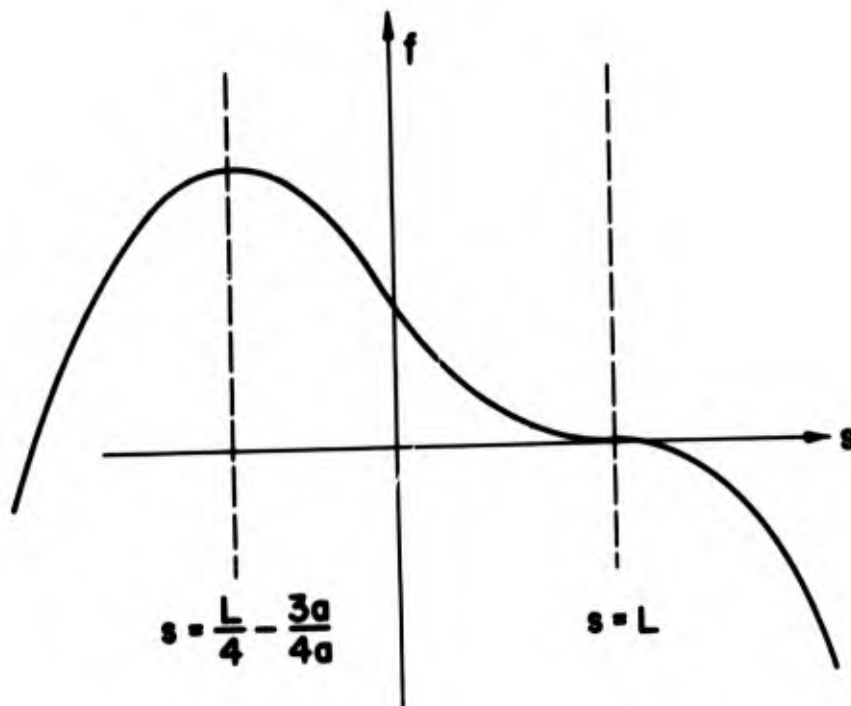


Figure H4.

Unclassified

Security Classification

DOCUMENT CONTROL DATA - R&D

(Security classification of title, body of abstract and indexing annotation must be entered when the overall report is classified)

1. ORIGINATING ACTIVITY (Corporate author) Colorado School of Mines Research Foundation, Inc. Golden, Colorado		2a. REPORT SECURITY CLASSIFICATION Unclassified	
		2b. GROUP	
3. REPORT TITLE MECHANICS OF PENETRATION OF PILES INTO PERMAFROST			
4. DESCRIPTIVE NOTES (Type of report and inclusive dates) Final Report			
5. AUTHOR(S) (Last name, first name, initial) Charest, Jacques; Duler, Philippe; and Rinehart, John S.			
6. REPORT DATE Sept 65		7a. TOTAL NO. OF PAGES 116	7b. NO. OF REFS 9
8a. CONTRACT OR GRANT NO. DA-11-190-ENG-92		8a. ORIGINATOR'S REPORT NUMBER(S)	
b. PROJECT NO			
c.		8b. OTHER REPORT NO(S) (Any other numbers that may be assigned this report)	
d.		CRREL Technical Report 122	
10. AVAILABILITY/LIMITATION NOTICES Distribution of this document is unlimited			
11. SUPPLEMENTARY NOTES		12. SPONSORING MILITARY ACTIVITY U. S. Army Cold Regions Research and Engineering Laboratory, Hanover, N.H.	
13. ABSTRACT Laboratory and field tests have been conducted to determine the feasibility of using rockets for driving piles. Phase I consisted of driving hollow circular model piles into artificial permafrost using guns. Measured parameters were the penetrations and impact velocities of piles having various masses and various external and internal diameters. The main purpose of Phase II was the measurement of parameters in order to find a physical meaning of the empirical equation developed in Phase I. The field test program consisted of driving thin, hollow, full-size piles into natural permafrost using a rocket as the driving agent, and measuring the same parameters as in Phase I. The results indicate that the use of rockets is technically feasible. It is estimated that a 6 in. nominal diameter pile of 0.56-in. wall thickness could be driven 6 to 8 ft into permafrost by a 100,000 lb thrust rocket having an 80 msec burning duration. To resist collapse upon impact with the permafrost, the pile should have either a reinforcement shoe or a minimum wall thickness of 0.56 in. A design of an integrated pile-rocket assembly meeting these requirements is proposed.			

14. KEY WORDS	LINK A		LINK B		LINK C	
	ROLE	WT	ROLE	WT	ROLE	WT
<p>Pile driving methods Foundation construction in permafrost</p>						

INSTRUCTIONS

1. ORIGINATING ACTIVITY: Enter the name and address of the contractor, subcontractor, grantee, Department of Defense activity or other organization (*corporate author*) issuing the report.

2a. REPORT SECURITY CLASSIFICATION: Enter the overall security classification of the report. Indicate whether "Restricted Data" is included. Marking is to be in accordance with appropriate security regulations.

2b. GROUP: Automatic downgrading is specified in DoD Directive 5200.10 and Armed Forces Industrial Manual. Enter the group number. Also, when applicable, show that optional markings have been used for Group 3 and Group 4 as authorized.

3. REPORT TITLE: Enter the complete report title in all capital letters. Titles in all cases should be unclassified. If a meaningful title cannot be selected without classification, show title classification in all capitals in parenthesis immediately following the title.

4. DESCRIPTIVE NOTES: If appropriate, enter the type of report, e.g., interim, progress, summary, annual, or final. Give the inclusive dates when a specific reporting period is covered.

5. AUTHOR(S): Enter the name(s) of author(s) as shown on or in the report. Enter last name, first name, middle initial. If military, show rank and branch of service. The name of the principal author is an absolute minimum requirement.

6. REPORT DATE: Enter the date of the report as day, month, year, or month, year. If more than one date appears on the report, use date of publication.

7a. TOTAL NUMBER OF PAGES: The total page count should follow normal pagination procedures, i.e., enter the number of pages containing information.

7b. NUMBER OF REFERENCES: Enter the total number of references cited in the report.

8a. CONTRACT OR GRANT NUMBER: If appropriate, enter the applicable number of the contract or grant under which the report was written.

8b, 8c, & 8d. PROJECT NUMBER: Enter the appropriate military department identification, such as project number, subproject number, system numbers, task number, etc.

9a. ORIGINATOR'S REPORT NUMBER(S): Enter the official report number by which the document will be identified and controlled by the originating activity. This number must be unique to this report.

9b. OTHER REPORT NUMBER(S): If the report has been assigned any other report numbers (*either by the originator or by the sponsor*), also enter this number(s).

10. AVAILABILITY/LIMITATION NOTICES: Enter any limitations on further dissemination of the report, other than those imposed by security classification, using standard statements such as:

- (1) "Qualified requesters may obtain copies of this report from DDC."
- (2) "Foreign announcement and dissemination of this report by DDC is not authorized."
- (3) "U. S. Government agencies may obtain copies of this report directly from DDC. Other qualified DDC users shall request through _____."
- (4) "U. S. military agencies may obtain copies of this report directly from DDC. Other qualified users shall request through _____."
- (5) "All distribution of this report is controlled. Qualified DDC users shall request through _____."

If the report has been furnished to the Office of Technical Services, Department of Commerce, for sale to the public, indicate this fact and enter the price, if known.

11. SUPPLEMENTARY NOTES: Use for additional explanatory notes.

12. SPONSORING MILITARY ACTIVITY: Enter the name of the departmental project office or laboratory sponsoring (paying for) the research and development. Include address.

13. ABSTRACT: Enter an abstract giving a brief and factual summary of the document indicative of the report, even though it may also appear elsewhere in the body of the technical report. If additional space is required, a continuation sheet shall be attached.

It is highly desirable that the abstract of classified reports be unclassified. Each paragraph of the abstract shall end with an indication of the military security classification of the information in the paragraph, represented as (TS), (S), (C), or (U).

There is no limitation on the length of the abstract. However, the suggested length is from 150 to 225 words.

14. KEY WORDS: Key words are technically meaningful terms or short phrases that characterize a report and may be used as index entries for cataloging the report. Key words must be selected so that no security classification is required. Identifiers, such as equipment model designation, trade name, military project code name, geographic location, may be used as key words but will be followed by an indication of technical context. The assignment of links, rules, and weights is optional.